

UNIVERSITÄTSKLINIKUM HAMBURG-EPPENDORF

Zentrum für Experimentelle Medizin
Institut für Osteologie und Biomechanik

Prof. Dr. med. Michael Amling

Acetylation of transcription factor TFEB: impact for nuclear translocation, gene activation and synthesis of lysosomal enzymes

Dissertation

zur Erlangung des Doktorgrades PhD
an der Medizinischen Fakultät der Universität Hamburg.

vorgelegt von:

Anastasia Laudicina
Spoleto (PG), Italy

Hamburg 2023

Angenommen von der Medizinischen Fakultät am 18.12.2023

Veröffentlicht mit Genehmigung der Medizinischen Fakultät der Universität Hamburg.

Prüfungsausschuss, der/die Vorsitzende: Prof. Dr. Thomas Braulke

Prüfungsausschuss, zweite/r Gutachter/in: Prof. Dr. Kerstin Kutsche

To my family

INDEX

1. Introduction.....	1
1.1. Lysosomes.....	1
1.2 Lysosomes diseases.....	2
1.3 Regulatory mechanism of lysosomal adaptation.....	3
1.3.1 Molecular players in lysosomal nutrient sensing pathways.....	3
1.4 Transcriptional regulation of lysosomal function.....	7
1.5 Transcription Factor EB (TFEB).....	9
1.5.1 Functional regulation of TFEB phosphorylation.....	10
1.5.2 Additional kinases involved in TFEB regulation.....	12
1.5.3 Acetylation of TFEB as novel posttranslational modification.....	12
1.6 Aim of the study.....	15
2. Material and Methods.....	16
2.1 Material.....	16
2.1.1 Equipment.....	16
2.1.2 Consumables.....	16
2.1.3 Chemicals.....	17
2.1.4 Kits.....	17
2.1.5 Oligonucleotides (oligo) for mutagenesis and sequencing.....	18
2.1.6 Media and supplements for cell culture.....	18
2.1.7 Software and data processing.....	19
2.1.8 Online website.....	19
2.2 Cell culture methods.....	20
2.3 Biochemical methods.....	20
2.3.1 Total cell extraction.....	20
2.3.2 Preparation of nuclear and Postnuclear Supernatant (PNS)/cytoplasmic fractions.....	20
2.3.3 Secretome analysis.....	21
2.3.4 Western blotting.....	21
2.3.5 Enzyme activity measurements.....	23
2.4 Molecular biology methods.....	23
2.4.1 Quantitative real-time PCR.....	23
2.4.2 Transcriptome.....	25
2.4.3 Site-directed mutagenesis.....	25
2.5 Confocal laser scanning microscopy.....	26
2.6 Statistical analysis.....	27
3. Results.....	28
3.1 Subcellular distribution of GFP-TFEB-wt and mutants.....	28
3.1.1 Transient transfection of the single K274 acetylation mimetic-mutation decrease TFEB nuclear translocation in steady-state condition.....	31
3.1.2 TFEB-acetylation mimetic mutation affect the phosphorylation at S142 and S211.....	32
3.2 Differential gene expression analysis of induced wild-type and TFEB K3R.....	34
3.2.1 Different gene-activation response to TFEB-wt and –K3R expression.....	36
3.3 Transcriptome analysis of TFEB-wt and –K3R.....	37
3.3.1 Short and long term TFEB transcription.....	37
3.3.2 TFEB wt and K3R regulated CLEAR-containing target genes.....	42
3.3.3 Validation of RNAseq data by RT-PCR analysis.....	45
3.4 Impact of TFEB wt and –K3R induced gene activation on protein synthesis of lysosomal enzymes.....	46

3.4.1 Identification of transmembrane soluble domain under TFEB expression.....	50
4. Discussion.....	53
4.1 TFEB acetylation at K237, K256 and K274 prevent its nuclear translocation.....	53
4.2 TFEB-K3A is retained in the cytoplasm in an mTORC1-independent manner.....	54
4.3 Transcriptome analysis upon TFEB-wt and -K3R expression.....	55
4.3.1 TFEB regulation of selected CLEAR-target genes.....	56
4.4 TFEB dependent soluble lysosomal protein translation.....	58
4.4.1 Transmembrane shedding after TFEB expression.....	59
5. Summary.....	62
6. Abbreviation and Supplementary Tables.....	65
7. Bibliography.....	68
8. Acknowledgements.....	78
9. Curriculum vitae.....	79
10. Eidesstattliche Erklärung.....	81

1. Introduction

1.1 Lysosomes

Lysosomes are best known as the primary center of metabolic pathways involved in the degradation and processing macromolecules. Moreover, they play a key role in diverse cellular processes, such as immune response (e.g. bacterial/virus inactivation), plasma membrane repair, fusion with other organelles (e.g. autophagosomes, endosomes), cell adhesion, and migration (Ballabio and Bonifacino, 2020). Lysosomes are single membrane-bound acidic organelles, present inside the cell in different numbers, morphology, size, membrane protein composition and enzyme content (Yang and Wang, 2021). Highly specialized cell types (e.g. melanocytes, cytotoxic T cells) contain lysosome-related organelles with unique functions and protein composition to support specific physiological roles (Ballabio and Bonifacino, 2020).

The catabolic functions of lysosomes are mediated by ~ 70 luminal lysosomal hydrolases (proteases, glycosidases, lipases, sulfatases, phosphatases, and nucleases) and accessory, enzyme-activators such as saposins or the cholesterol binding protein NPC2, which are mostly involved in the degradation or transfer of lipids (Ballabio and Bonifacino, 2020). The acidification of the lysosomal lumen (pH 4.6) is required for the catalytic activity of many lysosomal hydrolases. The multi-subunit v-ATPase regulates the H⁺ influx supported by a counterflux of cations (Na⁺ and K⁺) or as anion co-transport mediated by ion channels or exchanger complexes localized in the lysosomal membrane (Kendall and Holian, 2021). In addition to ion transporter complexes, lysosomal membranes comprise ~ 250 integral membrane proteins, responsible for structure and protection (e.g. LAMP1/2), and the egress of the degraded products and metabolites for subsequent re-utilization (Saftig and Klumperman, 2009). Furthermore, at least 50 associated proteins (e.g. mTOR, Rag-GTPases) are found on the cytoplasmic surface of lysosomes interacting with lysosomal vATPases and integral lysosomal amino acid or cholesterol transporter to form dynamic signaling platforms by sensing metabolic, oxidative or energetic changes, both in the lumen of the lysosome and in the cytoplasmic environment (Ballabio and Bonifacino, 2020; Fig. 1.1). Moreover, by receiving both extracellular and intracellular cargo material, lysosomes play an indispensable role in endocytic and autophagic pathways, respectively (Bouhamdani et al., 2021). In particular, autophagy, an evolutionary conserved catabolic pathway, relies on proper lysosomal functions for both constitutive turnover of cytoplasmic components (such as short lived cytosolic or misfolded proteins, damaged organelles), or providing energy supply for cells during nutrient starvation (Di Malta et al., 2019). Finally, recent discoveries on the

transcriptional regulation of lysosome biogenesis and functions changed completely the view of lysosomes as multifunctional and dynamic compartments able to adapt to environmental conditions (Ballabio and Bonifacino, 2020).

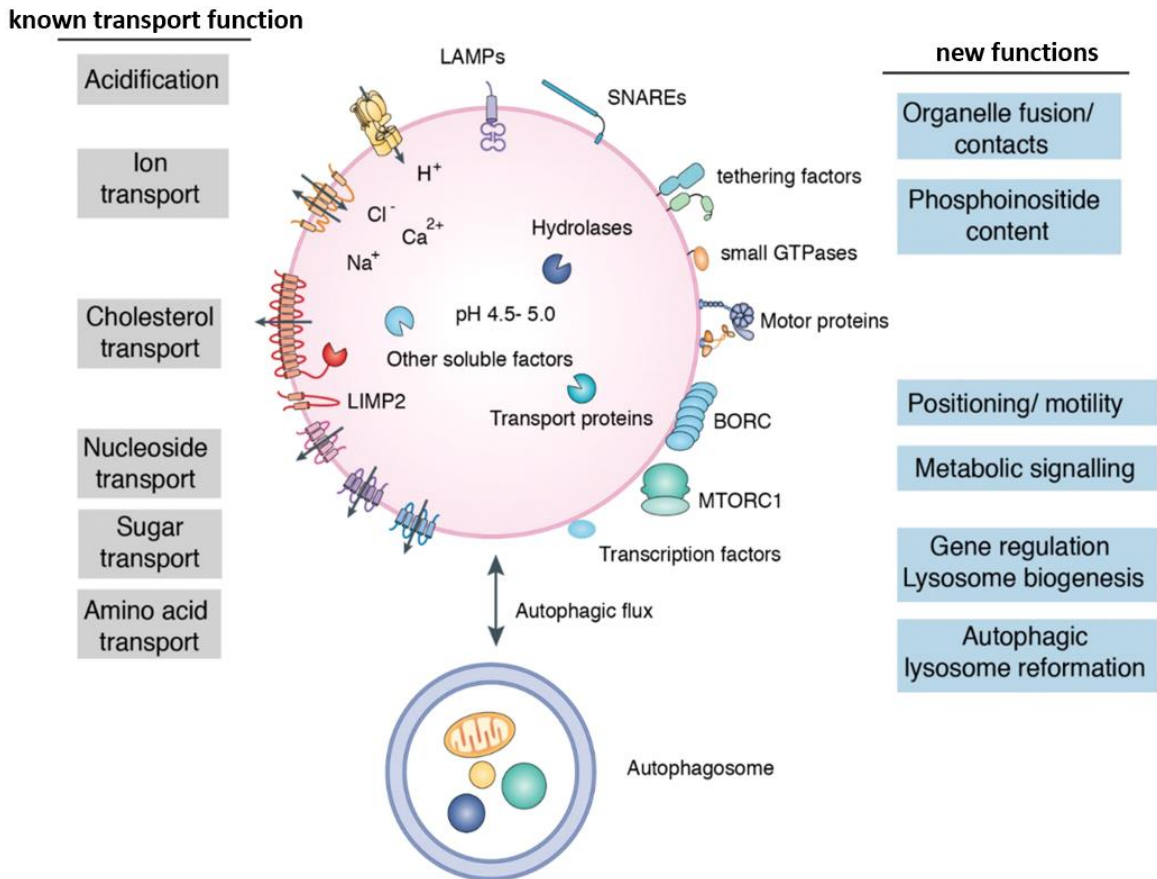


Fig. 1.1 Schematic representation of the lysosome and related functions – Lysosomal luminal, transmembrane and associated proteins are displayed. Lysosomes can fuse with autophagosomes for degradation of the cargo in the last step of the autophagy flux. In addition to the transport functions known since decades (grey boxes, left), various novel lysosomal properties and pathways have been discovered in the past 10 years (light blue, right) (readapted from Ballabio and Bonifacino, 2020).

1.2 Lysosome diseases

The biological significance of lysosomes is emphasized by ~ 70 human hereditary rare genetic disorders. Bi-allelic mutations in genes encoding lysosomal hydrolases, membrane proteins but also non-lysosomal genes involved in lysosomal biogenesis, cause lysosomal dysfunctions and subsequent progressive storage disorders (LSDs), classified according to the major non-degraded lysosomal materials such as mucopolysaccharidoses (MPS), sphingolipidoses, or glycoproteinoses (Platt et al, 2018). The incidence of these LSDs ranged from 1:20,000 to 1:1,000,000.

In the last 15 years lysosomal biogenesis and functions also have been associated with more common diseases, especially neurodegenerative disorders, cancer, inflammatory and autoimmune diseases, and metabolic disorders (Bajaj et al., 2019). In particular, neuronal accumulation of non-degraded aggregates in the cytoplasm and the subsequent cell death is a common pathophysiological feature observed in many neurodegenerative disorders including Alzheimer (AD), Parkinson (PD), Huntington disease (HD), and frontotemporal dementia (Deneubourg et al., 2022). In this regard, recent discoveries highlight lysosomal proteases such as cathepsin K and cathepsin D as potential therapeutic targets in PD or AD, to promote the degradation of α -synuclein and $\alpha\beta$ -amyloid plaque aggregates, respectively (Hook et al., 2020; McGlinchey et al., 2020).

1.3 Regulatory mechanism of lysosomal adaptation

As the primary key regulators of metabolism, lysosomes integrate both nutrient and growth factor availability signals by modulating the protein composition, degradation processes, size, morphology, and distribution of these organelles (Bouhamdani et al., 2021). For instance, lysosomal Ca^{2+} channels respond to pH variations, cellular stress, or small molecules such as ATP, phospholipids and sphingosine, allowing thus a selective Ca^{2+} release based on the upstream stimuli. Lysosomal Ca^{2+} signaling mediates various lysosomal functions, such as lysosome reformation, endosome-lysosome fusion, autophagosome-lysosome fusion, or lysosomal exocytosis (Ballabio and Bonifacino, 2020).

Numerous discoveries in the past 15 years demonstrate the existence of transcriptional programs controlling lysosomal biogenesis and functions as a response to metabolic signals (Sardiello et al., 2009; Settembre et al., 2011; Slade and Pulinilkunnil, 2017). Finally, the increasing broad spectrum of transcription factors and repressors acting downstream of the cell metabolic request(s) highlight the key-role of lysosomes as a multifunctional signaling hub (Ballabio and Bonifacino, 2020).

1.3.1 Molecular players in lysosomal nutrient sensing pathways

One of the major regulators of cell growth and metabolism is the mechanistic target of rapamycin (**mTOR**), a serine-threonine kinase that controls the balance between anabolism and catabolism in response to environmental conditions (Saxton and Sabatini, 2017). mTOR is part of two protein kinase complexes: **mTOR complex-1 (mTORC1)** and **mTORC2**. mTORC1 is composed of mTOR, the mammalian lethal with SEC13 protein **8 (mLST8)** which interacts and stabilizes the catalytic activity of mTOR, and the **Regulatory-associated protein**

of mTOR (**RAPTOR**), that is fundamental for substrate recognition and targeting mTORC1 to the surface of lysosomes. mTORC2 shares some components with mTORC1 such as mLST8 the rapamycin-insensitive companion of mTOR (**RICTOR**) and the mammalian stress-activated map kinase-interacting protein 1 (**mSIN1**) (Battaglioni et al., 2022).

Seminal works demonstrate the dual role of mTORC1 in the integration of metabolic signals. mTORC1 promotes cell growth by phosphorylation of anabolic effectors involved in protein synthesis such as p70S6 kinase S6K (at T371/389), or by inhibition of eukaryotic initiation factor 4E-binding protein 1 (**4EBP1**, at T37/46, S65, T70) (Battaglioni et al., 2022; *Translation pathway* in Fig. 1.2). Furthermore, mTORC1 inhibits the lipid metabolism by phosphorylation of the AMP-activated kinase (**AMPK** at S356/345/377) and Lipin1 (at S106, S472), but activates glucose metabolism via phosphorylation of the eukaryotic translation initiation factor **eIF2B** (at S2/67) (Battaglioni et al., 2022; *Lipid & Glucose metabolism* in Fig. 1.2). In addition, mTORC1 regulates growth factor signaling via phosphorylation of the insulin receptor-binding protein GRB10 (at S474, S476), or by inhibition of the insulin receptor substrate 1 (**IRS1**) at S422/423, and S636/639 (Battaglioni et al., 2022; *Growth factor signaling* in Fig. 1.2). Finally, mTORC1 regulates its own activity by phosphorylation of RAPTOR (at S859/863), its endogenous inhibitor DEPTOR (at S293/299, T295), or the proline-rich AKT1 substrate 1 **PRAS40** (at S183/212/211) (Battaglioni et al., 2022; *mTOR regulation* in Fig. 1.2).

On the other hand, mTORC1 represses catabolic processes by phosphorylation of downstream effectors. Phosphorylation of microphthalmia/transcription factor E (**MiT/TFE**) family members, specifically TFEB (at S122, S142, S211) and TFE3 (at S321) leading to their inactivation (Vega-Rubin-de-Celis et al., 2017; Settembre et al., 2012; Martina et al., 2012; Roczniak-Ferguson et al., 2012; Martina et al., 2014; *Lysosome biogenesis* in Fig. 1.2). In nutrient-rich conditions, mTORC1 phosphorylates and inactivates the unc51-like autophagy activating kinase 1 **ULK1** (at S757) and blocks autophagy (*Autophagy* in Fig. 1.2). Reversely, under nutrient-rich conditions mTORC1 phosphorylates the tumor suppressor protein UVRAG (at S498, S550/571), important in the autophagosome-lysosome reformation (ALR) process that is initiated by lysosomal tubulation and is essential in maintaining lysosomal function and cell survival (Munson et al., 2015; *Autophagy* in Fig. 1.2).

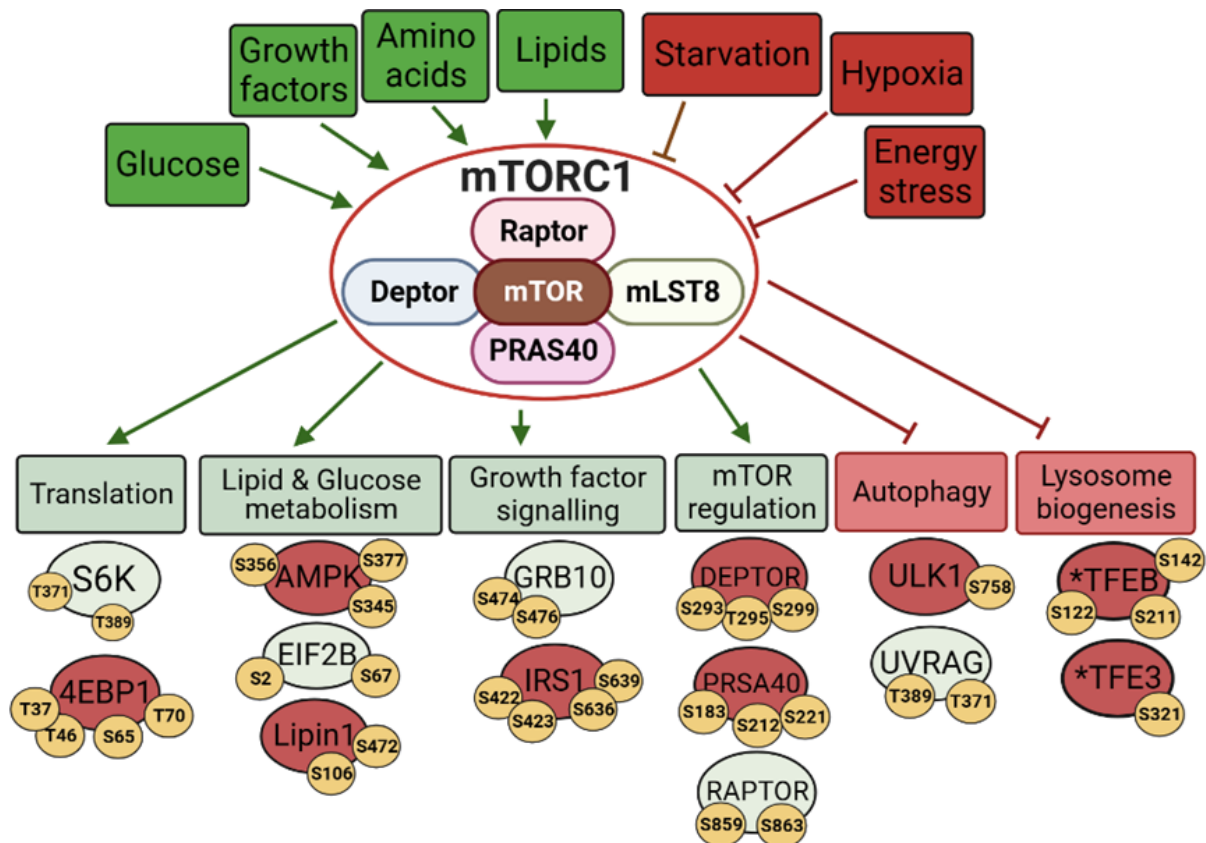


Fig. 1.2 Schematic representation of mTORC1 metabolic signaling – mTORC1 is a multiprotein complex localized at the cytoplasmic surface of lysosomes and is activated by metabolic basal signals (upper left green boxes), or inhibited by cell stress signals (upper right, red boxes). In the presence of fed-cell signals, mTORC1 integrates different stimuli and activates specific response(s) (green squares boxes) by phosphorylation at specific Ser or Thr residues (small yellow circles) of downstream effectors by activating (light green ovals) or inhibiting the proteins (red ovals). mTORC1 activation shutdown catabolic pathways (red square boxes). *TFEB and TFE3 are regulators of autophagy processes as well (*Picture create with BioRender*).

mTORC2 regulates cell metabolism and cell survival by phosphorylation of AKT (known as protein kinase B; at T308, S473) which subsequently phosphorylates and inactivates its downstream targets such as glycogen synthase kinase-3 β (GSK3 β) and transcription factor FOXO1/3a (Sun et al., 2023). Moreover, mTORC2 regulates cytoskeletal remodeling and cell migration by phosphorylation of members of the PKC kinase family (Saxton and Sabatini, 2017). Finally, mTORC2-catalyzed phosphorylation of serine/threonine-protein kinase **SGK1** (at S422) regulates cell survival and ion homeostasis (Saxton and Sabatini, 2017; Sun et al., 2023).

The active mTORC1 complex integrates metabolic signals from both the cytoplasm and the lysosomal lumen by upstream amino acid nutrient sensors through distinct mechanisms. In the cytoplasm, the leucine sensor Sestrin, the arginine sensor (**CASTOR**), and the S-adenosylmethionine (**SAM**) sensor upstream of mTORC1 (**SAMTOR**), respond to the amino

acid levels by direct binding and regulation of **GATOR1** (**GAP** towards **Rags 1**) complex, leading to mTORC1 dissociation from lysosome surface under low amino acid levels. The arginine level in the lumen of lysosomes is sensed by the integral lysosomal membrane protein solute carrier SLC38A9.

Recent discoveries led to the subdivision of canonical and non-canonical mTORC1 signaling pathways. In both pathways, mTORC1 is recruited at the lysosomal surface by Rag-GTP/GDPases (heteromeric complexes composed by RagA/B-**GTP** bound to RagC/D-**GDP**), associated with the lysosomal Lamtor1-5 (**Ragulator**) complex. The Ragulator-Rag complex specifically interacts with the v-ATPase, maintaining the low lysosomal pH, and various cytosolic and lysosomal proteins sensing the amino acid level. High essential amino acid concentrations mediate the activation of mTORC (Fig. 1.3; Napolitano et al., 2022).

In the **canonical signaling process**, the recruited mTORC1 at the lysosomal surface is activated by binding of the activated Rheb-GTP protein and allows the phosphorylation of its substrates S6K and 4EBP1. Concomitantly, the GTPase-activating properties of the Rheb inhibitor **Tuberous Sclerosis Complex (TSC)** has to be blocked by growth factor-initiated TSC phosphorylation (Battaglionni et al., 2022; Napolitano et al., 2022; Fig. 1.3 A).

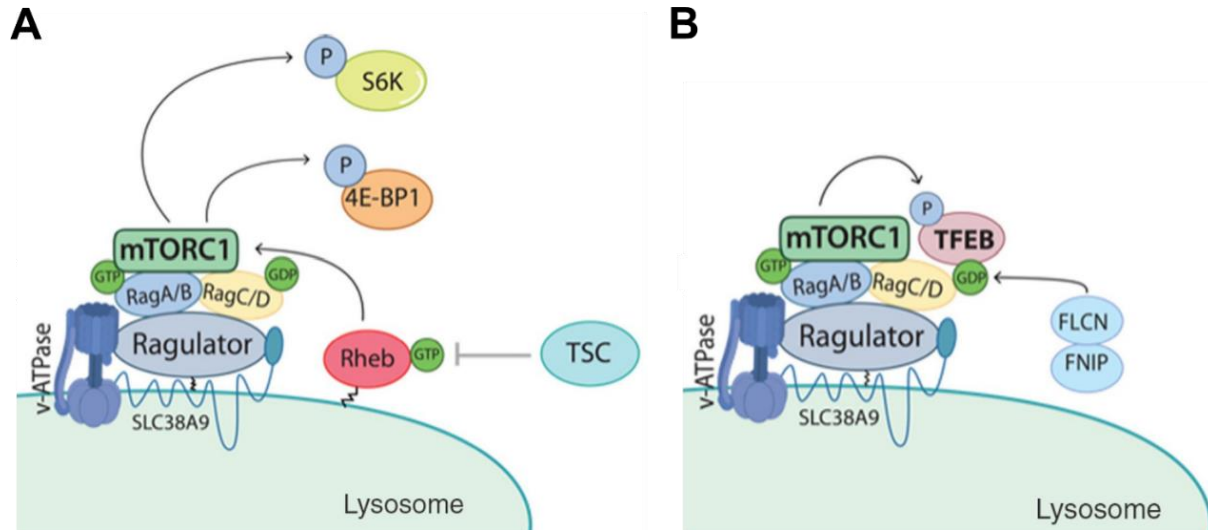


Fig. 1.3 Canonical and non-canonical signaling pathway of mTORC1 – (A+B) The recruitment of mTORC1 to the lysosome surface is modulated by Rag-GTP/GDPases, and the Ragulator complex. The Ragulator complex associates with the v-ATPase and interacts with SLC38A9 amino acid transporter. (A) In the canonical-pathway mTORC1 activation relies on the TSC/Rheb-GTP axis, which leads to the phosphorylation of S6K and 4EBP1. (B) In the non-canonical mTORC1 pathway, FLCN–FNIP-RagC/D-GDP negatively regulates TFEB by the activated mTORC1 phosphorylation (*readapted from Napolitano et al., 2022*).

In the **non-canonical pathway**, the substrate-recruitment to mTORC1 is regulated by the **FLCN:FNIP1/2** (folliculin:folliculin-interacting protein1/2) complex. Under nutrient-rich

conditions FLCN:FNIP1/2 dissociates from the cytoplasmic surface of lysosomes allowing the conversion from RagC/D-**GTP** into RagC/D-**GDP**. Subsequently, RagC/D-GDP recognizes TFE3 and TFEB, which are then recruited to the lysosome surface for phosphorylation by mTORC1.

AMPK is an additional nutrient and energy sensor recruited to the lysosome surface. AMPK is activated by stress-signals and starvation, which subsequently leads to repression of anabolic processes and promotion of the autophagy pathway through phosphorylation of down-stream effectors such as the transcriptional **bromodomain**-containing protein **4 (BRD4)** repressor. Other down-stream substrates of AMPK are shared with mTORC1 (e.g. TFE(B), ULK1), further emphasizing the crosstalk of diverse molecular players involved in lysosomal nutrient response (Vara-Ciruelos et al., 2019). Finally, GSK3 β is another fundamental molecular player in lysosomal nutrient sensing. GSK3 β regulates cell metabolism by activating catabolic pathways upon insulin withdrawal. GSK3 β phosphorylates and inactivates glycogen synthase, while activation of ULK1 promotes the initiation of autophagy (Ryu et al., 2021; Martínez-Fàbregas et al., 2022).

1.4 Transcriptional regulation of lysosomal function

In addition to growth control, the aforementioned kinases regulate the biogenesis, subcellular distribution, and activity of lysosomes by inhibiting or promoting nuclear localization of transcription factors. Bioinformatic approaches revealed the presence of one or multiple tandem copies of 10-base-pair E-box sequences enriched in the promoter region of genes with lysosomal-autophagy-related function, named as **Coordinated Lysosomal Enhancement And Regulation (CLEAR)** network (Sardiello et al. 2009; Palmieri et al., 2011; Settembre et al. 2013). The CLEAR-motifs can be recognized by MiT/TFE members (Palmieri et al., 2011; Martina et al., 2014; Ploper et al., 2015; Fig 1.4 A). The MiT/TFE members promote lysosomal biogenesis and autophagy by nuclear translocation under cell-stress and nutrient withdrawal. Vice-versa, at steady-state condition MiT/TFE members are found inactive in the cytoplasm (Martina et al., 2014; Puertollano et al., 2018). MiT/TFE belong to a larger **basic helix-loop-helix leucine zipper (bHLH-Zip)** transcription factors family, recognizing the same canonical E-box motif which overlap with the CLEAR-sequence site (Hemesath et al., 1994, Sardiello et al., 2009). Further studies revealed another bHLH transcription factor MYC, as repressor of lysosomal biogenesis. Particularly, under basal metabolic conditions, MYC interacts with **histone-deacetylases 2 (HDAC2)**, and the lysosomal gene-activation is inhibited allosterically

occupied the CLEAR sites on the promoters of lysosomal genes, and of TFEB/TFE3 inhibiting the lysosomal gene-activation (Annunziata et al., 2019; Fig. 1.4 B).

Furthermore, other transcription factors which do not directly bind the CLEAR-motif have been described as regulators of lysosomal biogenesis and/or autophagy. For instance, under nutrient-rich conditions, the zinc-finger transcription factor (ZKSCAN3) inhibits lysosomal biogenesis and autophagic flux by binding the promoter region of numerous lysosomal-autophagy genes through a specific KRDGGG DNA motif (Chauhan et al., 2013; Fig. 1.4 C). On the other hand, the generation of lysosomal oxygen-reactive species results in signal transducer and activator of transcription 3 (STAT3) activation, thus promoting selectively the transcription of lysosomal hydrolases without triggering autophagy genes (Martínez-Fàbregas et al., 2018; Fig. 1.4 D). Finally, BRD4 is an emerging lysosome-autophagy repressor on epigenetic level by binding acetylated histones on the promoter region of diverse lysosomal genes in normal metabolic cell conditions (Sakamaki et al., 2017; Fig. 1.4 E).

In conclusion, several activators and repressors have been identified and are required to cooperate in specific transcriptional responses to adapt to intracellular cues (amino acid levels, oxygen stress) and environmental changes.

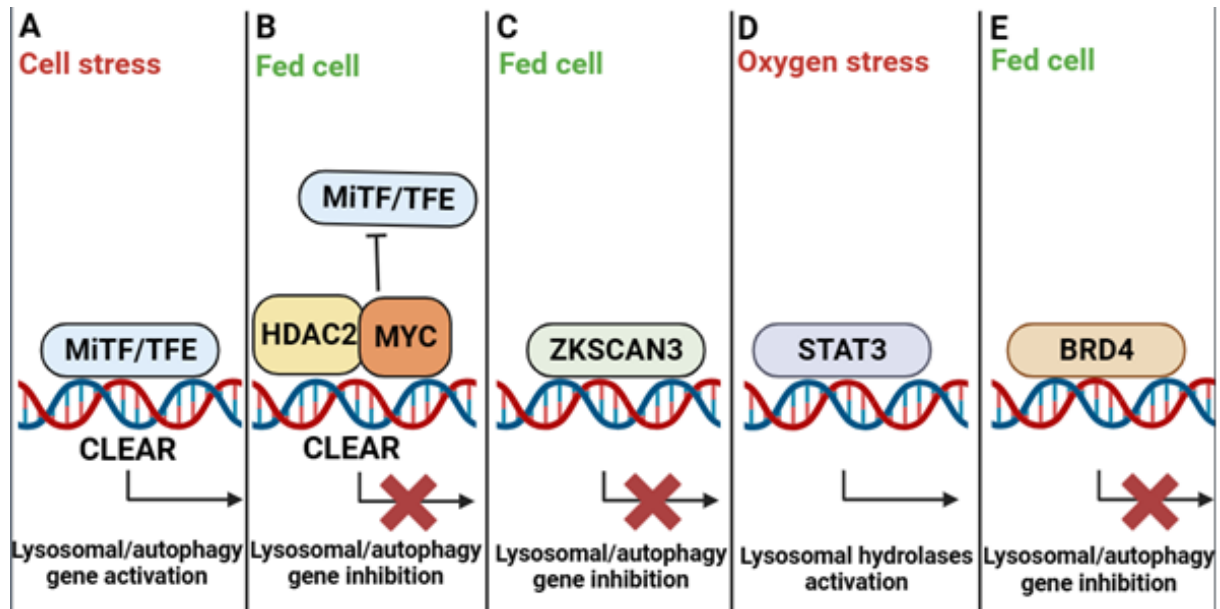


Fig. 1.4 Transcriptional regulation of lysosome biogenesis and autophagy genes - (A) MiT/TFE helix-loop-helix family members bind the CLEAR motifs in stress conditions activating lysosomal and autophagy genes. (B) CLEAR motifs are also recognized by MYC-HDAC2 complex under basal metabolic condition, which blocks CLEAR-containing target genes activation by allosteric occupation of the promoter region. (C) Activation of lysosomal biogenesis and autophagy flux is inhibited through occupation of the promoter region by ZKSCAN3 in nutrient-rich condition. (D) Oxygen stress results in nuclear translocation of STAT3 and activation of lysosomal hydrolases without triggering autophagy flux. (E) BRD4 binds acetylated histones on promoter regions of lysosomal/autophagy genes repressing their transcription under basal metabolic condition.

1.5 Transcription Factor EB (TFEB)

TFEB is the best characterized member of the MiT/TFE family, which includes also MiTF, TFE3 and TFEC. The full-length TFEB protein comprises 476 amino acids (aa). All the MiT/TFE members share the same basic helix-loop-helix motif (bHLH; comprising TFEB aa 235-288), required for DNA binding, and the leucine-zipper (LZ) dimerization domain (TFEB aa 298-319). LZ allows homo- or hetero-dimerization of TFEB with the other members of the MiT/TFE family for DNA binding. An activation domain (AD, TFEB aa 156-165) is required for upstream regulation and shared by TFEB, TFE3 and MiTF (Sato et al., 1997), but missing in TFEC (Zhao et al., 1993). TFEB was found to control the transcription of 471 CLEAR motif-containing genes involved in a plethora of diverse basic cellular processes, among them a subcategory of 73 lysosomal-autophagy genes, shown in Table 1.1 (Sardiello et al., 2009; Palmieri et al., 2011). However, the kinetics and selection of TFEB-target genes, the role of the variable number as well as the position of the CLEAR motifs in relation to the transcription start site, are poorly understood.

Table 1.1 – CLEAR motif-containing lysosome-autophagy genes^a

Category encoded proteins	Gene name
Lysosomal hydrolases and accessory proteins	<i>ASAHI, CTSA, CTSB, CTSD, CTSF, GAA, GALNS, GBA, GLA, GLB1, GNS, GUSB, HEXA, HEXB, IFI30, NAGLU, NEU1, PLBD2, PPT1, PSAP, SCPEP1, SGSH, TPP1</i>
Lysosomal membrane	<i>GLMP (Clorf85), CD63, CLCN7, CLN3, CTNS, MCOLN1, SLC36A1, LAMP1, TMEM55B</i>
Lysosomal acidification	<i>ATP6AP1, ATP6V0A1, ATP6V0B, ATP6V0C, ATP6V0D1, ATP6V0D2, ATP6V0E1, ATP6V1A, ATP6V1B2, ATP6V1C1, ATP6VID, ATP6V1E1, ATP6V1G1, ATP6V1H</i>
Non-lysosomal proteins involved in lysosomal biogenesis	<i>NAGPA, GNPTG, IGF2R, M6PR, BLOC1S1, BLOC1S3, HPS1, HPS3, HPS5, SUMF1</i>
Autophagy	<i>BECN1, GABARAP, HIF1A, NRBF2, PRKAG2, RAB7A, RRAGC, SQSTM1, STK4, UVRAG, VPS8, VPS11, VPS18, VPS26A, VPS33A, VPS35, WDR45</i>

^aPalmieri et al., 2011

Remarkably, TFEB overexpression activates the transcriptional program of i) lysosomal biogenesis by enhancing the acidification of lysosomes and degradation rate of macromolecules, ii) multiple steps in the autophagic-flux, iii) lysosomal positioning and fusion processes between lysosomes and other subcellular organelles or with the plasma membrane (lysosomal exocytosis), and iv) integrated stress response (ISR) (Martina et al., 2014; Medina et al., 2011; Settembre et al., 2011; Gambardella et al., 2020). TFEB-induced gene activation

patterns were found to be cell-type and tissue dependent, controlling e.g. the lipid metabolism in the liver, bone resorption by osteoclasts, or metabolic adaptive responses in skeletal muscles (Tan et al., 2022). Taking together, the global coordination of the major cellular catabolic pathways led to the renomination of TFEB as the master regulator of intracellular clearance and lysosomal function. Moreover, constitutive TFEB overexpression in cellular and mouse models of human diseases has been reported to promote the cellular clearance of non-degraded accumulated material in neurodegenerative diseases, and metabolic and lysosomal storage disorders (Tan et al., 2022). Despite the benefits, constitutive TFEB overexpression also has been associated with the onset and sustainment of various types of cancer, including renal cell carcinoma, non-small-cell lung carcinoma, or pancreatic ductal adenocarcinoma, emphasizing cell type-specific functions and highlighting the dual role of TFEB upon its constitutive overexpression (Bahrami et al., 2020).

1.5.1 Functional regulation of TFEB phosphorylation

The functional activity of TFEB is primarily regulated by the transcriptional control of its own expression, and its capability to recognize the promoters of target genes (Sardiello et al., 2009; Cesana et al., 2023). In addition, the transcriptional activity of TFEB requires dynamic and fine-regulated translocation mechanisms into the nucleus. Since the present thesis is focused on nuclear translocation processes of TFEB, published data will be summarized in more detail. The subcellular localization of TFEB is strictly dependent on nutrient availability where TFEB reversibly translocate between the nucleus upon cell-stress responses (e.g. starvation), and export into the cytoplasm under nutrient re-establishments (Li et al., 2018; Napolitano et al., 2018).

On the molecular level, the different subcellular localizations of TFEB are associated with posttranslational modifications (PTMs). The best investigated TFEB PTM is phosphorylation at specific serine residues mediated by different kinases. In nutrient-rich conditions, both TFEB and the mTORC1 kinase are recruited to the lysosome surface, mediated by RagC/D-GDP followed by mTORC1 activation (Sancak et al., 2010; Cui et al., 2023). The first N-terminal 30 amino acids of TFEB have been shown to be responsible for this RagC/D binding and lysosomal localization (Martina et al., 2013; Cui et al., 2023). In addition to the activation of the ribosomal S6 kinase, or inactivation the translational 4EBP1 repressor by phosphorylation (see Fig. 1.2), mTORC1 phosphorylate TFEB at serine residues S122, S142 (also phosphorylated by nutrient-responsive ERK2 kinase), and S211 (Settembre et al., 2012; Martina et al., 2012; Rocznik-Ferguson et al., 2012; Vega-Rubin de Celis et al., 2017; Fig. 1.5

A). After phosphorylation by mTORC1, TFEB dissociates from the lysosomal surface by unknown molecular mechanisms. Phosphorylation at S211 is recognized by members of YWHA/14-3-3 chaperone family that sequesters and retains TFEB inactive in the cytoplasm (Martina et al., 2012; Rocznik-Ferguson et al., 2012; Fig. 1.5 B). It has been hypothesized that 14-3-3 binding to phosphorylated S211 TFEB prevent its nuclear translocation by masking the Nuclear Localization Signal (NLS aa 235-252) (Martina et al., 2012; Rocznik-Ferguson et al., 2012). Moreover, amino acid substitution of either S142 or S211 to alanine (S142A or S211A) or the treatment of cells with the mTORC1 inhibitor torin1, leads to a constitutive TFEB nuclear localization (Settembre et al., 2011; Martina et al., 2012; Fig. 1.5 C)

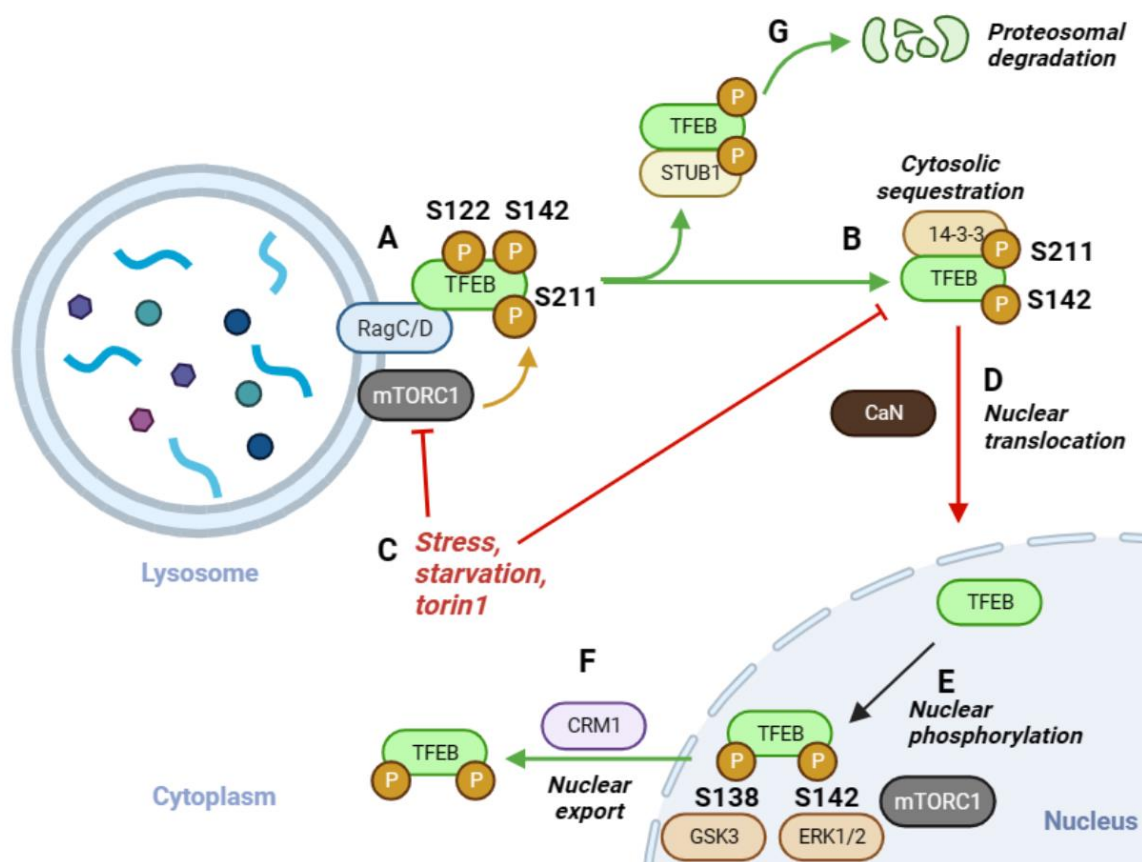


Fig. 1.5 TFEB phosphorylation regulation – (A) At steady-state (nutrient-rich) both mTORC1 and TFEB are recruited at the lysosomal surface, promoting mTORC1-mediated phosphorylation of TFEB at S122, S211 and S142. (B) Phosphorylation at S211 is recognized by 14-3-3 proteins which bind and sequester TFEB in the cytoplasm. (C) Cell stress, starvation and/or torin1 treatment lead both to mTORC1 inhibition and weakly phosphorylated TFEB. (D) Dephosphorylation by calcineurin (CaN) at S142/S211 sites, promote TFEB nuclear translocation. (E) In the nucleus, TFEB is proposed to be phosphorylated at S138 and S142 by GSK3 and ERK1/2, respectively. (F) The nuclear export is mediated by the exportin CRM1. (G) Phosphorylation at S211 is recognized by STUB1 promotes TFEB protein degradation via ubiquitin proteasome pathway (picture re-adapted from BioRender Template; Adithi Pisapati and Dr. Thomas Pulinkunnil, Dalhousie University).

Phosphorylation of TFEB prevents its nuclear import, while cell stress promotes TFEB nuclear translocation by both mTORC1 inactivation and TFEB dephosphorylation (Franco-Juárez et

al., 2022). The starvation-associated release of lysosomal Ca^{2+} by MCOLN1 (Mucolipin, TRP Cation Channel 1) leads to the activation of the phosphatase calcineurin (CaN) which subsequently dephosphorylates TFEB at S142 and S211 and promotes the nuclear translocation of TFEB (Medina et al., 2015; Fig. 1.5 D). The mechanisms how TFEB localized in the nucleus can exit the compartment is rather unclear. A nuclear export signal of TFEB (NES, aa 140-150) has been identified and the phosphorylation at S142 and S138 in the proximity of NES appear to be required for the nuclear export of TFEB under conditions of nutrient replenishment (Li et al., 2018; Napolitano et al., 2018; Fig. 1.5 E). It has been proposed that the phosphorylated S138 and S142 form a motif which is recognized by exportin-1 (CRM-1) associated with TFEB inactivation and re-localization to the cytoplasm (Fig. 1.5 F). Finally, phosphorylation at S142 and S211 is recognized under nutrient-rich conditions by E3 ubiquitin ligase (STUB1) which promotes TFEB protein degradation through ubiquitin proteasome system (Sha et al., 2017; Fig. 1.5 G). Additional structural or PTM requirements for the select degradation of phospho-S142/S211 TFEB are unknown.

1.5.2 Additional kinases involved in TFEB regulation

Recent discoveries propose upstream phosphorylation-mediated mechanisms required for TFEB localization at lysosomes, followed by mTORC1 phosphorylation and sub-sequential inactivation. Under amino acid replacement conditions, phosphorylation of TFEB at S3 by the upstream **mitogen-activated protein kinase 3 (MAP4K3)** initiates the recruitment of TFEB to lysosomes, followed by mTORC1 phosphorylation and subsequent inactivation (Hsu et al., 2018). Similarly, it was reported that TFEB can be phosphorylated at S134 and S138 by GSK3 β resulting in cytoplasmic retention through binding to 14-3-3 protein. In parallel, the phosphorylation at these sites leads to the recruitment of TFEB to lysosomes (Li et al., 2016); however, how mechanistically these two phosphorylation sites modulate TFEB lysosomal recruitment is still unknown. Finally, upon starvation, AMPK phosphorylates TFEB at multiple serine residues localized in the C-terminus such as S466, S469, and S467, which promote TFEB transcriptional activation (Paquette et al., 2021).

1.5.3 Acetylation of TFEB as novel posttranslational modification

In addition to phosphorylation, recent studies reported on the acetylation of TFEB at lysine residues with partially contradictory effects on its transcriptional activity. So far, the studies have been performed in different cell types and inhibitor treatment protocols, and provide no clear insights into the mechanisms how TFEB acetylation regulates the transcription of target

genes. Bao et al. (2016) proposed based on their data that TFEB-K116 needs to be deacetylated in the nucleus by **sirtuin-1** (SIRT-1) to promote transcriptional activation in a TFEB phosphorylation-independent manner but neither providing information on the TFEB phosphorylation status nor on its subcellular distribution. In addition, four lysine residues were found to be acetylated (K91, K103, K116 and K430) in human colon cancer (HCT116) cells upon histone deacetylase inhibitor treatment with suberoylanilide hydroxamic acid (**SAHA**) (Zhang et al., 2018). The simultaneous lysine-to-arginine substitution of K91/103/116/430R decreases both TFEB nuclear translocation and transcriptional activation in HCT116-SAHA treated cells, leading to the hypothesis that acetylation acts as a positive nuclear translocation signal for TFEB. Moreover, siRNA knockdown of the **acetyl-CoA acetyltransferase 1** (**ACAT1**) or the lysine deacetylase, HDAC1, resulted in a significant reduction and increase, respectively, in TFEB transcriptional activity (Zhang et al., 2018). The significance of the presented data is difficult to assess because of lacking various required control conditions in particular for western blotting approaches, a low number (only 4) of selected target genes regulated by TFEB on the mRNA level, and insufficient methods and conditions to evaluate the lysosome functions in dependency of the general deacetylation inhibitor SAHA.

Recent discoveries suggest that lysine acetyltransferase GCN5 (also known as KAT2), represses TFEB transcriptional activity by promoting TFEB nuclear acetylation on lysines K116, K274 and K279. The authors proposed that acetylation at both K274 and K279 disrupt TFEB dimerization required for DNA binding and gene activation (Wang et al., 2020). Li and colleagues (2022) treated HeLa cells stably expressing TFEB-EGFP with the histone deacetylase inhibitor trichostatin A (TSA) and detected TFEB-EGFP in the nucleus associated with an increased expression of lysosomal and autophagic genes (Li et al., 2022). Using mass spectrometry these authors demonstrated that TFEB is acetylated at K116, K236, K237 and K431 under TSA treatment. Moreover, the authors have reported that acetylation at K236/237 interferes with 14-3-3 binding which explains an enhanced nuclear translocation of acetylated TFEB-K236/237 (Li et al., 2022). siRNA knockdown of HDAC5 and HDAC9 promote nuclear translocation of TFEB, and *in vitro* acetylation assays reveal that TFEB is acetylated at K116, K236/K237, and K431 by the acetyltransferase elongator subunit 3 (ELP3) in an mTORC1-independent manner (Li et al., 2022). However, it has been recently demonstrated that ELP3 primarily acts as a tRNA acetyltransferase (Dauden et al., 2019) rather than mediating lysine acetylation of target proteins.

In preliminary experiments performed in collaboration of Prof. Bräulke's laboratory and the mass spectrometry expertise of Dr. Winter's group (University of Bonn), all previously

described phosphorylated serine residues and seven acetylated lysine residues, K116, K237, K256, K264, K274, K279, and K430, have been identified in the cytoplasmic fraction of TFEB-overexpressing HeLa Tet-On cells under nutrient-rich steady-state conditions. The acetylated sites at K237, K256, K264, and K274 of TFEB are located in the DNA binding domain (DBD/ bHLH-LZ) (Fig. 1.6).

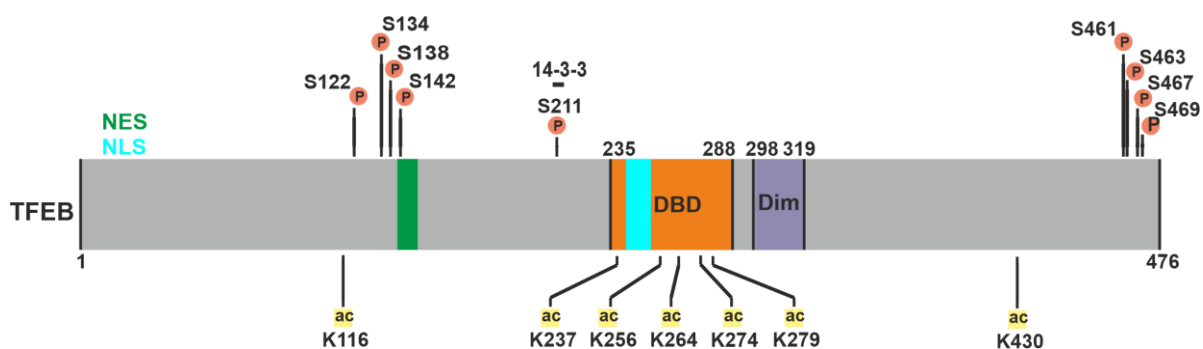


Fig. 1.6 Schematic representation of TFEB domain structures - The phosphorylated serine residues and the seven acetylated lysine residues identified via mass-spectrometry are shown with the related position. The nuclear localization-sequence (NLS, turquoise) and nuclear-export sequence (NES; green) are shown; the DNA-binding domain (DBD; orange) and the dimerization domain (Dim; violet) are indicated.

There are still many open questions on the molecular mechanism behind phosphorylation/acetylation interaction and communication on TFEB regulation. Furthermore, the stoichiometry of TFEB PTMs is completely unclear, as well as which residues are simultaneously modified and form unique subpopulations of TFEB molecules capable for i) nuclear translocation, ii) DNA-binding and transcriptional activation of select target genes, and iii) homo- or hetero-dimerization of TFEB with other members of the MiTF family, are still not elucidated.

1.6 Aim of the study

Phosphorylation and acetylation have been described to regulate the transcriptional activity of TFEB, a crucial component in the adaptation of the lysosome-autophagy pathway to changing environmental or internal cues, in various cell types and conditions. Although the biological significance of the phosphorylation sites and their modifying kinases/phosphatases have been intensively studied, the few studies on the functional impact of TFEB acetylation at various lysine residues led to contradictory conclusions.

Seven acetylated lysine residues have been previously identified by mass-spectrometry analysis (K116, K237, K256, K264, K274, K279, and K430) in TFEB expressed in HeLa cells in our group. Homology-based three-dimensional (3D) structure modelling of human TFEB dimers reveals that the acetylated residues K237, K256 and K274 appear to be directly involved in the binding of DNA. Therefore, the main focus of the present thesis was directed on these residues and the overall objective was to molecularly define how acetylation mimetic exchanges of K237, K256 and K274 to alanine (K3A) or non-acetylation mimetic substitutions by arginine (K3R) affect i) the subcellular distribution, ii) the transcriptional activity, and iii) the synthesis of soluble lysosomal enzymes as indicator of lysosomal biogenesis.

This study will address the following questions:

1. Do the acetylated (K3A) or the non-acetylated (K3R) form of TFEB support the cytoplasmic localization or the translocation into the nucleus? Are phosphorylation and acetylation of TFEB interlinked?
2. Which genes, in particular lysosomal and autophagy genes, are differentially regulated by TFEB and mutant proteins in HeLa cells depending on their inducible expression level under nutrient-rich conditions?
3. Does the induced expression of TFEB changes the soluble lysosomal proteome synthesized in 24 h in a functionally significant manner?

2. Material and Methods

2.1 Material

2.1.1 Equipment

Equipment (Model)	Company
Balances (AC100, TE2101)	Mettler Toledo, Sartorius
Block heater	Kleinfeld Labortechnik
Centrifuges (5418, 5415R)	Eppendorf
Dounce homogenizer	Wheaton
Electrophoresis chamber (Agagel Midi Wide)	Biometra
Horizontal shaker	Labotek
Imager (Chemi Doc XRS)	Bio-Rad
Incubator	Innova CO-170
Luna ^{II} Automated Cell Counter	Labtech
Microwave	Whirlpool
Mini Blot Module	Life Technologies
Mini Gel Tank	Life Technologies
Nano Drop	Thermo Scientific
pH meter (MP220)	Mettler Toledo
Photometer (Multiscan GO)	Thermo Scientific
Pipettes	Eppendorf
Pipette controller (Pipetus®)	Hirschmann
Real-time PCR Thermocycler (MxPro3000)	Agilent
Sonicator	Hielscher UP50H
Water bath	Schütt Labortechnik

2.1.2 Consumables

Consumable	Company
Amicon® Ultra-0.5 ml centrifugal filters (10 kDa cut-off)	Merk Millipore
Coverslip	Assistant
Disposable material for cell culture	BD Falcon, Sarstedt, Nunc
Disposable lab consumables	BD Falcon, Sarstedt, Nunc
Disposable scraper	Sarstedt
Dialysis membranes	Spectrum
Gel electrophoresis combs	Hoefer
Microplate 96 multiwell	Sarstedt
Nitrocellulose membrane	Amersham Protran
Nitrocellulose membrane filter (0.22 µm)	Millipore
NuPage 4-12% Bis-Tris gels	Life Technologies
Whatmann paper	Whatman GmbH

2.1.3 Chemicals

Chemical	Company
Acrylamide	Roth
Aqua-Poly/Mount®	Assistant
β-mercaptoethanol	Sigma-Aldrich
Bovine serum albumin (BSA)	Serva
DAPI	Life Technologies
Dimethylsulfoxide (DMSO)	Roth
Dithiothreitol (DTT)	Sigma
Doxycycline	Clontech
Ethanol	Merck
Isopropanol	Roth
LDL-Sample Buffer	Thermo Fisher Scientific
Milk powder non-fat dry	Roth
NNN'N'-Tetramethylethylenediamine (TEMED)	Sigma
Nonidet 40 (NP40)	Roche
PageRuler™	Thermo Fisher Sci
Paraformaldehyde (PFA)	Roth
Protease inhibitor cocktail	Sigma
PhosStop	Roche
Sodium dodecyl sulfate (SDS)	Sigma
Torin1	Tocris
Triton X-100	Sigma
jetPEI	Polyplus

2.1.4 Kits

Kit	Company
Clarity Western ECL Substrate Kit	BioRad
Roti-Quant Universal BCA-Assay	Carl Roth
High capacity cDNA Reverse Transcription kit	ThermoFischer Sci
IDT Gene Expression Assay	IDT
RNAeasy extraction kit	Qiagen
QIAschredder	Qiagen

2.1.5 Oligonucleotides (oligo)¹ for mutagenesis and sequencing

Oligo name	Oligo sequence 5' to 3'	Application
TFEB-K237A	Fw: GGCCAAGGAGCGGCAGAAAG GC AGACAATCACAACCTTAATTG Rv: CAATTAAGTTGTGATTGTCT GC CTTCTGCCGCTCCTTGGCC	SDM
TFEB-K237R	Fw: GGCCAAGGAGCGGCAGAAAG CG AGACAATCACAACCTTAATTG Rv: CAATTAAGTTGTGATTGTCT CG CTTCTGCCGCTCCTTGGCC	SDM
TFEB-K256A	Fw: GACGAAGGTTCAACATCAATGACCGCATC GCG GAGTTGGGAATGCTGATCCCCA AAG GCC Rv: GGCC TT GGGGATCAGCATTCCCAACTC CGC GATGCGGTCATTGATGTTGAACCTTCGTC	SDM
TFEB-K256R	Fw: GACGAAGGTTCAACATCAATGACCGCATC CGG GAGTTGGGAATGCTGATCCCCA AAG GCCAAT Rv: ATTGGCC TT GGGGATCAGCATTCCCAACTC CGG GATGCGGTCATTGATGTTGAACCTTCGTC	SDM
TFEB-K274A	Fw: GCCAATGACCTGGACGTGCGCTGGAAC GCG GGCACCATCCTCA AAG GCCTCTGTGGATTAC Rv: GTAATCCACAGAGGC CTT GAGGATGGTGCC CGC GTTCCAGCGCACGTCCAGGTCATTGGC	SDM
TFEB-K274R	Fw: GCCAATGACCTGGACGTGCGCTGGAAC GCG GGCACCATCCTCA AAG GCCTCTGTGGATTAC Rv: GTAATCCACAGAGGC CTT GAGGATGGTGCC CGG GTTCCAGCGCACGTCCAGGTCATTGGC	SDM
TFEB-S142A	Fw: CAACAGTGCTCCCAAT GCA CCCATGGCCATGCTGC Rv: GCAGCATGGCCATGGGT TGC ATTGGGAGCACTGTTG	SDM
TFEB-S211A	Fw: GTCACCAGCAGC GCC TGCCCTGCGG Rv: CCGCAGGGCAG GGC GCTGCTGGTGAC	SDM
IRES-M1_fw	TAGTGAACCGTCAGATCG	Sequencing
GFP_C_fw	CAAAGACCCCAACGAGAAG	Sequencing
TFEB_int_F	GAATGTGTACAGCAGCGAC	Sequencing

Fw¹: forward; rv: reverse; int F: internal forward primer; codons targeted by site-directed mutagenesis (SDM) are highlighted in bold.

2.1.6 Media and supplements for cell culture

Media and supplements	Company
Dulbecco's modified Eagle Medium (DMEM)	Thermo Fisher Sci
Fetal bovine serum (FBS)	Thermo Fisher Sci
GlutaMAX™ (100×)	Thermo Fisher Sci
Penicillin (1mg/ml), Streptomycin (1mg/ml)	Thermo Fisher Sci
PBS 10x	Thermo Fisher Sci
Opti-MEM™	Thermo Fisher Sci
Trypsin/EDTA solution (0.05%)	Thermo Fisher Sci
Earle's Balanced Salt Solution EBSS	Thermo Fisher Sci

2.1.7 Software and data processing

Software	Company
Corel Draw 2019	Corel
Endnote	Thomson Reuter
ImageJ 1.4.10	NIH
Microsoft Office	Microsoft
Quantity One-4.6.7	Bio-Rad
GraphPad Prism 10	GraphPad
Fiji	PerkinElmer
SnapGene	Snap Gene
MxPro	Stratagene

2.1.8 Online website

Online Program/Databases	Web site
NCBI Database	http://www.ncbi.nlm.nih.gov/
DAVID tool	DAVID Functional Annotation Bioinformatics Microarray Analysis (ncicrf.gov)
Venn Diagram	InteractiVenn - Interactive Venn Diagrams

2.2 Cell Culture methods

HeLa Tet-On 3G (HeLa TO) cells were purchased from Takara. HeLa TO cells were cultured in Dulbecco's Modified Eagle's Medium (DMEM) supplemented with 10% fetal bovine serum (FBS), GlutaMAX and 1% penicillin/streptomycin (P/S). The cells were transiently transfected with pTRE3G-IRES-MSC1-EGFP-TFEB-wild-type (wt) or TFEB mutants (table 2.2.1) using jetPEI® kit according to the manufacture's protocol. The day after, GFP-TFEB-wt and mutants were induced with 1 µg/mL doxycycline for 24h or 3h.

HeLa TO stable expressing GFP-TFEB-wt, -K3A and -K3R were previously generated and validated in Prof. Thomas Bräulke's laboratory.

Table 2.2.1 – Plasmid constructs used for transient transfection of HeLa TO cells

Plasmid	Name of the construct
pTRE3G-IRES-M1-eGFP-TFEB-wt	TFEB wild type
pTRE3G-IRES-M1-eGFP-TFEB-K3A	K237/256/274A
pTRE3G-IRES-M1-eGFP-TFEB-K274A	K274A
pTRE3G-IRES-M1-eGFP-TFEB-S142/211A	S142/211A
pTRE3G-IRES-M1-eGFP-TFEB-K3A+S142/211A	K237/256/274A+ S142/211A
pTRE3G-IRES-M1-eGFP-TFEB-K274A+S142/211A	K274A+S142/211A

2.3 Biochemical methods

2.3.1 Total cell extraction

After removing the medium and washing the cells two times with cold 10 mM PBS, cold lysis buffer A (50mM Tris/HCl pH 7.4, 150mM NaCl, 1% TX-100, 1% Protease Inhibitor Cocktail, 1% Phosphatase Inhibitor) was added directly to the cells (500µL for 60mm or 800µL for 100mm dishes). The cells were scraped and the lysate was transferred to a 1.5mL Eppendorf tube and incubated in the cold room under rotation. After 30 min, the samples were centrifuged at 15.000g for 15 min at 4°C. The supernatant was moved to a new Eppendorf tube and the protein concentration of cell lysates was quantified using a BCA assay Kit, following the manufacturer's instruction for the plate format.

2.3.2 Preparation of nuclear and Postnuclear Supernatant (PNS)/cytoplasmic fractions

Cells were resuspended in 500µL lysis buffer B (10 mM Tris/HCl pH 7.4, 0.3% NP-40, protease and phosphatase inhibitors), and homogenized with 25 strokes in a 1mL Dounce homogenizer, followed by centrifugation at 1.000g for 5 min at 4°C. The postnuclear supernatant was collected representing the cytoplasmic (cyt) fraction. The nuclear (nuc) pellet was washed with lysis buffer B, wash buffer A (10mM Tris/HCl pH 7.4, 1% Protease Inhibitor

Cocktail, 1% Phosphatase Inhibitor) and resuspended in the same volume as the cytoplasmic fraction in lysis buffer B. The cytoplasmic and nuclear fractions were sonicated three times for 5s (100% amplitude per cycle, 30 sec interval between steps) and incubated for 30 min under rotation at 4°C. After centrifugation at 15.000g for 15 min, cyt and nuc supernatants were collected and equal volumes were analysed by western blotting.

2.3.3 Secretome analysis

To analyze the newly synthesized lysosomal enzymes in dependency of TFEB, HeLa TO cells stable expressing TFEB-wt and -K3R were induced with doxycycline for 24h in serum-free Opti-MEM supplemented with 10mM NH₄Cl. As control HeLa Tet-On 3G cells were used. Conditioned media were collected, and centrifuged at 800g for 5 min at 4°C to remove cell debris. Afterwards, the media were dialyzed using Spectra/Por®3 Dialysis Membrane (Spectrum, MWCO: 3.5 kDa) overnight against 10mM PBS and analyzed by MS in collaboration with D. Winter (University of Bonn).

2.3.4 Western blotting

For western blotting analysis of media 24h serum-free conditioned media (OptiMEM) were collected and 10-fold concentrated using Amicon Ultra-0.5mL centrifugal filters (10kDa cut-off). Aliquots of extracts from cells and media were solubilized in reducing SDS sample buffer (125mM Tris/HCl pH 6.8, 1% SDS, 10% glycerin, 10mM DTT, 0.1mM β -mercaptoethanol, Coomassie® Blue R) for 5 min at 95°C or LDS sample buffer supplemented with 400mM DTT for 10 min at 70°C, separated by SDS-PAGE NuPage 4-12% Bis-Tris (Fig. 4.2-4.5) or 10% acrylamide self-made SDS gels (Fig. 4.6-7 and Fig. 4.17) and transferred onto nitrocellulose membranes with transfer buffer (1M Tris-HCl pH 8.7, 192mM glycine, 20% methanol). The membranes were blocked 25mM Tris/HCl pH 7.4, 150mM NaCl (TBS) containing 0.5% Tween and 5% non-fat milk powder or 5% BSA, and then incubated overnight with the primary antibodies listed in Table 2.3.1.

Table 2.3.1 – Primary antibodies

Primary antibodies	Species	Dilution (WB)	Company/Reference
GFP	rabbit	1:1,000	Life Technologies/A11122
TFEB p-S138	rabbit	1:15,000	Gift of A. Ballabio (Napolitano et al., 2018)
TFEB p-S142	rabbit	1:1,000	Millipore/3602264
TFEB p-S211	rabbit	1:1,000	Cell signalling/37681
GPNMB (E4D7P)	rabbit	1:1,000	Cell signalling/ 38313S
Histone H4 (L64C1)	mouse	1:1,000	Cell signalling/2935
TFEB	rabbit	1:1,000	Cell signalling/4240
α -tubulin	mouse	1:2,000	Sigma/T9026
GAPDH	mouse	1:2,000	Santa Cruz Biotech/sc25778
LaminA	mouse	1:1,000	Merck Millipore/MAB3540
pGRN	mouse	1:1,000	R&D/AF2557
PSAP	sheep	1:1,000	Abcam/64466
CTSB	goat	1:1,000	R&D/ AF953
CTSD	rabbit	1:1,000	Calbiochem/ IM16
GBA	mouse	1:1,000	R&D/MAB7410

After three washes with TBST, the membrane was incubated with secondary horseradish peroxidase (HRP)-coupled antibodies in 5% non-fat milk powder or 5% BSA (Table 2.3.2) for 1 h at room temperature at a dilution of 1:5,000. Immunoreactive proteins were detected by enhanced ECL solution kit and imaging in a Chemidoc Imaging system. Densitometric analyses of the immunoblots were performed using ImageJ software (NIH) and normalized to loading controls.

Table 2.3.2 – Secondary antibodies

Secondary antibodies (HRP)	Dilution	Company/Reference
anti-rabbit IgG	1:5,000	Biozol/JIM-111-035-003
anti-mouse IgG	1:5,000	Jackson/115-035-003
anti-goat IgG	1:5,000	Biozol, JIM-305-035-003

2.3.5 Enzyme activity measurements

The activities of lysosomal enzymes were measured in both cell extracts (see 2.3.1) and conditioned media. All the fluorometric assays were performed in 96 well plates. All enzyme substrates (Table 2.3.3) were diluted in 2x substrate buffer (200mM Na-citrate pH 4.6, 0.2% Triton X-100 and 0.4% BSA). 2µg of total protein extract and 10µl of concentrated medium were adjusted to a volume of 15µl with water. 15µL of reaction buffer was added to reach 30µL as the final total volume. As blank samples, 15µl of lysis buffer A or Opti-MEM were used. For β-hexosaminidase activity, the reaction set was incubated at 37 °C for 30 min. For β-galactosidase, α-mannosidase, and α-fucosidase activity measurements, the reaction samples were incubated at 37 °C for 18h. The enzyme reactions were stopped by the addition of 140µl of stop buffer (0.4M glycine/NaOH, pH 10.4). The absorption was then measured at 405 nm using a photometer.

Table 2.3.3 – Enzyme substrate

Enzyme substrates	Enzyme activity	Company
4-Nitrophenyl-N-acetyl-β-D-glucosaminide	β-hexosaminidase	Sigma
4-Nitrophenyl-α-D-mannopyranoside	α-mannosidase	Sigma
4-Nitrophenyl-β-D-galactopyranoside	β-galactosidase	Sigma
4-Nitrophenyl-α-L-fucopyranoside	α-fucosidase	Sigma

The activity (A) was calculated according to the following equation:

$$\text{Activity} = \frac{\Delta E_{405} / \text{min} * V_m}{\epsilon * d * V_p}$$

A = enzyme activity [U; 1 U = 1 µmol/min]

ΔE/min = change in absorbance per minutes

ε = extinction or absorbance coefficient [for 4-nitrophenol 18.45 /µmol*cm;]

VP = sample volume during the reaction [15 µl]

VM = measured volume [170 µl]

d = layer thickness of the solution [1 cm]

2.4 Molecular biology methods

2.4.1 Quantitative real-time PCR

RNAs were isolated from cultured cells using the RNeasy extraction kit and measured with Nanodrop. 1µg of total RNA was reversed transcribed using High-Capacity cDNA Reverse Transcription Kit according to the manufacturer's instruction. Quantitative real-time PCR was performed with Mx3000/Mx3005P Real-Time PCR system with PrimeTime Gene Expression Master Mix using pre-designed forward and reverse primers (Table 2.4.1) in triplicates. The

relative mRNA expression levels of analysed genes were normalized to the *ACTB* mRNA in the same cDNA sample using the comparative CT method ($2^{-\Delta\Delta T}$).

Table 2.4.1 - RT-PCR primers

Target gene	Company	Product number
ACP5	Integrated DNA Technologies	Hs.PT.56a.38600579.g
ACTB	Integrated DNA Technologies	Hs.PT.39a.22214847
ASAH1	Integrated DNA Technologies	Hs.PT.56a.2283675
ATP6V0D2	Integrated DNA Technologies	Hs.PT.58.1072618
CTSB	Integrated DNA Technologies	Hs.PT.58.1907042
CTSD	Integrated DNA Technologies	Hs.PT.58.27568031
CTSS	Integrated DNA Technologies	Hs.PT.58.3625679
GPNMB	Integrated DNA Technologies	Hs.PT.58.5010635
NEU4	Integrated DNA Technologies	Hs.PT.58.40899979
PSAP	Integrated DNA Technologies	Hs.PT.58.744083
RILP	Integrated DNA Technologies	Hs.PT.58.22883761
RRAGD	Integrated DNA Technologies	Hs.PT.58.27161067
SQSTM1 / p62	Integrated DNA Technologies	Hs.PT.58.39829257
TFEB	Integrated DNA Technologies	Hs.PT.58.22483241
TFEC	Integrated DNA Technologies	Hs.PT.58.26872107
USP2	Integrated DNA Technologies	Hs.PT.58.28252823
WIPI1	Integrated DNA Technologies	Hs.PT.58.27403765
CTSK	TaqMan	Hs00166156_m1
GRN	TaqMan	Hs00963707_g1

2.4.2 Transcriptome

Total RNA of triplet replicates were isolated from control and stably expressing GFP-TFEB HeLa TO cells using QIAshredder and RNeasy extraction kit according to the manufacturer's instruction. RNA amount was measured with Nanodrop, and the samples were analyzed by RNA sequencing in collaboration with N. Fischer (UKE/Leibniz-Institut für Virologie, Hamburg).

Normalization and differential expression analyses were carried out with DESeq2, thereby defining differentially expressed genes (DEGs) if a fold change ≥ 1.5 and adjusted P-value ($p\text{-value}_{adj} \leq 0.05$) was detected.

2.4.3 Site-directed mutagenesis

Single or simultaneous amino acid substitutions at Lys237, Lys256 and Lys274 by arginine (R) or alanine (A) were introduced by site-directed mutagenesis generating the GFP-TFEB-K3R or -K3A mutants, respectively. In addition, the phosphorylation sites Ser142 and Ser211 were single or double mutated to alanine (TFEB-S142/211A) into the wt or mutant GFP-TFEB-K274A and K3A constructs. Oligonucleotides used for cloning, mutagenesis and sequencing were synthesized by Eurofins Genomics (Table 2.4.2). All the plasmids were sent for sequencing to SEQLAB, Göttingen.

2.4.2 Oligonucleotides (oligo)¹ for mutagenesis and sequencing

Oligo name	Oligo sequence 5' to 3'	Application
TFEB-K237A	Fw: GGCCAAGGAGCGGCAGAAG GC AGACAATCACAACCTTAATTG Rv: CAATTAAGTTGTGATTGTCT GC CTTCTGCCGCTCCTTGGCC	SDM
TFEB-K237R	Fw: GGCCAAGGAGCGGCAGAAG CG AGACAATCACAACCTTAATTG Rv: CAATTAAGTTGTGATTGTCT CG CTTCTGCCGCTCCTTGGCC	SDM
TFEB-K256A	Fw: GACGAAGGTTCAACATCAATGACCGCATC CGCG GAGTTGGGAATGCTGATCCCCA AG GCC Rv: GGC CTT GGGGATCAGCATTCCCAACTC CGCG GATGCGGTCATTGATGTTGAACCTTCGTC	SDM
TFEB-K256R	Fw: GACGAAGGTTCAACATCAATGACCGCATC CGGG GAGTTGGGAATGCTGATCCCCA AG GCCAAT Rv: ATTGGC CTT GGGGATCAGCATTCCCAACTC CGCG GATGCGGTCATTGATGTTGAACCTTCGTC	SDM
TFEB-K274A	Fw: GCCAATGACCTGGACGTGCGCTGGAAC CGCG GGCACCATCCTCA AGG CCTCTGTGGATTAC Rv: GTAATCCACAGAGGC CTT GAGGATGGTGCC CGCG GTTCCAGCGCACGTCCAGGTCATTGGC	SDM
TFEB-K274R	Fw: GCCAATGACCTGGACGTGCGCTGGAAC CGGG GCACCATCCTCA AGG CCTCTGTGGATTAC Rv: GTAATCCACAGAGGC CTT GAGGATGGTGCC CGCG GTTCCAGCGCACGTCCAGGTCATTGGC	SDM
TFEB-S142A	Fw: CAACAGTGCTCCCAAT GC ACCCATGGCCATGCTGC Rv: GCAGCATGGCCATGGGT GC ATTGGGAGCACTGTTG	SDM
TFEB-S211A	Fw: GTCACCAGCAGC GCCT GCCCTGCGG Rv: CCGCAGGGCAG GGCG CTGCTGGTGAC	SDM
IRES-M1_fw	TAGTGAACCGTCAGATCG	Sequencing
GFP_C_fw	CAAAGACCCCAACGAGAAG	Sequencing
TFEB_int_F	GAATGTGTACAGCAGCGAC	Sequencing

Fw¹: forward; rv: reverse; int F: internal forward primer; codons targeted by site-directed mutagenesis (SDM) are highlighted in bold.

2.5 Confocal laser scanning microscopy

Cells grown on 12 mm cover slips were washed twice with PBS followed by fixation with 4% paraformaldehyde (PFA) diluted in PBS for 20 min at RT. After fixation, cells were washed twice with quenching solution (50mM NH₄Cl in PBS), incubated with quenching solution for 5 min, washed with PBS and permeabilized with 0.1% Triton X-100 in blocking solution (3%

BSA in PBS) for 10 min at room temperature. The cells were blocked for 1h with blocking solution at room temperature followed by incubation with TFEB antibody (1:50) in blocking solution over night at 4°C. The next day the cells were washed with PBS and incubated with Alexa647 secondary antibody (1:500 abcam) in blocking solution for 2h followed by washing with PBS. Nuclei were stained with 2.5 µg/mL DAPI diluted in PBS for 10 min, washed with PBS, and the coverslips were sealed in mounting medium Aqua-Poly/Mount. Images were taken with a Leica TCS SP8 digital scanning confocal microscope (Leica DMI 6000; 63 X magnification).

2.6 Statistical analysis

GraphPad was used to perform the statistical analysis of the data. Statistical analysis was performed using unpaired two-tailed Student's t tests. Asterisks indicate statistically significant differences * p -value < 0.05; ** p -value < 0.01; *** p -value < 0.001

3. Results

3.1 Subcellular distribution of GFP-TFEB and mutants

To investigate the biological significance of selected K237, K256 and K274 lysine residues localized in the DNA-binding domain, we substitute through site-directed-mutagenesis (SDM) procedure the aforementioned lysines to alanine (A) or arginine (R). The simultaneous K-to-A replacement (TFEB-K3A) mimics the neutral charges of acetylated TFEB at these sites, given by the replacement of a charged amino acid (+1) to an uncharged one (0). On the other hand, the simultaneous K-to-R replacement (TFEB-K3R), mimics a de-acetylated TFEB, due to the introduction of a positively charged amino acid (+1; Fig. 3.1 A). To gain insight into the structural environment of acetylated lysine residues *in silico*, homology-based three-dimensional (3D) structure modelling of human TFEB dimer based on the 76% sequence identity to the mouse MiTF/CLEAR box structure that was previously performed (PDB: 6G1L; Möller et al., 2019). Thereby, these mimetic mutations affect the electrostatic surface of the TFEB-DNA binding pocket (Fig. 3.1 B).

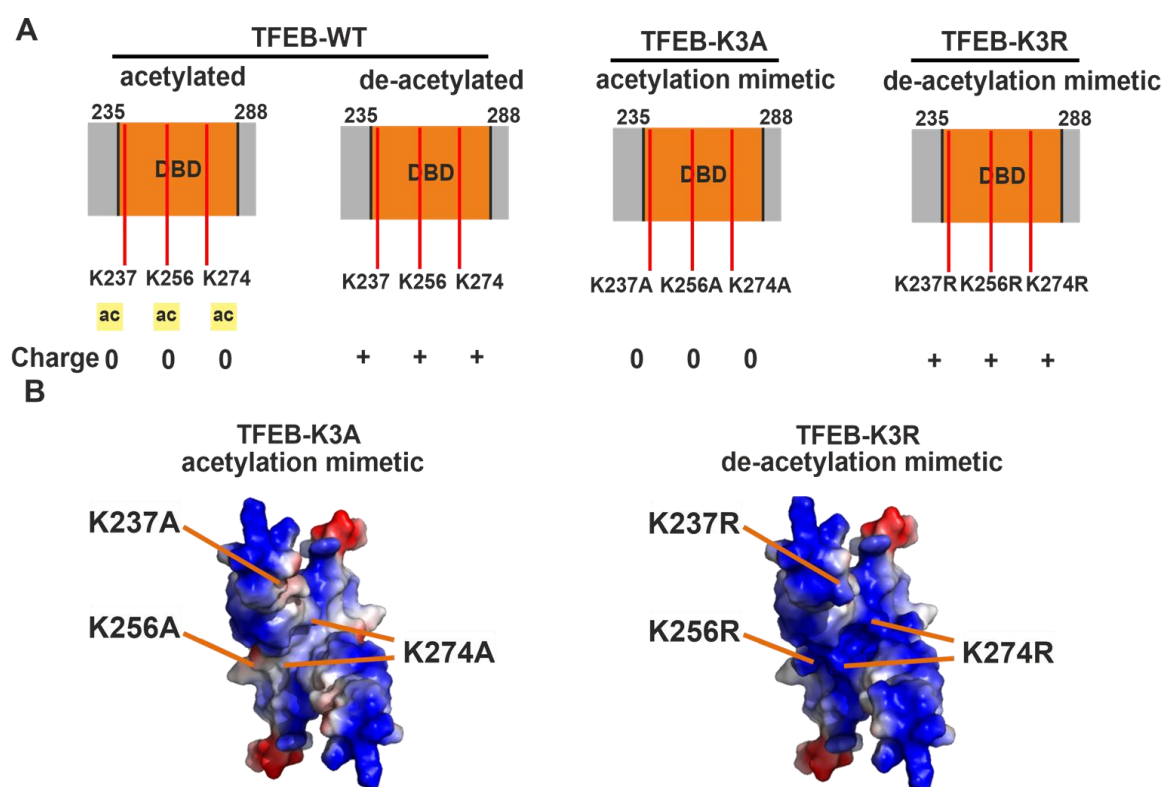


Fig. 3.1 GFP-TFEB is acetylated in the DNA binding domain at K237, K256 and K274 residues - (A) Schematic presentation of acetylated lysine residues K237, K256 and K274 in the DNA binding domain (DBD) and charge effects in the K-to-A acetylation mimetic TFEB K3A and K-to-R de-acetylation mimetic K3R mutants. (B) Surface electrostatic charges (positive: blue / negative: red / neutral: white) of TFEB-K3A and -K3R DNA-binding pockets. The selected lysine residues are indicated.

To examine the biological significance of the acetylated lysine residues K237, K256 and K274, we generated triple mutants of wild-type (wt) GFP-TFEB substituting these residues by alanine (K3A) or arginine (K3R), and selected stably, low and uniform expressing HeLa 3G TO cell clones. Since the acetylated residues were found only in the cytoplasmic fraction of TFEB, we investigated the nuclear/cytoplasm distribution of GFP-TFEB-wt and the mutants in both steady-state conditions and under treatment with the mTORC1 inhibitor torin1. The endogenous TFEB in HeLa 3G TO cells was used as control in both approaches. Thus, GFP-TFEB-wt, -K3A and -K3R expression was induced for 24h with 1 μ g/mL doxycycline. For torin1 treatment, 90 min before the end of the 24h of induction-time, cells were starved in EBSS medium for 30 min, followed by the addition of 250nM torin1 for 1h in EBSS. Afterwards, two different approaches were performed: the distribution of GFP-TFEB-wt and the mutants was analysed either by TFEB confocal immunofluorescence microscopy, or after subcellular fractionation into the nucleus fraction (nuc) and the post nuclear-supernatant (here referred as “cyt”). Afterwards, the nuc and the cyt-fractions were analysed by western blotting. Both immunofluorescence microscopy and western blot analysis revealed the majority (75%) of GFP-TFEB-wt molecules in the cytoplasm and 25% in the nuclear fraction at steady-state condition. Upon selective mTORC1 inhibitor torin1 treatment, nuclear localization of GFP-TFEB-wt increased 3-fold (Fig. 3.2 C and G), resembling the expected distribution profile of endogenous TFEB (Fig. 3.2 B and F). On the other hand, the -K3R mutant shows a comparable distribution pattern in immunofluorescence microscopy analysis at steady-state (60% cytoplasm and 40% nuclear), and a torin1-dependent translocation into the nucleus of 60% of total TFEB-K3R (Fig. 3.2 I). The failure to detect an effect of torin1 treatment on the nuclear translocation of GFP-TFEB-K3R (Fig. 3.2 E) is presently unclear. In GFP-TFEB-K3A expressing cells a high cytoplasmic localization was observed (>85%) which is resistant to torin1 treatment (Fig. 3.2 D and H). Together, these data suggest that the acetylation-mimicking K3A mutant lost the capability to translocate into the nucleus in an mTORC1-independent manner.

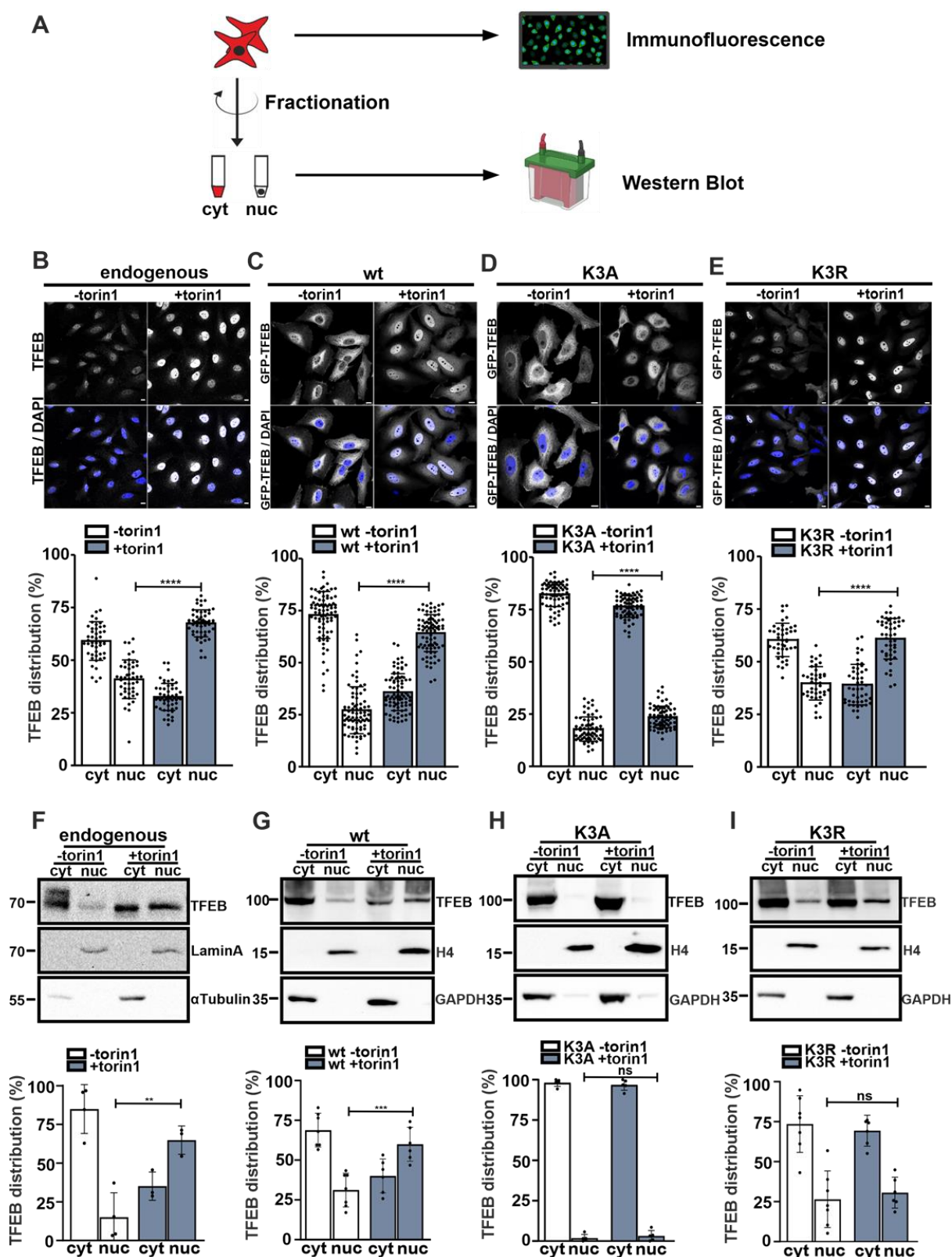


Fig. 3.2 mTORC1-independent cytoplasmic retention of acetylation mimetic TFEB K3A mutant - (A) Schematic experimental protocol to determine the nuclear and cytoplasmic distribution of TFEB by subcellular fractionation and immunofluorescence confocal microscopy. The expression of wt, -K3A and -K3R was induced by doxycycline (1 μ g/mL) in stable HeLa clones for 24h in nutrient-rich medium or treated with torin1 (250nM) for 60 min in starvation medium. Endogenous TFEB in HeLa cells was used as a control. (B, C, D, E) Nuclear and cytoplasmic localization of endogenous TFEB, GFP-TFEB and mutants analysed by IF microscopy using TFEB staining (white false color) and nuclei marker DAPI (blue). TFEB signal alone (white false color) or merged with DAPI signal (grey and blue) are displayed, scale bars: 10 μ m. Quantification of GFP-TFEB puncta in the is

shown beneath each condition (n=2-3). (F, G, H, I) Subcellular fractionation of endogenous TFEB and GFP-TFEB-wt, and mutants 24 h after doxycycline induction without or with torin1 treatment monitored by immunoblotting. The positions of molecular mass marker proteins are indicated. LaminA, H4, α Tubulin, and GAPDH were used as marker for nuclear and cytoplasmic localization, respectively. The respective blots were quantified and normalized against LaminA/H4 or α Tubulin/GAPDH, n = 5-6 experiments. (Values are mean \pm SD).

3.1.1 Transient transfection of the single K274 acetylation mimetic-mutation decrease TFEB nuclear translocation in steady-state condition

Since the simultaneous K-to-A acetylation mimetic mutation of TFEB-K3A determinate its cytoplasmic retention, we wondered whether or not the single K237A, K256A and K274A substitution alone retain TFEB in the cytoplasm. Thus, GFP-TFEB-wt and the single GFP-TFEB-K237A, -K256A and -K274A mutants were transiently expressed in HeLa TO cell and TFEB expression induced with doxycycline (1 μ g/mL) for 24h. Subsequently the localization of the different GFP-TFEB forms was analysed by immunofluorescence microscopy (Fig. 3.3 A). Transient overexpression of GFP-TFEB-wt resulted in a high nuclear localization (75%). The single exchange mutants TFEB-K237A and -K256 led to a slightly reduced nuclear localization level of 59 and 62%, respectively. In contrast, 28% of the single substituted -K274A mutant was translocated into the nucleus only suggesting a main role of acetylated K274 in cytoplasmic retention of TFEB. To confirm these data, subcellular fractionation experiments were performed with HeLa TO cells transiently expressing GFP-TFEB-wt, K274A, the double -K237/274A (K2A) mutant, and the triple -K237/256/274A mutant (K3A) mutant. The representative western blot of the subcellular fractionation experiment is shown in Fig. 3.3 B. Densitometric quantification revealed about 30% GFP-TFEB-wt, but ~70% of the -K274A mutant in the cytoplasmic fraction, supporting the immunofluorescence data. For both double -K237/274A and -K3A mutants about 90% were detected in the cytoplasmic fraction. Taking together, the single exchange at -K274A is sufficient to retain the majority of overexpressed TFEB in the cytoplasm retention. The double exchange mutant -K237/274A reaches a similar retention level as K3A.

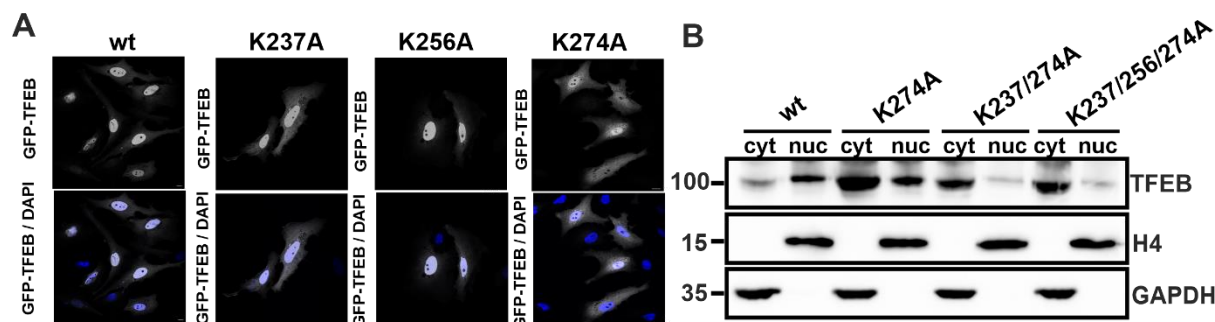


Fig. 3.3 Single exchange mutant K274A decreases strongly the nuclear translocation of TFEB – (A) HeLa TO were transiently transfected with GFP-TFEB-wt and the single exchange mutants -K237A, -K256A, and -K274A cDNAs followed by doxycycline induction for 24h. GFP (white) and DAPI (blue) stainings, scale bar: 10µm. Mean of each 30 transfected cells were used for quantification (B) HeLa TO were transfected with the indicated expression constructs, induced by doxycycline for 24 h, and subcellular fractionation. Aliquots of nuclear and cytoplasmic fractions were analysed by western blotting. TFEB expression was normalized to H4 or GAPDH immunoreactive bands, respectively (n=1).

3.1.2 TFEB-acetylation mimetic mutation affect the phosphorylation at S142 and S211

To evaluate whether the lysine-to-alanine mutation of TFEB K3A affect the phosphorylation of TFEB at S142 and S211 in cytoplasmic and nuclear fractions, specific phospho-antibodies recognizing phospho-S142 and phospho-S211 residues of TFEB were used. The double serine-to-alanine TFEB mutant S142/S211A served as control. About 62% of transiently expressed GFP-TFEB-wt are localized in the nuclear fraction of which 53% and 20% are phosphorylated at S142 and S211, respectively (lane 1 and 2, Fig. 3.4 A and B). In contrast, 18% of the TFEB-K3A mutant was found in the nucleus but lacking phosphorylated S142 and S211 residues (lane 3 and 4, Fig. 3.4 A and B). The simultaneous exchange of S142 and S211 by alanine (S142/211A) leads to the fast nuclear translocation of TFEB into the nucleus (lane 5 and 6, Fig. 3.4 A). Surprisingly, the introduction of S142/211A into the TFEB K3A mutant was not sufficient to abolish the cytoplasmic retention effect of K3A (lane 7 and 8, Fig. 3.4 A and B). Quantification of the phospho-S142 and S211 blots in relation to the TFEB protein immunoreactivity suggest that the phosphorylation of S211 is impaired by the K3A mutation, in particular in the cytoplasm, whereas the pS142/TFEB ratio is not changed (Table S1). The single exchange mutant TFEB-K274A affects the phosphorylation status of both S142 and S211 (lane 5 and 6, Fig. 3.4 B).

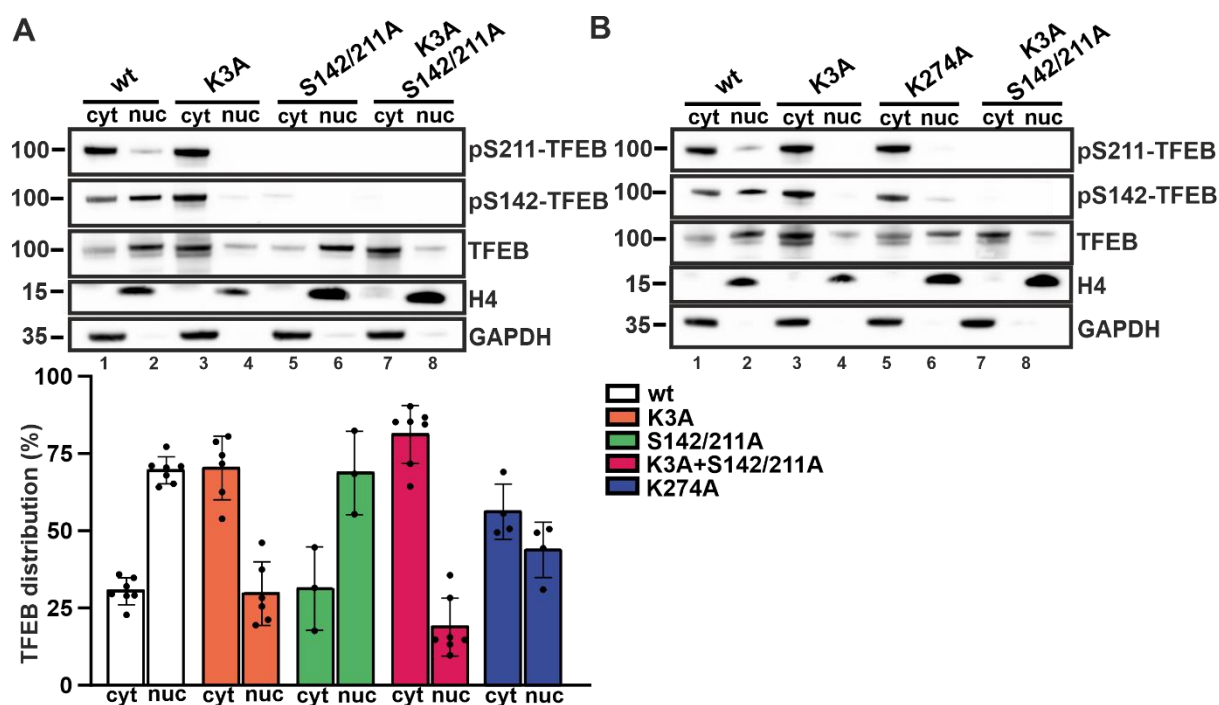


Fig. 3.4 Both single -K274A and combined -K237/256/274A acetylation mimetic mutation increase TFEB cytoplasmic phosphorylation at S142 and S211 – (A+B) HeLa TO were transfected with GFP-TFEB-wt, -K3A, -S142/211A, and -K3A+S142/211A. GFP-TFEB expression was induced for 24h by 1 μ g/mL dox, followed by subcellular fractionation. Nuclear and cytoplasmic fractions were analysed by western blot against TFEB and specific phosphorylated TFEB S142 and S211 forms. H4 and GAPDH were used as loading control for nuclear and cytoplasmic fractions, respectively. The positions of protein molecular mass in kDa are displayed. In the lower panel the normalized TFEB cytoplasmic (against GAPDH) and the nuclear (against H4) expression and distribution is shown (n=3).

Since the single and triple exchange mutants -K274A and -K3A affect the mTORC1-mediated phosphorylation of TFEB at S142 and S211, the phosphorylation of S138 analyzed.

Densitometric evaluation of the blot reveals phosphorylation at S138 in the cytoplasmic fraction of both -K3A (87%) and -K274A (81%) compared to the -wt (29%). In conclusion, the acetylation mimetic mutation at K274A or in the triple mutant K237/256/274A increased the cytosolic phosphorylation of TFEB at S138 (Fig. 3.5).

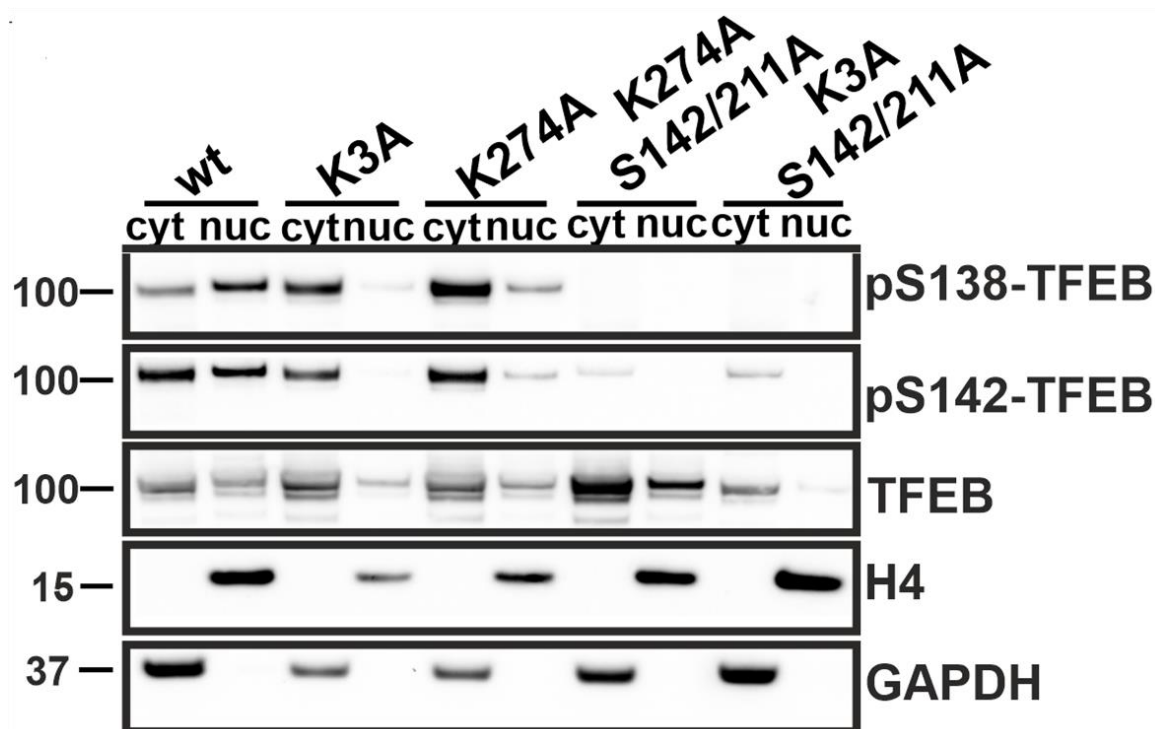


Fig.

3.5 -K274A and -K3A mutations affect S138 phosphorylation in cytoplasmic fractions - HeLa TO cells expressing GFP-TFEB-wt, -K3A, -K274A, -K274A+S142/211A, and -K3A+S142/211A upon doxycycline induction were processed for subcellular fractionation into cytoplasmic (cyt) and nuclear (nuc) fractions, and western blotting. Equal amounts of subcellular fractions were loaded.

3.2 Differential gene expression analysis of induced wild-type and TFEB K3R

To analyse the transcriptional activity of wild-type (wt) and mutant GFP-TFEB-K3R HeLa TO cells in response to doxycycline-induced expression two experimental protocols were used based on the protein expression of TFEB. The expression of TFEB was induced with 1 μ g/ml for 3h, and either harvest (chase 0h), or chased the cells in the absence of dox for various time periods (Fig. 3.6 A). Densitometric evaluation of the western blots under the tested conditions revealed a maximum GFP-TFEB protein concentration after 21h of chase (4.7-fold increase compared to GFP-TFEB synthesized during 3h dox-induction; Fig. 3.6 B). The GFP-TFEB protein expression after 24h continuous dox-induction, the most frequently used condition in literature, was almost similar as the GFP-TFEB protein level in the 3h dox/21h chase condition (Fig. 3.6 C). When the relative TFEB protein level after 3h dox \pm 21h chase in dox-free medium and 24h continuous dox induction were compared with the respective mRNA level of TFEB under identical conditions, the real-time PCR analysis showed that the transcript level of GFP-TFEB was 3.1-fold higher after 24h dox induction in comparison with the 3h dox induction period. During the following 21h chase period the GFP-TFEB transcript level decreased by 44% (Fig. 3.6 D).

In conclusion, TFEB transcripts generated during 3h dox induction require about 21h to be translated into the TFEB protein. Extended dox-induction periods for 24h resulted in a 3-fold higher mRNA level than after 3h dox induction whereas the TFEB protein was similar. These data suggest 21h chase lead to the same protein level as continuously induced 24h, in a physiological way without activating continuously in loop TFEB-gene transcription.

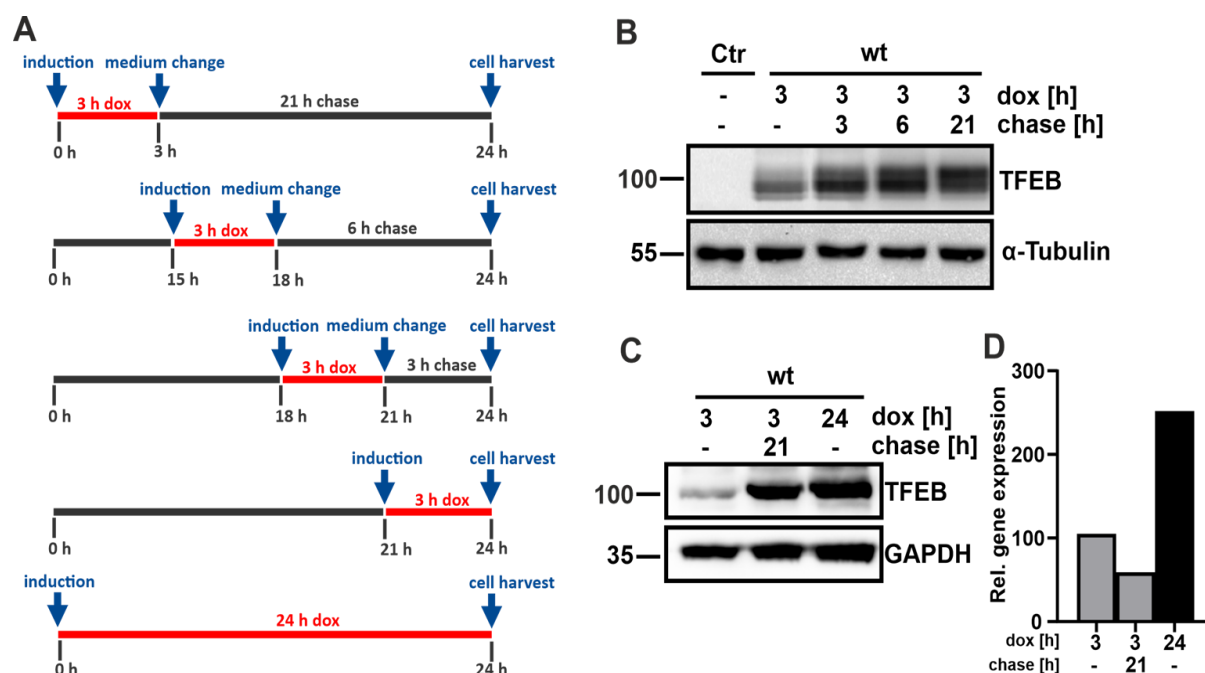


Fig. 3.6 Optimization of dox-induced TFEB-GFP expression in HeLa TO cells - (A) Experimental protocol of doxycycline (dox; 1 µg/ml) induced TFEB expression ± chase in the absence of dox in HeLa Tet-on cells. (B) HeLa TO cells stably expressing GFP-TFEB-wt were induced with dox for 3 h and either harvested or chased in dox-free medium for the indicated time periods. Non-transfected HeLa TO cells were used as control (Ctr). Cell extracts were analysed by western blotting. α-tubulin was used for equal loading. (C) TFEB western blot for direct comparison between the three dox-induction protocols. GAPDH was used as loading control. (D) The relative mRNA level of TFEB was determined in HeLa TO cells induced with dox under identical conditions as in (C) by real-time PCR. The values are calculated as fold change by setting the endogenous TFEB transcript level as 1.

Next, to investigate the stability of the GFP-TFEB protein, after 3h dox induction of TFEB, the dox-free time of chase was prolonged up to 45h (Fig. 3.7 A and B). The densitometric evaluation of the blot reveals after 45h dox-free chase a reduction of the GFP-TFEB protein level to 36% of the TFEB amounts under the 3h dox + 21h chase condition. From these data it can be concluded that the half-life of GFP-TFEB in HeLa cells is about 19-20h.

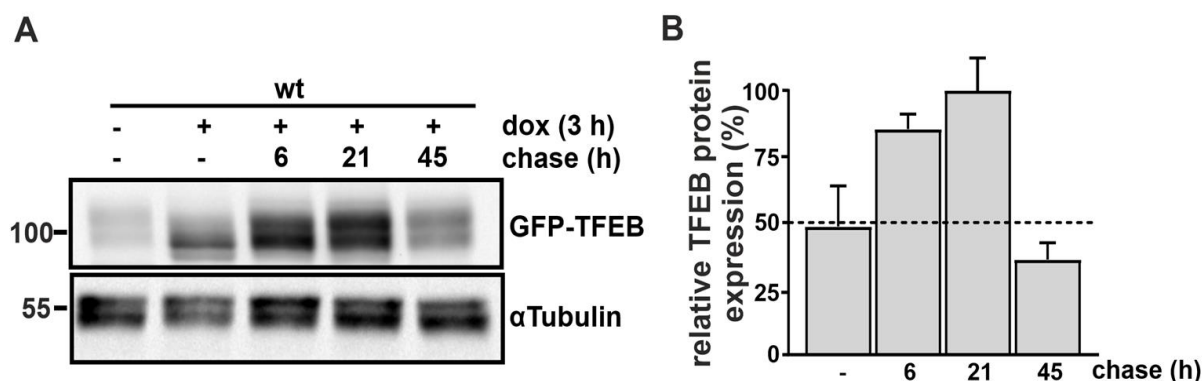


Fig. 3.7 Stability of GFP-TFEB protein in HeLa cell line - (A) Extracts from cells stably expressing GFP-TFEB-wt were either not induced (control) or treated for 3h with dox, followed by the indicated time periods of dox-free chase incubation, were analysed by GFP western blotting. α Tubulin was used as loading control. (B) Quantification of densitometric analysis of A. GFP-TFEB expression values were normalized to the α Tubulin intensity. GFP-TFEB expression 3h dox+ 21h was set as 100% (n=3).

3.2.1 Different gene-activation rates upon TFEB-wt and -K3R expression

Since TFEB-K3A does not translocate into the nucleus, the transcriptional activities of GFP-TFEB-wt and the -K3R mutant were compared. HeLa TO cells stably expressing TFEB wt and -K3R were induced for 3 h followed by different time periods in dox-free chase medium. Non-induced HeLa TO cells were used as control. The RNA of these cells were prepared and the transcript level of the *ACP5* and *WIPI1* genes coding for the lysosomal tartrate-resistant acid phosphatase, and the autophagy-related WD repeat domain phosphoinositide-interacting protein 1, respectively, were quantified by real-time PCR and related to the actin (*ACTB*) expression. The *ACP5* and *WIPI1* transcript levels in non-induced HeLa TO cells were subtracted.

Real-time PCR analysis for the *ACP5* gene activation by TFEB-wt follows a sigmoid curve over time reaching a plateau 3h dox + 21h chase corresponding to a 38-fold increase in comparison with the transcript level after 3h dox treatment (Fig. 3.8). Prolonged chase periods for 45 h resulted in a decrease of the *ACP5* mRNA by 34%. In contrast, the highest level *WIPI1* mRNA is reached after 6 h chase (3.2-fold higher than the 3h dox treatment), which slowly decreases during the following 40h of chase. Upon -K3R induction for 3h the maximum of *ACP5* mRNA was reached after 45h chase (corresponding to 10% of the transcript level activated by TFEB-wt).

A similar time course was determined for the *WIPI1* expression upon -K3R activation reaching 54% of the TFEB-wt activity. The low transcriptional activation of *ACP5* by the K3R mutant suggest that the replacement of the lysine residues by arginine reduces drastically the affinity

for the CLEAR motif in the *ACP5* promotor whereas the recognition/binding capability of K3R to the CLEAR motif in the *WIP11* promotor is moderately impaired.

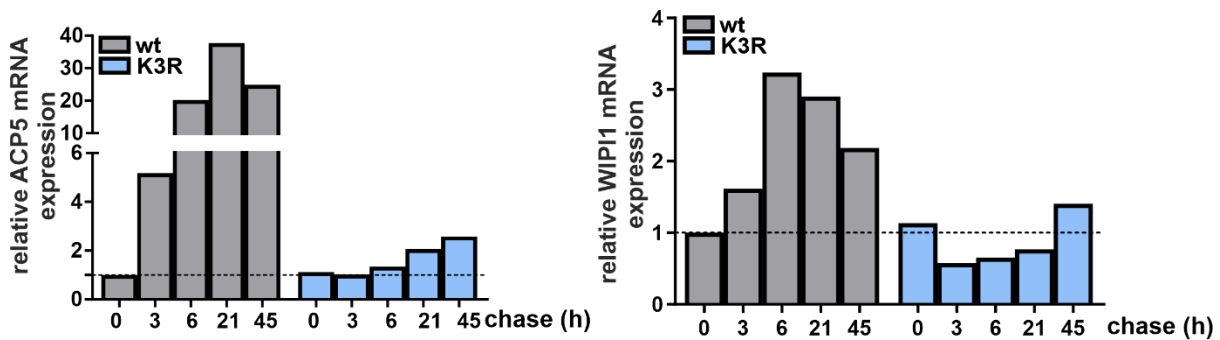


Fig. 3.8 Transcriptional activation of *ACP5* and *WIP11* in response to TFEB and -K3R mutant induction- HeLa TO cells stably expressing GFP-TFEB-wt and -K3R were induced for 3 h and either harvested (0 h chase) or chased for the indicated time in dox-free medium. Non-transfected HeLa TO cells (-) were used as control. The mRNA expression of *ACP5* (left) and *WIP11* (right) were determined by real-time PCR and normalized for the *ACTB* transcript level.

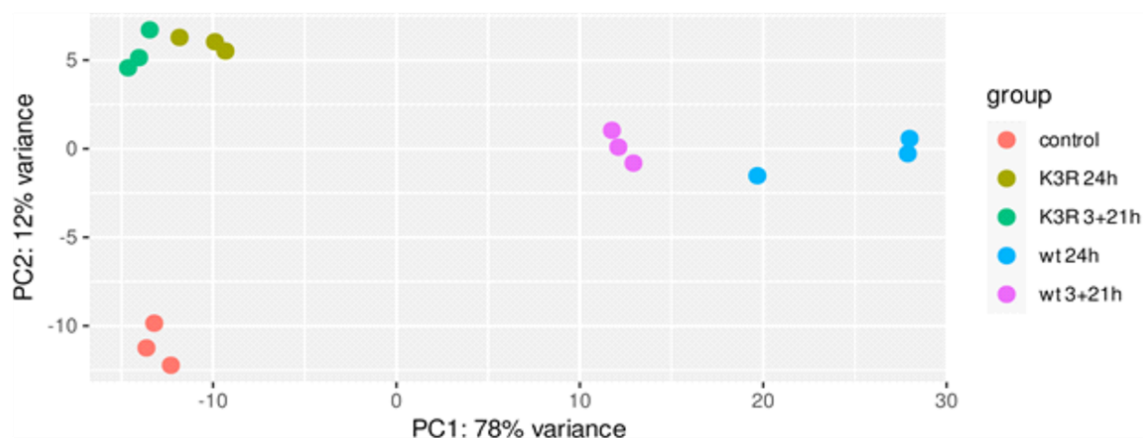
3.3 Transcriptome analysis of TFEB-wt and -K3R

3.3.1 Short and long term TFEB transcription

After establishing two reliable TFEB-induction protocols, TFEB-dependent transcriptome analysis were performed after 3h dox + 21h chase and 24h continuous dox induction of wt and TFEB K3R expression. GFP-TFEB-wt and -K3R stably expressing clones in HeLa cells were induced to express both short-TFEB 3h followed by 21h chase (wt 3+21h, K3R 3+21h) or long-term continuously induced 24h (wt 24h; K3R 24h). The basal gene expression profile of non-transfected HeLa cells was used as reference control. Purified RNA were collected for each condition in triplicates and processed for RNA sequencing in collaboration with Prof. Nicole Fischer (UKE/Leibniz-Institut für Virologie, Hamburg).

To test the quality of the samples analysed principal component analyses (PCA) were performed. The data revealed TFEB-wt or K3R-dependent clustering of samples, indicating differential regulation of TFEB wt and TFEB K3R gene expression. In contrast, the differences between the 24h continuous dox administration and the 3h dox + 21h chase of TFEB wt showed a more pronounced similarity of the samples, and these samples were different from the mutant (Fig. 3.9 A). Transcriptional profiling of HeLa cells expressing TFEB-wt or -K3R according to the 3h dox + 21h chase and the continuous 24h dox protocols related to the expression profile of control cells revealed a large number of differentially expressed genes (DEGs, $\log_2\text{FC} \geq 1.5$ or ≤ -1.5 and multiple testing adjusted p-value (padj.) ≤ 0.05) detected under all conditions (Fig. 3.9 B).

A



B

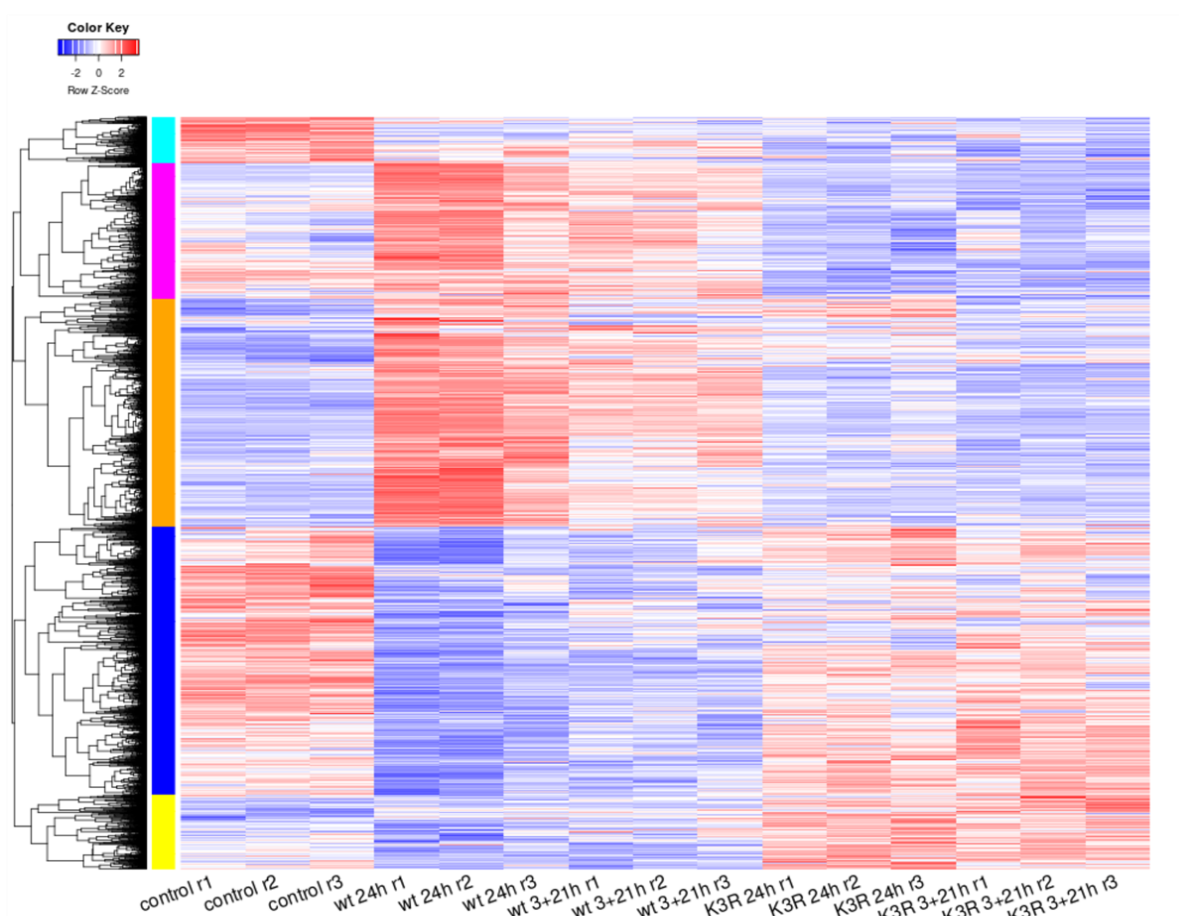


Fig. 3.9 RNA-seq analysis of differentially expressed genes in wild-type and TFEB K3R mutant cells – GFP-TFEB-wt and -K3R stably expressed in HeLa TO cells were induced with 1 μ g/mL dox either for 3h + 21h chase (short term) or for 24h continuously (long term). Total purified RNA samples were evaluated by (A) principal component analysis (PCA) of global gene expression values of three independent sets of experiments. Each dot represents a single sample and the cluster demonstrate the variance between the respective samples. (B) Heatmap depicting the expression levels of differentially expressed genes (DEGs) across control, wt 24h, wt 3+21h, K3R 24h, and K3R 3+21h groups. Each replicate's scaled expression is represented by the row Z-score, visualized through a red-blue gradient where red indicate high and blue low expression. Criteria for consideration: an absolute log₂-fold change ≥ 0.585 (equivalent to a 1.5-fold change in expression) and an adjusted p-value ≤ 0.05 . Genes are hierarchically clustered based on their expression patterns. Five primary clusters are marked in cyan, magenta, orange, blue, and yellow, comprising 388, 1142, 1906, 2247, and 628 genes respectively. All the statistical and clustering analysis was performed via R-script.

Several thousand differentially regulated genes were found in all four conditions (wt 3+21h, wt 24h, K3R 3+21h, K3R 24h), compared to the basal non-induced TFEB control cells. K3R 3+21h or K3R 24h-expressing cells displayed a trend towards more down than upregulated genes, whereas TFEB-wt expressing cells showed a comparable numbers for up- and downregulated transcripts (Fig. 3.10 A and B; Fig 3.11 A and B). TFEB expression induced a significant upregulation of 1145 at 3+21h and 2221 genes at 24h dox treatment and downregulation of 1174 (50.6%) and 1967 (47%) genes at 3+21h and 24h dox respectively. In contrast, -K3R expression significantly upregulated 379 (30%) and 526 (40%) genes at 3+21h or 24h dox treatment, respectively, while considerably more genes were downregulated at the conditions included: 884 (70%) and 777 (60%) genes, respectively. Interestingly, the number of significantly dysregulated genes in TFEB-K3R expressing cells does not increase with prolonged dox treatment.

From all differentially regulated genes in TFEB-wt and -K3R expressing cells 587 genes (16.4%) and 756 (13.8%) were dysregulated in both wt and -K3R mutant after 3+21h and 24h dox treatment, respectively. 134 (8.8% (3+21h)) and 274 genes (10% (24h)) were up-regulated, while 355 (17.2% (3+21h)) and 370 transcripts (13.5% (24h)) were found commonly down-regulated.

To gain insight which cellular compartments might be coordinately regulated by TFEB-wt and -K3R, Gene Ontology (GO) enrichment analysis were performed. This revealed that annotations of *lysosome*, *lysosome membrane* and *lysosomal lumen* were significantly enriched by TFEB-wt under both conditions of dox-induction, while only the *lysosomal lumen* was found to be enriched after -K3R expression independent of the dox induction protocol (Fig. 3.10 C; 3.11 C).

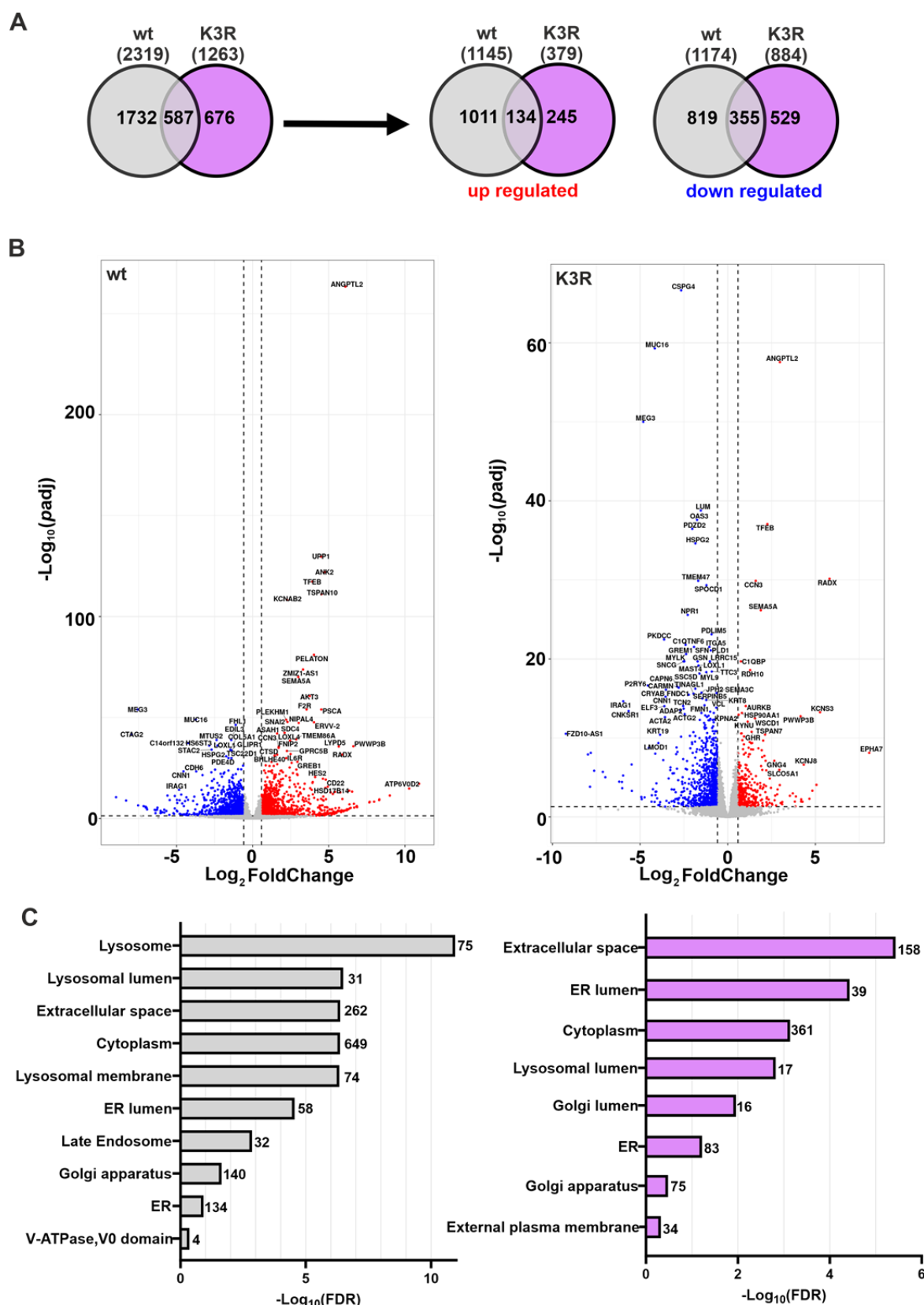


Fig. 3.10 RNAseq analysis of wild-type and TFEB-K3R HeLa TO cells induced by 3h dox + 21h chase protocol - (A) Venn diagram showing the overlap of 823 genes between all differentially expressed genes (DEG) in TFEB-wt and TFEB-K3R expressing cells (3h dox+21h chase) and their subdivision into up- and down-regulated genes. (B) Volcano plots showing DEGs for all genes in TFEB-wt versus control and TFEB-K3R related to control HeLa cells. Up-regulated genes are highlighted in red, down-regulated genes are highlighted in blue. (C) GO enrichment analysis of cellular compartments of TFEB-wt and -K3R expressing cells. The number of the genes is given.

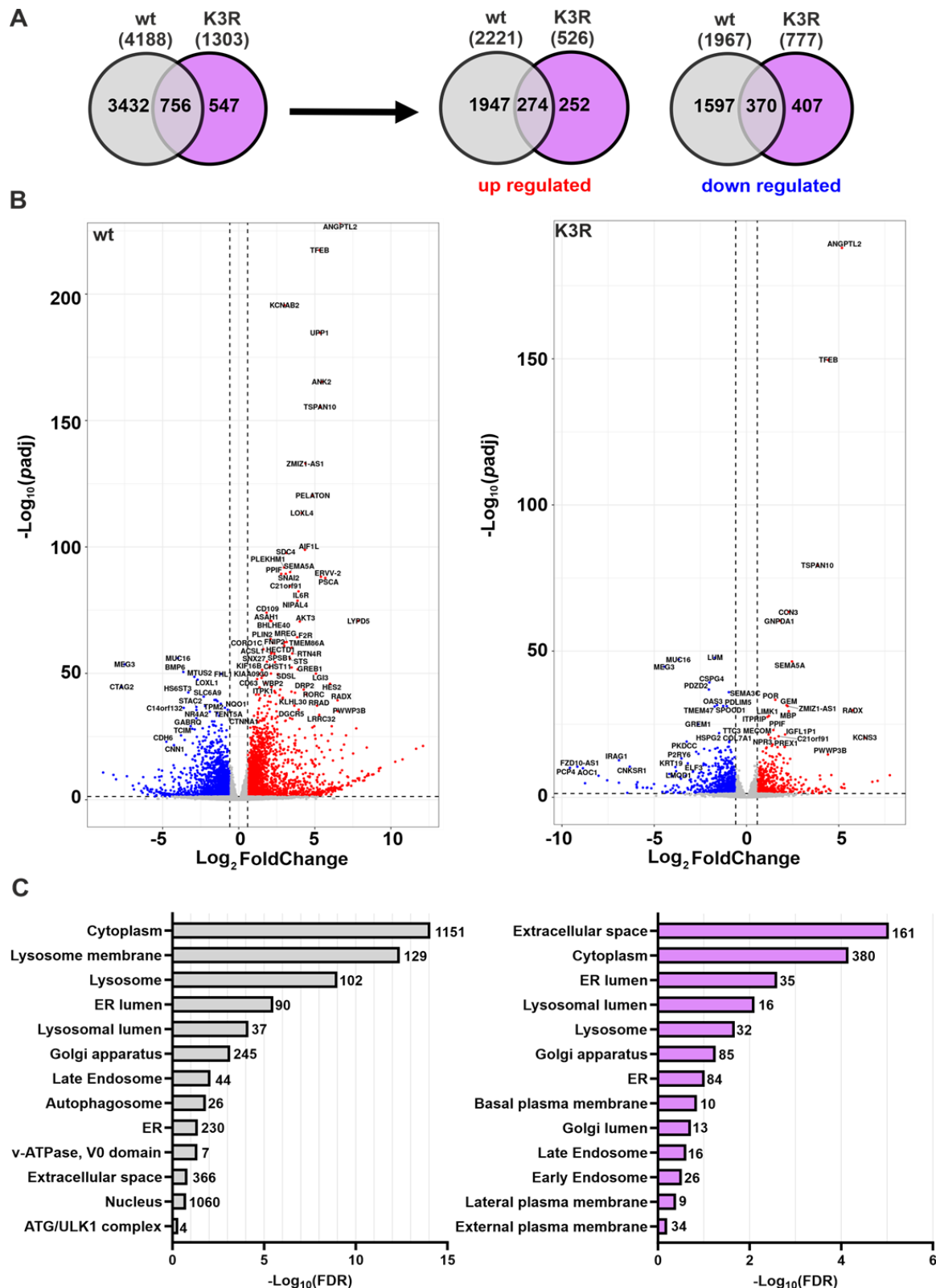


Fig. 3.11 RNA-seq analysis of wild-type and TFEB-K3R HeLa TO cells following 24h continuous dox treatment - (A) Venn diagram showing the overlap of 1016 genes between all DEGs in TFEB-wt and TFEB-K3R expressing cells (24h continuous dox) and their subdivision into up- and down-regulated genes. (B) Volcano plots showing DEGs for all genes in TFEB-wt versus control and TFEB-K3R versus control HeLa cells. Up-regulated genes are highlighted in red, down-regulated genes are highlighted in blue. (C) GO enrichment analysis of cellular compartments of TFEB-wt and -K3R expressing cells. The number of the genes is given.

3.3.2 TFEB wt and K3R regulated CLEAR-containing target genes

Genome-wide mapping of TFEB target sites in HeLa cells revealed 471 TFEB direct targets called the CLEAR network (Palmieri et al., 2011). Similarly, we found 102 of 471 TFEB target genes to be differentially expressed in HeLa TFEB-wt cells under 3h dox+21h chase condition, of which 99 show upregulation, including 10 genes of luminal lysosomal enzymes, *ASAH1*, *CTSA*, *CTSB*, *CTSD*, *GBA*, *GLA*, *NAGLU*, *NEU1*, *SGSH*, and the sphingolipid activator *PSAP*, as well as 5 autophagy related genes, *NRBF2*, *PRKAG2*, *RRAGC*, *VPS18* and *VPS8* (Fig. 3.12). Three TFEB target genes were significantly downregulated. In contrast, in HeLa cells expressing TFEB-K3R 3+21h we identify 17 TFEB target genes with 7 of 10 equally regulated in wt and -K3R cells (Fig. 3.12 A). No genes of lysosomal hydrolases or autophagy-related were significantly activated upon -K3R induction (Fig. 3.12 C).

After 24h continuous dox treatment we found 190 significantly dysregulated TFEB target genes in HeLa TFEB-wt cells of which 177 were upregulated among them 12 significantly activated luminal lysosomal genes, *ASAH1*, *CTSA*, *CTSB*, *CTSD*, *GBA*, *GLA*, *GNS*, *HEXA*, *NAGLU*, *NEU1*, *PSAP*, *SGSH*. Thirteen target genes including the lysosomal *GAA* transcript were significantly downregulated. (Fig. 3.13 A and B). Upon identical conditions of doxycycline-mediated induction of -K3R, 38 differentially expressed TFEB target genes were identified of which 31 were also dysregulated in dox-induced TFEB-wt cells; 26 genes have been commonly found to be upregulated in dox-induced TFEB-wt cells, and 2 being significantly downregulated in both (Fig. 3.13 A). In contrast to the 3h dox + 21h condition, three transcripts of lysosomal genes, *CTSA*, *CTSD*, and *PSAP*, were activated after 24h continuous induction of the -K3R mutant. Furthermore, 24h dox-treatment of K3R-expressing cells, did not activate autophagy-related genes with the exception of *SQSTM1* and *PRKAG2* (Fig. 3.13 C).

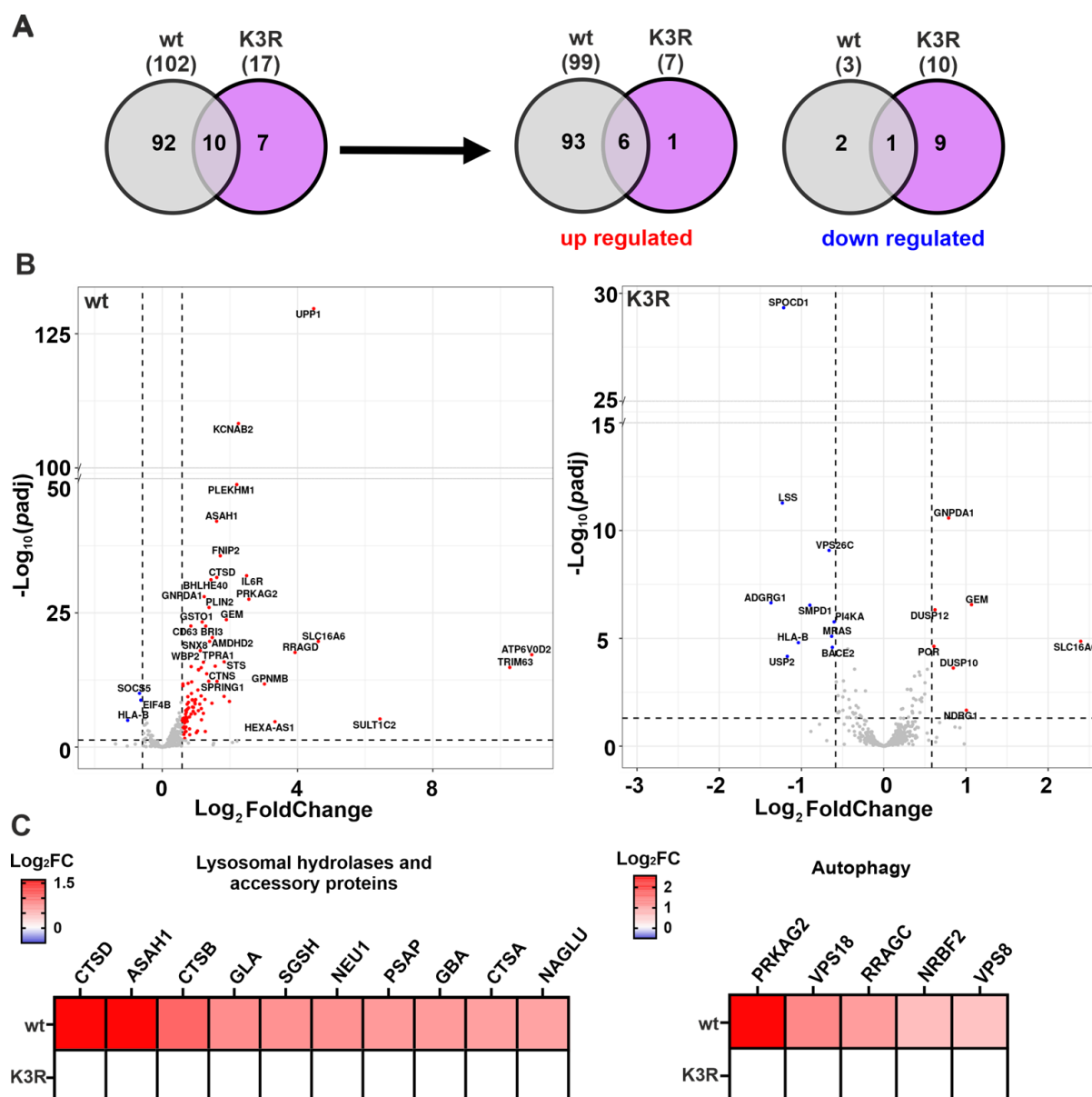


Fig. 3.12 TFEB target gene expression in wt and TFEB-K3R HeLa cells induced by 3h dox +21h chase protocol - (A) Venn diagram showing that in TFEB wt and TFEB K3R expressing cells (3h dox+21h chase) 102 and 17 TFEB target genes were differentially expressed, respectively. The majority of DEGs were upregulated by TFEB-wt. (B) Volcano plots showing the expression of TFEB target genes in TFEB-wt versus control and TFEB-K3R versus control HeLa cells induced for 3h with dox followed by 21h chase in the absence of dox. Significantly up-regulated genes are highlighted in red, significantly down-regulated genes are highlighted in blue. Non-significant dysregulated genes are shown in grey. (C) Heatmaps of differentially expressed genes (Log₂FC) for lysosomal hydrolases and accessory proteins, and autophagy genes in TFEB-wt and -K3R HeLa cells.

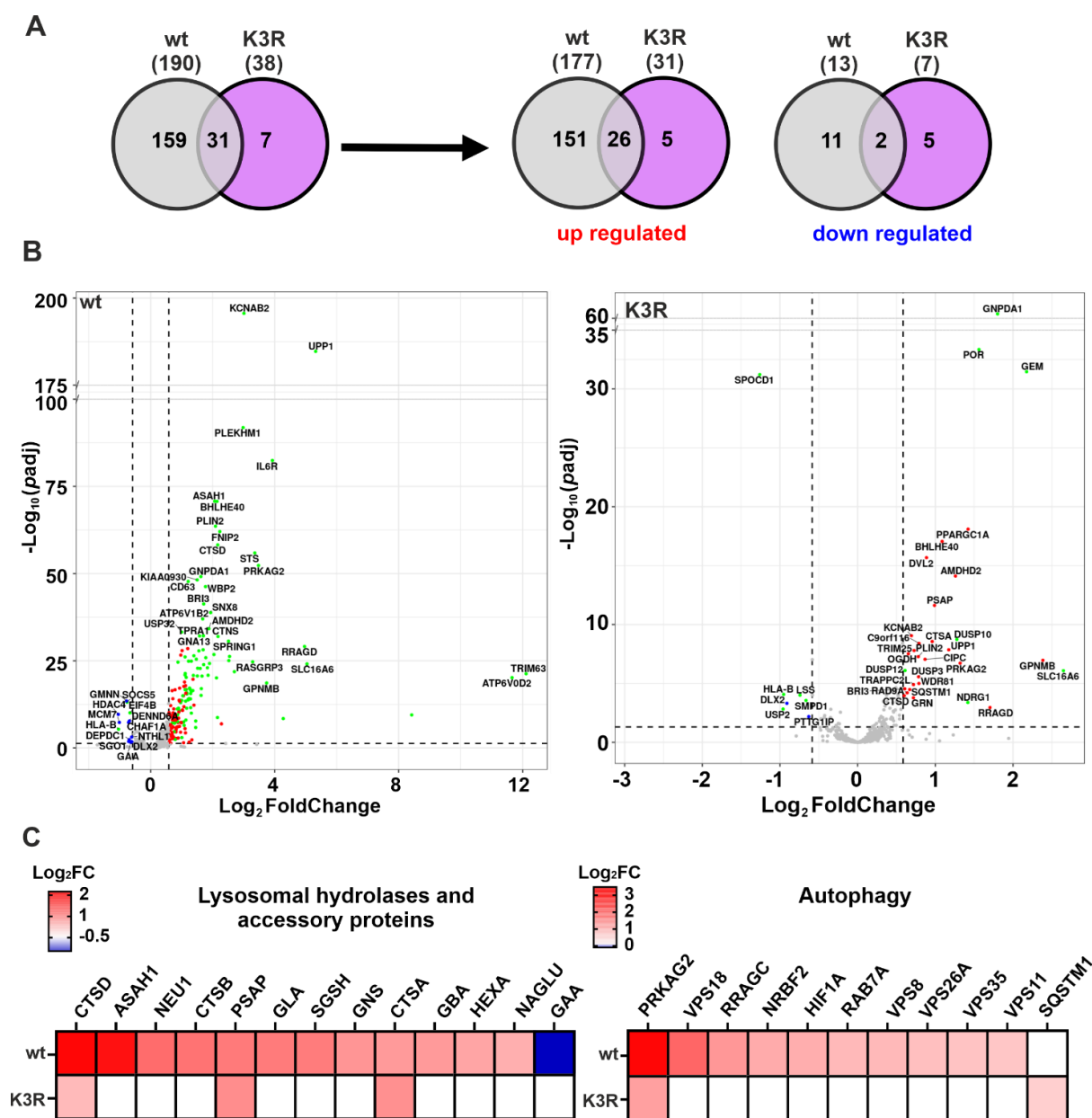


Fig. 3.13 TFEB target gene expression in TFEB-wt and -K3R HeLa cells following 24h dox treatment - (A) Venn diagram showing that upon 24 h continuous dox induction of TFEB-wt and TFEB-K3R 190 and 38 target genes, respectively, were differently expressed; the majority of target genes were upregulated under these conditions. (B) Volcano plots showing differentially expressed TFEB target genes in TFEB-wt versus control and TFEB-K3R versus control HeLa cells induced for 24h with dox. Significantly up-regulated genes are highlighted in red, significantly down-regulated genes are highlighted in blue. DEGs which have also been significantly dysregulated in cells under 3h dox + 21h chase condition (Fig.3.12) are highlighted in green. Non-significant dysregulated genes are shown in grey. (C) Heatmaps of differentially expressed genes (Log_2FC) for lysosomal hydrolases and accessory proteins, and autophagy genes in TFEB-wt and -K3R HeLa cells.

Of note, the *GPNMB* gene, one of the most activated target genes of TFEB (Palmieri et al., 2011) encoding a transmembrane glycoprotein NMB, was found also in the TFEB-wt upregulated target gene set under both condition, but only upon 24h continuous dox-treatment in the K3R-expressing HeLa cells. In contrast, the *GNPDA1* mRNA coding for the glucosamine-6-phosphate isomerase 1, seems to be highly upregulated in -K3R expressing cells (Fig. 3.12 B, 3.13 B).

Together, our RNAseq data derived from two experimental conditions reveal that both, the number of dysregulated genes overall and TFEB- targets genes (CLEAR network) correlate with the TFEB transcript level. With few exceptions identical genes for lysosomal enzymes and genes related to autophagy are activated by TFEB-wt under both doxycycline induction conditions, whereas the gene landscape activated by the -K3R mutant differs significantly from TFEB-wt.

3.3.3 Validation of RNAseq data by RT-PCR analysis

To evaluate the RNAseq data, we examined the expression of various lysosome and autophagy-related genes and some non-lysosomal target genes (*USP2*, *GPNMB*, *TFEC*). RNA was isolated and purified from stable TFEB-wt and -K3R expressing HeLa TO cells induced with 1µg/mL dox for 24h. Non-transfected HeLa TO cells were used as control. The relative mRNA expression level of the selected genes were analysed by RT-PCR, normalized against *ACTB* expression and calculated according to the comparative CT method ($2^{-\Delta\Delta T}$) (Fig. 3.14). In TFEB wt expressing cells the mRNA level of all tested target genes were increased, whereas the effect of -K3R were always lower or not changed. Surprisingly the mRNA of *ACP5*, coding for the soluble lysosomal acid phosphatase 5, was strongly activated by TFEB-wt but only marginal by -K3R (Fig. 3.14). The transcript level of TFEB-wt was found to be 3-fold higher than the TFEB-K3R mutant transcripts (32% of the TFEB-wt; Fig. 3.14 B). Similarly, the dox-induced expression of TFEB-wt resulted in a 37-fold increase in *TFEC* mRNA level in comparison with untreated controls whereas K3R led to an 8-fold elevated *TFEC* expression.

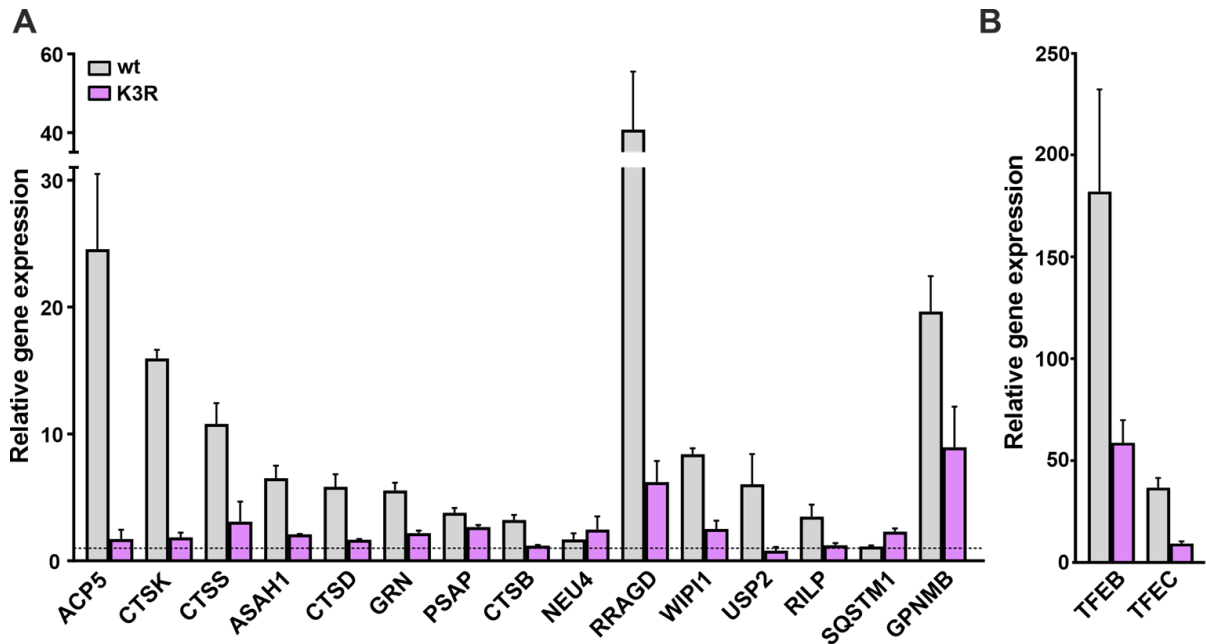


Fig. 3.14 Validation of selected genes of the RNAseq data set – (A) RT-PCR expression analysis of transcripts coding soluble lysosomal proteins (*ACP5*, *CTSK*, *CTSS*, *ASAHI*, *CTSD*, *GRN*, *PSAP*, *CTSB*, *NEU4*), autophagy-related proteins (*RRAGD*, *WIP1I*, *USP2*, *SQSTM1*), and *GPNMB* in HeLa TO cells expressing TFEB-wt and -K3R upon 24 h continuous doxycycline treatment. The relative mRNA levels of three independent RNA preparations (mean \pm SD) are shown related to the respective non-doxycycline treated control HeLa TO cell values (set to 1; dotted line). (B) Relative transcript level of *TFEB* and *TFEC* in HeLa TO expressing TFEB-wt and -K3R cells upon 24 h dox-induction. The endogenous *TFEB* mRNA amounts of non-treated control cells were subtracted.

3.4 Impact of TFEB-wt and -K3R induced gene activation on protein synthesis of lysosomal enzymes

TFEB-wt induction for 24h leads to the activation of 12 genes encoding lysosomal hydrolases under nutrient rich conditions (see 3.3.2). To examine the consequences of this long-term transcriptional activation on the rate of newly synthesized lysosomal enzymes, extracts of cells expressing TFEB wt and -K3R mutant were analysed for the protein level of two lysosomal hydrolases, α -mannosidase and cathepsin B (*CTSB*) by western blotting. Neither the abundance nor the proteolytic processing to mature enzyme forms were affected by the 24h expression of wt or TFEB-K3R mutant in comparison with non-transfected HeLa control cells (data not shown). These results suggest that the protein level of intracellular lysosomal enzymes at steady state is too high to distinguish a significant increase of small amounts of newly synthesized hydrolases induced by TFEB within 24h.

Moreover, the sensitive fluorometric measurements of lysosomal enzyme activities in HeLa cells and media upon the 3h dox + 21h TFEB induction protocol failed to identify any significant transcription factor-induced variations in the selected enzyme levels (Table S2).

Next, we applied an experimental approach to detect all newly synthesized soluble lysosomal proteins which reach lysosomes in a defined time through the major transport route depending on mannose 6-phosphate (M6P) receptors (MPR). MPRs recognize M6P residues on newly synthesized lysosomal enzymes and mediate their sorting from the secretory pathway in the *trans* Golgi network (TGN) to the endosomal compartment. The low pH in endosomes results in dissociation of MPR-lysosomal enzyme complexes followed by the delivery of the enzymes to lysosomes, whereas the MPRs recycle to the TGN for another round of transport. A small percentage of lysosomal enzymes escape to binding to MPRs and are secreted mostly as inactive precursor forms (Fig. 3.15; Braulke et al., 2023). Treatment of cells with NH_4Cl leads to a fast alkalinization of all acidic compartments and prevents the pH-induced dissociation of M6P-containing lysosomal enzymes from their cargo receptors. Subsequently ligand-occupied MPRs return to the TGN and the plasma membrane unable for binding and proper sorting of newly synthesized lysosomal enzymes that results in their hypersecretion (Fig. 3.15).

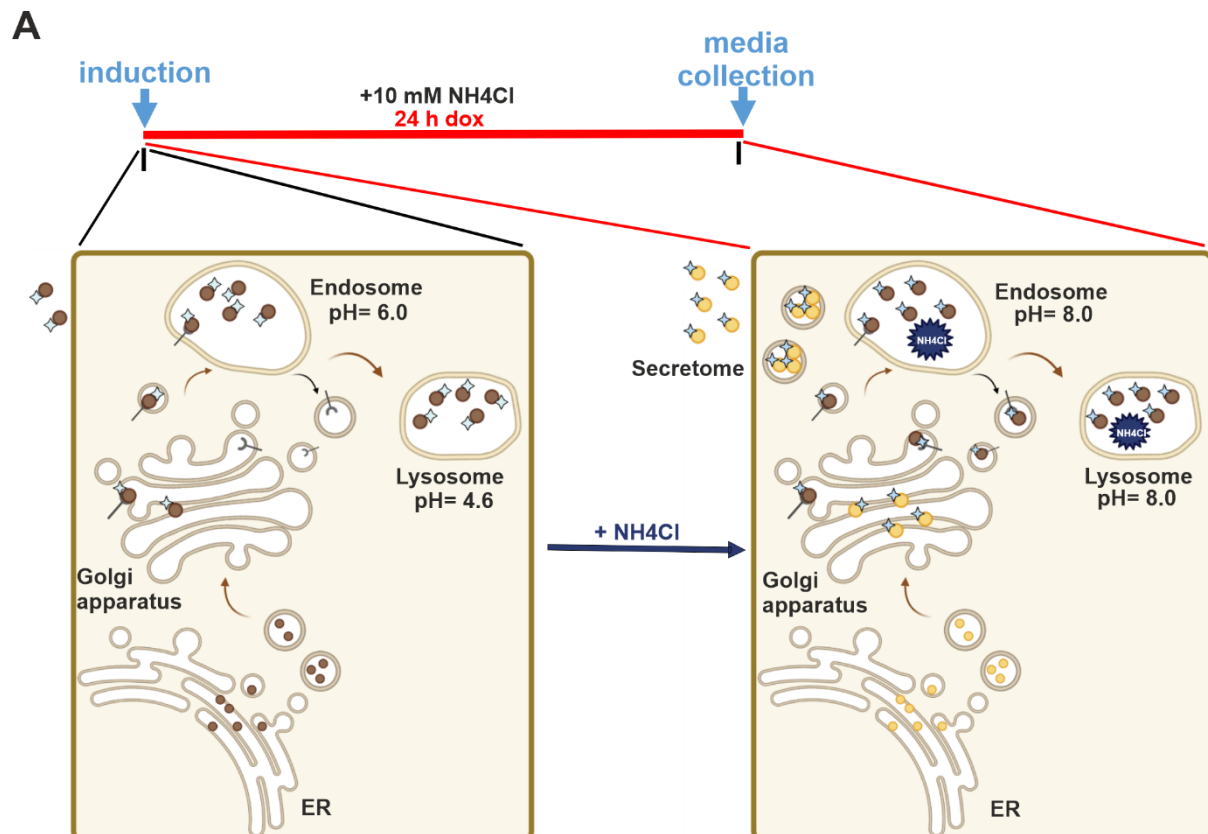


Fig. 3.15 Schematic representation of NH_4Cl -dependent secretion of newly synthesized lysosomal enzymes upon TFEB expression – Lysosomal hydrolases are synthesized in the ER and modified in the *cis*-Golgi with M6P residues. M6P-containing enzymes are recognized by M6P-receptors (MPR) in the *trans*-Golgi network (TGN) and sorted to endosomes, where the low pH (pH=6) allows the dissociation of lysosomal enzymes from MPR. The lysosomal enzymes are further transported to lysosomes whereas MPRs recycle to the TGN for another round of transport (left panel). The presence of NH_4Cl increases the pH of all the acidic compartments, inhibiting the dissociation of M6P-containing lysosomal enzymes from MPR, which return to the TGN in an occupied state. As a consequence, all the newly synthesized lysosomal enzymes are no longer sorted in the TGN to the lysosome but hypersecreted into the medium (right panel).

Thus, stably expressing TFEB-wt and -K3R HeLa TO cells were induced for 24h with 1µg/mL dox in serum-free OptiMEM supplemented with 10mM NH₄Cl. Afterwards, the media were collected, dialyzed and analyzed by comparative mass-spectrometry (MS; in collaboration with PD Dominic Winter, University of Bonn). Media of non-doxycycline treated HeLa TO cells were used as controls (Fig. 3.16 A).

In the medium of dox-induced TFEB-wt cells 480 proteins have been identified, among them 27 soluble lysosomal enzymes and accessory proteins of which 18 (ACP5, ASAH1, CPVL, CTSD, CTSF, CTSH, CTSS, GBA, GLA, GRN, GUSB, HYAL1, IFI30, MAN2B1, PLA2G15, PSAP, SGSH, SMPDL3A) were significantly increased in comparison with controls (Fig. 3.16 B). In contrast, 324 proteins were found to be differently expressed in media of K3R expressing cells in comparison with controls. Among them 22 lysosomal enzymes and accessory proteins but only cathepsin S (CTSS) was significantly increased (Fig. 3.16 C). In conclusion, continuously 24h-induced TFEB-wt led to an increased protein synthesis of only 18 lysosomal hydrolases, while under the same conditions only the amounts of CTSS were significantly elevated by the TFEB-K3R mutant.

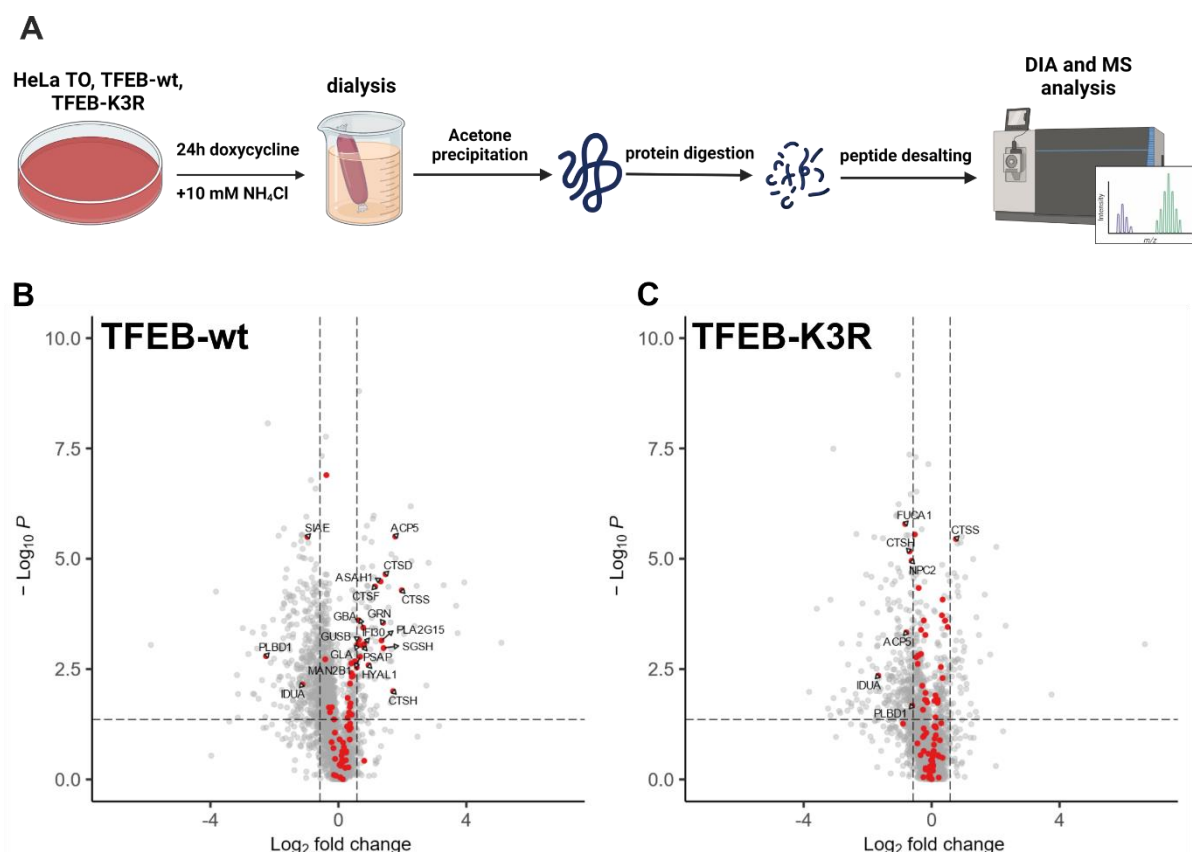


Fig. 3.16 Analysis of newly synthesized soluble lysosomal proteins upon TFEB expression - (A) Schematic experimental protocol to analyze the newly synthesized soluble lysosomal secretome generated during the 24 h doxycycline-induced TFEB-wt and K3R expression. (B and C) Volcano plots outlining the distribution of soluble lysosomal enzymes (red dots) synthesized and hypersecreted upon NH₄Cl treatment during 24 h dox induction of TFEB-wt (B) and TFEB-K3R (C). Data was graphed log₂ (ratio) of TFEB-wt or TFEB-K3R vs non-dox treated cells against the $-\log_{10}$ (p -value). The dashed line indicates the 0.05 p -value cut off ($n=4$).

To evaluate the secretome data, western blot experiments were performed. TFEB-wt and -K3R stably expressing in HeLa TO were induced for 24 h with 1 μ g/mL dox in serum-free OptiMEM media supplemented with or without 10 mM NH₄Cl. Aliquots of cell extracts and serum-free 10-fold concentrated were analysed by pGRN, CTSB, CTSD, PSAP western blotting. The β -glucocerebrosidase, GBA, was used as internal control for a non-M6P modified lysosomal enzyme.

Western blot analysis revealed a strong increase in the band intensity for pGRN, CTSB precursor form and CTSD-precursor form under NH₄Cl treatment in the media compared to the not-NH₄Cl treated (Fig. 3.17 A) indicating that the majority of these enzymes are transported via an M6P-dependent pathway to lysosomes. However, no obvious differences among TFEB-wt, -K3R and the control media could be detected although the abundance of GRN and CTSD were clearly increased in the MS data set. The equal band intensities of GBA in the media of TFEB-wt and -K3R with or without NH₄Cl treatment supports the concept of M6P-independent, NH₄Cl resistant transport mediated by the lysosomal integral membrane

protein LIMP-2 (Reczek et al., 2007). The slightly increased secretion of pro-saposin (PSAP) upon treatment with NH_4Cl are in agreement with previous data that this precursor form of the accessory protein reaches the lysosome via both intracellular MPR-dependent routes and via secretion recapture processes mediated by the LRP-1 receptor (Quian et al., 2008; Hiesberger et al., 1998). However, PSAP as well as all other tested lysosomal proteins are detected intracellularly as precursor forms upon NH_4Cl treatment because the lysosomal proteases involved in their proteolytic maturation are catalytically inactive due to the increased alkaline pH.

In conclusion, western blot analysis is not sensitive enough to verify the small or moderate increases in the abundance of soluble lysosomal proteins tested here (GRN, PSAP, CTSB, CTSD) differentially expressed in the MS-based secretome analysis upon TFEB-wt or -K3R-induced expression.

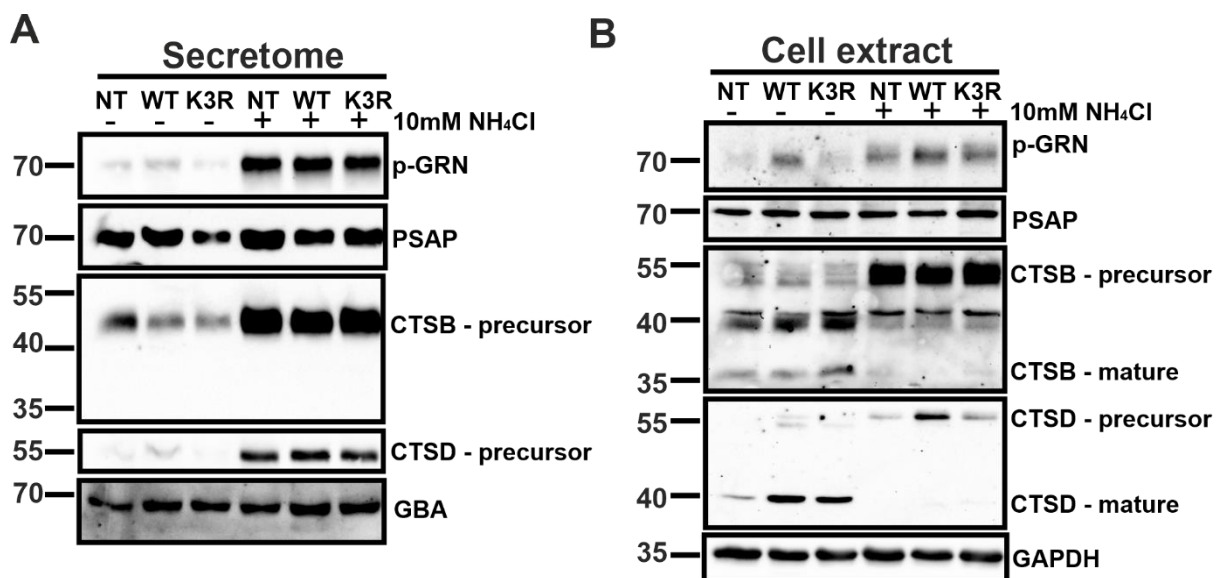


Fig. 3.17 Evaluation of mass-spectrometry data - TFEB-wt and -K3R stably expressing in HeLa TO were induced for 24 h with $1\mu\text{g/mL}$ dox in serum-free OptiMEM media supplemented with 10 mM NH_4Cl or not. Afterwards, the media was collected and concentrated. Both $10\mu\text{L}$ media (A) and cell extract (B) were analysed by western blot +/- NH_4Cl against different selected lysosomal proteins (pGRN, CTSB, CTSD, PSAP). The lysosomal hydrolases GBA was used as internal control for the secretome, while GAPDH was used as loading control for the cell extract. The relative protein molecular mass are displayed in kDa.

3.4.1 Identification of transmembrane soluble domain under TFEB expression

Among non-lysosomal proteins identified in the media of TFEB-wt and -K3R mutant expressing cells, there were surprisingly peptides from several transmembrane proteins, such as GPNMB, one of the most upregulated TFEB target genes, TMEM59, SPRING1, or glycosyl- and sulfotransferases (B4GALT5, CHST11). In addition some low-abundant commonly peptides have been found such as p62, NUDCD2 and ADAMTS13, suggesting a possible

TFEB-dependent regulation of proteases cleaving in the transmembrane domain or in the luminal domain of the mentioned transmembrane proteins (shedding) and releasing a soluble protein domain (Fig. 3.18 A and B).

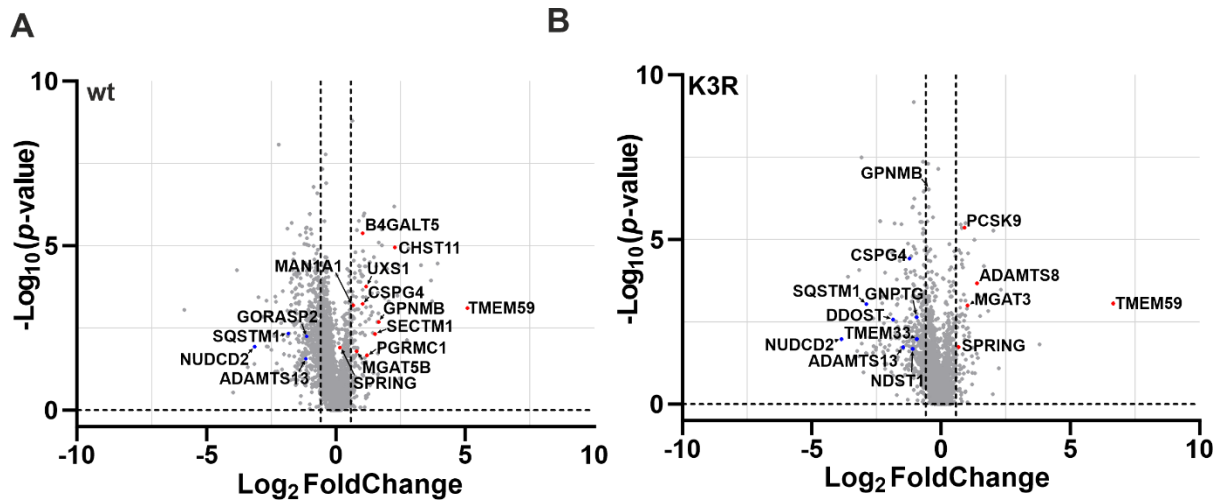


Fig. 3.18 - Volcano plots of selected transmembrane proteins detected in the secretomes of HeLa cells upon dox-induction of TFEB-wt (A) and K3R mutant (B) for 24 h (n=4)

In Fig. 3.19 it is shown that the expression of TFEB-wt- increased the amounts of the 130 kDa integral membrane GPNMB protein in cell lysates and the soluble 110 kDa GPNMB form in the medium. K3R led to a moderate increase in the cell lysate, whereas the formation of the soluble GPNMB in the medium was not altered. In the presence of NH_4Cl both the cellular and the soluble GPNMB in the medium were strongly increased in non-doxycycline induced control cells. NH_4Cl treatment elevated the 130 kDa cellular and 110 kDa soluble GPNMB in TFEB-wt expressing cells and media only marginally. In K3R expressing cells the NH_4Cl effect on GPNMB in cells and medium resembles the NH_4Cl effect in non-doxycycline treated control cells. Together, NH_4Cl treatment activated both the *GPNMB* mRNA dependent on dox-induced TFEB (Fig. 3.19 B) and resulted in similar amounts of cellular GPNMB membrane protein forms as well as the the soluble form (Fig. 3.19 A). Moreover, additional bands <100kDa are visible in wt and K3R cell samples in particular in the presence of NH_4Cl .

Since the NH_4Cl treatment block the M6P-pathway leading to the hypersecretion of soluble-lysosomal hydrolases (Fig.3.15), similarly to the hypersecretion of lysosomal hydrolases which are not modified with M6P residues-due to the deletion of *N*-acetylglucosamine-1-phosphotransferase (GNPTAB). To examine whether in *GNPTAB* KO cells GPNMB is highly expressed intracellularly and secreted into the medium, HeLa TO-control and HeLa TO-*GNPTAB* KO cells were transiently transfected with GFP-TFEB-wt or not and the GFP-TFEB-wt protein expression induced for 24h with dox. Cell extracts and media were analysed by

alpha-subunit of phosphotransferase, TFEB, CTSB, GPNMB, and western blotting. Intracellularly GPNMB was only expressed and secreted into the medium by GNPTAB KO cells (Fig. 3.19 C). The overexpression of TFEB in these cells show no effect of the GPNMB expression.

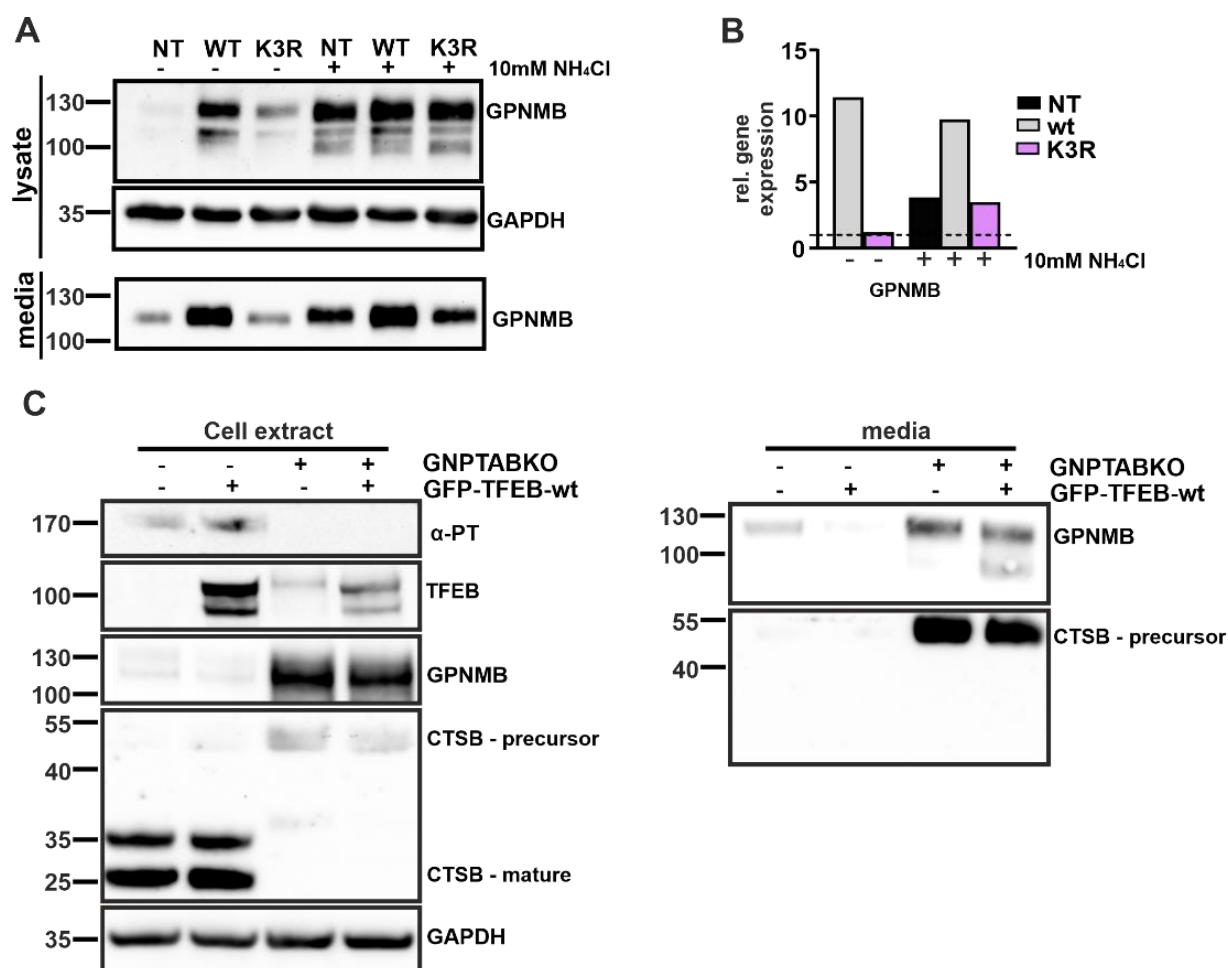


Fig. 3.19 NH₄Cl increases both intracellular expression and the secretion of the soluble GPNMB domain - (A) TFEB-wt and -K3R stably expressing in HeLa TO were induced for 24 h with 1μg/mL dox in serum-free OptiMEM supplemented or not with 10mM NH₄Cl. Non-dox treated (NT) HeLa TO cells were used as controls. Extracts of cells and media were analysed by western blotting. (B) HeLa TO TFEB-wt and -K3R stably expressing cells were induced for 24 h with dox in the absence or presence of 10mM NH₄Cl. The relative GPNMB mRNA level were analysed by real-time PCR normalized for *ACTB* and calculated according to the comparative CT method ($2^{-\Delta\Delta T}$). (C) HeLa TO and HeLa TO-*GNPTAB* KO cells were transiently transfected with GFP-TFEB-wt or not and the GFP-TFEB-wt protein expression was induced for 24h with 1μg/mL doxycycline. Cell extracts and conditioned media were analysed by western blotting. The media was collected and concentrated. The positions of molecular mass marker proteins are indicated in kDa.

4. Discussion

The crucial role of the transcription factor EB (TFEB) activity in the regulation of lysosome biogenesis and autophagy depends on its subcellular localization and the recognition of CLEAR motifs in the promotor region of lysosomal and autophagy-related target genes. While the impact of various serine (S) phosphorylation sites for the shuttling of TFEB between the cytoplasm and the nucleus are well studied (Puertollano et al., 2018), the function of acetylated lysine (K) residues are incompletely understood and controversially discussed. In this project, the role of three acetylated lysine residues, K237, K256, and K274, located in the DNA binding domain of TFEB was analysed in more detail. A number of new insights into i) the fine regulation of TFEB translocation into the nucleus in dependence of posttranslational modifications, ii) the transcriptional activity of TFEB and mutant forms under nutrient rich conditions, and iii) the significance of TFEB-induced transcription of lysosomal target genes on the lysosomal homeostasis based on the proteomic analysis of newly synthesized lysosomal enzymes.

4.1 TFEB acetylation at K237, K256 and K274 prevent its nuclear translocation

Previous studies in our laboratory identified seven acetylated lysine residues of TFEB in the cytoplasm but not in the nuclear fraction of TFEB expressing HeLa Tet-on cells. The focus of the present thesis was the characterization and the functional impact of the TFEB acetylation sites K237, K256, and K274. These residues of human TFEB are conserved between the different MiTF family members and preserved in mouse, rat, macaca, apes, bovine, chicken, amphibia and zebrafish. Aside from that, they are located in the DNA-binding/ helix-loop-helix and leucine zipper (bHLH-LZ) domain and directly involved in DNA binding in agreement with *in silico* 3D- structure modelling data of human TFEB dimers (performed by Dr. Henning Tiedow, University of Hamburg; Pogenberg et al., 2012). Because the positively charged lysine 237, 256 and 274 side chains in TFEB are mostly involved in electrostatic interactions with the phosphate moieties of the DNA, removal of these positive charges as occurring in acetylated lysines will directly impair DNA binding. From these data it can be concluded that the acetylated cytoplasmic TFEB needs to be deacetylated before or immediately after translocation into the nucleus.

By site-directed mutagenesis, the positive charge of the non-acetylated K237, K256 and K274 residues of TFEB shifted to non-charged residues upon acetylation, which is mimicked by simultaneous substitution of K237, K256 and K274 with alanines (K3A). The stoichiometry of

TFEB acetylation is not known but preliminary immunoprecipitation experiments of GFP-TFEB and subsequent TFEB and pan acetyl-lysine western blots suggest a low acetylation state in the cytoplasm of ≤ 3 percent of total TFEB. Thus, it should be considered that the K3A mutagenesis affects all expressed TFEB molecules and therefore provides a more general effect on localization and function than the small subpopulation of *in vivo* acetylated TFEB forms. The predominant localization of TFEB-K3A analysed by immunofluorescence microscopy, and subcellular fractionation was found in the cytoplasm (Fig. 3.2) in agreement with the TFEB-PTM mass spectrometry.

The present data here are in contrast with results reported by Wang et al. (2020) who reported that the histone acetyltransferase GCN5 mediates the acetylation of TFEB at K274 and K279 after entering the nucleus in HeLa or HEK293 cells. Subsequently, the acetylation at these sites inhibits the transcriptional activity TFEB through disrupting the hetero- or homodimerization of TFEB. However, only in an *in vitro* assay GCN5 was able to acetylate TFEB at K116, K274 and K279. The exchange of these lysine residues by arginine and its overexpression in HEK293 cells led to even a stronger target gene expression than the wild-type TFEB.

As control for the acetylation-mimetic K3A mutant, the lysine residues K237, K256 and K274 were substituted by arginines (K3R) resembling their non-acetylated status (Fig. 3.1). At steady-state, the induced K3R mutant shows a comparable distribution pattern as the endogenous TFEB (Fig. 3.2).

4.2 TFEB-K3A is retained in the cytoplasm in an mTORC1-independent manner

The mTORC1-mediated phosphorylation of TFEB at S122, S142 and S211 have been shown to prevent the nuclear entry of TFEB whereas the simultaneous exchange of S142 and S211 by alanine (S142/211A) leads to the fast nuclear translocation of TFEB into the nucleus (Settembre et al., 2011; Martina et al., 2012). To evaluate whether the lysine-to-alanine mutation of TFEB K3A affect the phosphorylation of TFEB at S142 and S211 two independent experimental approaches have been applied. First, the subcellular distribution of the K3A mutant was analysed in HeLa TO cells in the presence of the mTOR-specific inhibitor torin1 (Settembre et al., 2012) and demonstrated that the high cytoplasmic localization of TFEB K3A is resistant to torin1 treatment (Fig. 3.2). Second, the S142/211A exchanges were introduced into the K3A mutant and examined by subcellular fractionation and western blotting. Surprisingly, the S142/211A constitutive nuclear translocation motif was not sufficient to abolish the cytoplasmic retention effect of K3A (Fig. 3.4). Together these data suggest that simultaneous acetylation of K237, K256, and K274 represent a dominant mTORC1-

independent cytoplasmic-retention signal over the S142/211A nuclear translocation motif (Martina et al., 2012; Rocznik-Ferguson et al., 2012).

Of note, among the lysine residues exchanged in the K3A mutant, K274 is the major lysine acetylated residue, since the single K274A mutant lead already to an increased cytoplasmic retention (Fig. 3.3 and 3.4). In addition, previous preliminary experiments performed in Prof. Braulke's group, have demonstrated a faster electrophoretic mobility of TFEB-K274A than K237A or K256A, suggesting a differential acetylation stoichiometry among different posttranslationally modified TFEB isoforms (UKE Hamburg, Nina Westphal, data not shown). The mechanism how acetylated TFEB is retained in the cytoplasm is still unknown. The mTORC1 phosphorylated TFEB at S211 have been shown to be recognized and retained in the cytoplasm by different forms of 14-3-3 proteins (Martina et al., 2012; Rocznik-Ferguson et al., 2012) and by the structurally and functionally 14-3-3 homologous protein α -synuclein in neuronal cells (Decressac et al., 2013). However, the seven 14-3-3 isoforms are known to bind to several hundred identified (mostly serine or threonine phosphorylated) protein interaction partners (Stevens et al., 2018) containing consensus motifs which do not fit with acetylated lysine residues.

Finally, this study provided new insight into the crosstalk between acetylation of K237, K256, and K274 and the phosphorylation of S142 (by ERK2/mTORC1), S211 (by mTORC1) and S138 (by GSK3 β) (Yang and Seto, 2008). The reduced phosphorylation level at S211 but unchanged phospho-S142 level of the acetylation-mimetic K3A TFEB form, suggest that the non-charged residues at position 237, 256 and 274 either prevent the accessibility for kinases or the recruitment of K3A to the lysosome surface which still need to be studied.

4.3 Transcriptome analysis upon TFEB-wt and -K3R expression

TFEB is a transcription factor that contributes to the regulation of a plethora different physiological functions. The capability to exert its transcription factor function is hierarchically given by i) its subcellular localization, ii) homo/hetero-dimerization, and iii) DNA-binding capacity (Takla et al., 2023). In this study, three lysine residues K237/256/274 located in the TFEB-DNA binding/ bHLH-LZ domain were selected to investigate the DNA-binding capacity and subsequent functional activity of TFEB-K3R mimicking the non-acetylated TFEB compared to the wild-type TFEB under two experimental conditions.

At present, the transient or inducible expression of TFEB for 24h is the most used protocol for the analysis of TFEB transcriptional activity. Here stably expressing GFP-TFEB-wt and K3R

HeLa cells are used which can be induced by doxycycline treatment to activate the transcription of TFEB and the K3R mutant. Whereas during a short dox-induction for 3h low amounts of immunoreactive TFEB protein was formed, the TFEB protein increased continuously during a dox-free chase period and reaches a maximum after 21h chase (Fig. 3.6). Depending on the chase time a TFEB band doublet could be observed consisting of a fast mobility (hypophosphorylated) nuclear TFEB form, and a band with slower electrophoretic mobility representing the phosphorylated cytoplasmic TFEB fraction. During further prolonged chase time periods a decrease in TFEB protein can be observed which might be due to proteasomal degradation (Sha et al., 2017), allowing the calculation of the approximate TFEB half-life of 19-20h (Fig. 3.7).

Several thousand differentially regulated genes were identified by RNAseq following the two inducible expression protocols for TFEB-wt and -K3R. Surprisingly, almost ~50% of the total dysregulated genes were found to be downregulated upon TFEB-wt activation. When these data were compared with the *Human Transcription Factor* list (Lambert et al., 2018), 273 additional transcription factor/repressor genes differentially-regulated in response to TFEB-wt. were found. Among them, TFEC was highly upregulated in response to TFEB induction. TFEC is the only transcription factor from MiT/TFE family members that inhibits TFE3-dependent transcription activation (Zhao et al., 1993).

4.3.1 TFEB regulation of selected CLEAR-target genes

TFEB recognize and activates 471 genes containing the 10 base pair E-box CLEAR-motif in the proximity of their promoter region (Sardiello et al., 2009; Palmieri et al., 2011), and it has been considered the master modulator of lysosomal biogenesis due to the presence of enriched CLEAR-motifs in the promoter regions of 73 lysosome-and autophagy-related genes. In category lysosomal hydrolases and accessory proteins, *CTSD*, *ASAHI* and *CTSB* were identified as the top three candidates highly upregulated in both long- and short-term TFEB-wt expression, while *HEXA* and *GNS* were found activated only after longer time of TFEB-induction, suggesting a different temporal mRNA progression profile of the selected genes in response to TFEB.

The time-dependent gene activation is a critical regulatory mechanism since each gene exhibits a specific kinetics of transcription. Furthermore, the 471 CLEAR-containing genes are not only TFEB target genes, since the CLEAR motifs are recognized also by both TFE3 and MiTF (Martina et al., 2014; Möller et al., 2019). In addition, MYC or BHE41 were described to recognize the CLEAR-motifs, acting as a transcriptional repressors for subsets of TFEB target

genes (Annunziata et al., 2019; Carey et al., 2020). In conclusion, both TFEB induction protocols revealed a high number of dysregulated genes, which exceed the number of CLEAR-containing TFEB target genes. More than 200 dysregulated transcription factors/repressors upon induction of TFEB results in the secondary regulation of numerous additional genes contributing to a coordinated adaptive response even under nutrient rich conditions.

Another aspect that influences the gene activation pattern initiated by TFEB is the number and the position of the CLEAR motifs in the promotor regions of target genes, and the functional impact of the variable number of these motifs is presently still unknown (Sardiello et al., 2009). A novel web-tool database integrates both experimentally validated approaches and software-based predicted binding sites to understand whether a set of genes of interest is modulated after TFEB perturbation (De Cegli et al., 2022; [TFEB \(tigem.it\)](https://www.tigem.it)). Recently, an additional study performed in HEK293 cells increased the number of TFEB-target genes up to 556 genes. Among them, some of the genes are found also in 471 target-genes list (such as *ASAHI*, *IFI30*), whereas novel genes coding for lysosomal enzymes are now considered as TFEB target genes, such as *ACP5*, which was found highly upregulated also in the present study. However, Gambardella et al. (2020), considered as TFEB-target genes only those which i) show an activation in response to increasing TFEB amounts and ii) contain CLEAR sites in the promoter region. Recently a new splice variant of TFEB coding for a smaller TFEB-protein has been identified (Park et al., 2021), which lacks both the bHLH and leucine zipper domain. The authors propose that the small-TFEB negatively regulates the autophagy pathway.

Since the three lysine residues K256, K264, and K274 are directly involved in DNA-binding (Pogenberg et al., 2012), it was unknown how the simultaneous replacement of these lysine residues to arginine impacts the ability of TFEB to recognize and activate lysosomal gene transcription under the conditions of TFEB induction. K3R expressing cells displayed a trend towards more down- than upregulated genes which differ dramatically from the gene pattern activated by TFEB-wt (Fig. 3.10 and 3.11). These data suggest that the substitution of lysine residues by arginine in the DNA-binding domain changes the affinity of TFEB for the CLEAR motifs or prevent the replacement of repressors such as the MYC/HDAC2 complex bound on the E-box-CLEAR sites (Annunziata et al., 2019). Upon the induced expression of TFEB-K3R almost ~60% of total regulated genes by the TFEB-wt, could not be activated independent on the TFEB-K3R protein level.

Short-time -K3R expression is not enough to activate any CLEAR-containing target genes coding for lysosomal hydrolases or autophagy-related proteins. However, prolonged -K3R activation led to a significant upregulation of both *p62/SQSTM1* and *PRKAG2* autophagy-

related genes as well as the lysosome hydrolase genes of *CTSD*, *PSAP*, and *CTSA*. Using the TFEBExplorer tool (De Cegli et al., 2022) each two CLEAR sites could be identified in the promotor regions of *CTSD*, *PSAP*, and *CTSA*, which might be required for a slow activation rate by the K3R mutant.

Furthermore, nuclear TFEB interacts with Max-like protein **X (MLX)**, MYC and inositol polyphosphate multikinase (**IPMK**), which reduce the affinity of TFEB for the CLEAR-motif, resulting in a subsequent decrease of the transcriptional activity (Chen et al, 2020; Wang et al, 2023). At present it is unknown whether the K3R mutant can interact with the MLX, MYC, and IPMK proteins.

4.4 TFEB dependent soluble lysosomal protein translation

The master regulator role of TFEB for the biogenesis of lysosomes is justified by its transcriptional activation of genes involved in the lysosome-autophagy pathway (Ballabio and Bonifacino, 2020; Tan et al., 2022). Our own transcriptome analysis (see 3.3) revealed that TFEB exerts also autophagy-lysosome-independent functions affecting directly and indirectly thousands of other genes involved in various pathways such as cytokine production, phagocytosis, mitochondrial biogenesis, glucose homeostasis or regulation of myelination. However, only few studies reported on the subsequent consequences of altered mRNA expression profiles by TFEB for the synthesis of lysosomal and autophagy-related proteins and the significance for the homeostasis of lysosomes. Common biochemical approaches (e.g. western blotting of cell extracts or immunofluorescence microscopy) are not suitable to answer this question. First to follow the kinetics, transport and maturation of newly synthesized lysosomal proteins need sensitive experimental approaches such as radioactive pulse-chase labelling followed by immunoprecipitation of distinct proteins from cultured (Kollman et al., 2013) or non-radioactive click-labelling of proteins (Ignacio et al., 2023). Second, the 70 lysosomal hydrolases are characterized by different half-lives, and third, the lysosomal enzymes are low abundancy proteins. Thus, here the dependency of almost all newly synthesized lysosomal enzymes of mannose 6-phosphate (M6P) modifications for efficient sorting in the TGN mediated by M6P receptors (MPRs) was used for an experimental approach combined with MS analysis. This approach is based on the addition of the weak base NH_4Cl during the 24h TFEB-wt and -K3R induction period to the medium which increases the pH in all acidic compartments and prevents the low-pH-dependent dissociation of MPR-newly synthesized M6P containing ligands in endosomes (Bräulke et al., 2023). Subsequently ligand occupied

MPR recycle back to the TGN and newly synthesized lysosomal enzymes cannot bind further to MPR and are missorted into the medium.

The MS analysis of the soluble, lysosomal secretome upon TFEB expression revealed a weak and moderate increase of lysosomal hydrolases which does not correlate with the transcript level of their coding genes mediated by TFEB.

The direct comparison between the lysosomal protein secretome data and the TFEB transcriptome by RNA sequencing, identified both acid ceramidase and the cathepsin D protease increased in their abundance similarly to the gene-activation level, while other up-regulated genes coding for lysosomal hydrolases (e.g. *GNS*, *HEXA*) were not detected in the proteome analysis, suggesting differential kinetics between gene activation and protein translation. Epitranscriptomic modifications, such as N6-methyladenosine (m6A), 5-methylcytosine (m5C), or N7-methylguanosine (m7G), regulate RNA transcription and translation, processes by affecting mRNA stability, splicing events, or the initiation of translation (Sun et al., 2023). No study addresses the role of transcriptional modifications (such as m6A) on transcripts of lysosomal hydrolases which might uncover novel insight into the regulatory mechanisms of translation of lysosomal proteins and the existence of cell type-dependent subpopulations of lysosomes with variable compositions of hydrolases, transporter, mTORC1-related and associated ubiquitin ligases (Akter et al., 2023). Of note, recently two m6A-modifications in the 3'-UTR of TFEB mRNA have been described upon hypoxia-treated cardiomyocytes which decreases the TFEB mRNA stability. Moreover, the downregulation of the METTL3 methyltransferase responsible for the m6A-modification of TFEB mRNA results in a 3- to 4-fold higher transcription of six TFEB target genes and enhances the autophagic flux (Song et al., 2019).

However, elevated level of only 18 out of ~70 known lysosomal hydrolases are found upon TFEB expression that raised the question whether these changes significantly alters the lysosome proteome and have an impact on lysosomal biogenesis in steady-state conditions (nutrient-rich condition).

4.4.1 Transmembrane shedding after TFEB expression

Among the peptides of lysosomal enzymes-detected in the secretome several soluble domains of transmembrane proteins (e.g. SPRING, GPMNB) has been identified. The extracellular domain cleavage is a post-translational modification which alters both the extracellular environment by modifying the ECM, and the plasma membrane composition by limited proteolysis of surface receptors/adhesion molecules (Shirakabe et al., 2017). The shedding is

mostly executed by members of a **disintegrin and metalloprotease (ADAM)** family of metalloproteases, but also by other proteases such as a **disintegrin and metalloprotease with thrombospondin type I motifs (ADAMTs)**, and by **proprotein convertases (PCs)** family members along the secretory pathway (Rose et al., 2021; Jaacks and Bernasconi, 2017).

Among the soluble-fragments found in the MS data set, **SPRING** soluble-domain were increased upon -K3R activation but not in TFEB-wt expressing cells. **SPRING** is a TFEB-target gene (Palmieri et al., 2011), and the protein is normally found intracellularly as a glycosylated Golgi-resident membrane protein, and recent discoveries suggest that is cleaved by **site-1 protease (S1P)** and secreted (Keshishian et al., 2015; Pernemalm et al., 2019; Loregger et al., 2020). Since neither the *SPRING* nor *S1P* gene were found to be upregulated upon TFEB-K3R induction, we hypothesise that the amount of the soluble **SPRING** fragment is caused by the increase of proteolytic activity of **S1P**.

Another soluble-domain identified is the transmembrane type I **glycoprotein non-metastatic protein B (GPNMB)**, of unknown function, that contains in the extracellular GPNMB domain 12 N-glycosylation sites (Maric et al., 2013). The GPNMB-promoter region is used as TFEB transcriptional activity marker, and it has been described as one of the most elevated TFEB target gene (Gambardella et al., 2020; Sambri et al., 2023). However, also TFE3, MiTF, and another transcription factors which do not belong to the MiTF family, called MAF-oncogene protein family 4 (MAFK4), are involved in GPNMB activation (Tsou et al., 2020). The soluble GPNMB domain is shedded by ADAM10 (Rose et al., 2010), and the soluble fragment is an emerging diagnostic marker for cancer progression (Murugesan et al., 2018), and for neurodegenerative disorders (Moloney et al., 2018). Although there is no direct evidence on the relationship between GPNMB and lysosome functions, the soluble GPNMB fragment has been suggest as diagnostic marker for the lysosome disorders Niemann-Pick type A, B and C1 (Eskes et al., 2023; Rodriguez-Gil et al., 2021), and Gaucher disease (van der Lienden et al., 2018; Eskes et al., 2023) which have in common the storage of different lipids (sphingomyelin, non-esterified cholesterol, glucosylceramide).

GPNMB transcript and protein are both upregulated upon TFEB-wt expression and by treatment of cells with NH_4Cl intracellularly and as soluble GPNMB fragment in the conditioned medium (Fig. 3.19). Since NH_4Cl treatment inhibits the M6P-dependent targeting of newly synthesized lysosomal enzymes to lysosomes and leads in parallel to non-functional lysosomes (due to the alkaline lysosomal pH). It is likely that the lysosomal accumulation of small amounts of variable non-degraded lipids results in lysosome-nucleus-signalling and fast upregulation of the GPNMB 'lipid sensor'. This is supported by preliminary data observed in

HeLa cells with CRISPR-targeted *GNPT*-deficiency (loss of M6P-modification of lysosomal enzymes resembling the human disease mucopolidosis type II; Braulke et al., 2023). Both intracellular and cleaved soluble GPNMB domains are highly elevated, but here independent of the TFEB re-expression (Fig. 3.19).

5. Summary

Lysosome degradative functions depend on ~ 70 lysosomal hydrolases and accessory proteins, as well as ~ 250 integral membrane proteins. The transcription factor EB (TFEB) has been described as the master regulator of lysosome biogenesis and autophagy. TFEB activity depends on its subcellular localization modulated by posttranslational modifications. mTORC1-mediated phosphorylation sequesters TFEB in the cytosol. We have identified seven conserved acetylated lysine residues (K116, K237, K256, K264, K274, K279 and K430) of TFEB in the cytoplasm of HeLa cells by MS analysis. *In-silico* modeling of dimeric human TFEB revealed that non-acetylated lysine residues K237, K256, K274 are directly involved in the binding of DNA. To examine the role of these acetylation sites for TFEB function, two main cell model systems have been generated in which K237, K256, K274 were replaced by alanine (K3A; acetylation-mimetic) or arginine (K3R; non-acetylated-mimetic GFP-TFEB)) and stably expressed in Tet3G HeLa cells in a doxycycline inducible manner. The experiments performed in the presented thesis provide novel insights on the role of TFEB acetylation:

- TFEB-K3A, but not K3R, is retained in the cytoplasm, even in combination with the simultaneous substitution of mTORC1 phosphorylation sites S142 and S211 by alanine (S142/211A). K274 seems to be the main acetylated residue and TFEB K274A is partially retained in the cytoplasm, but K237/274A is sufficient for complete sequestration of TFEB.
- RNA sequencing under two conditions of TFEB expression revealed significant changes of several thousand mRNAs, among them 190 known TFEB targets including 23 lysosome- and autophagy-related genes. The gene expression profile activated by K3R is reduced and differs strongly from wild-type TFEB suggesting that i) TFEB translocation into the nucleus results in secondary regulation of numerous genes, and ii) the K-to-R exchange reduces the recognition of CLEAR-motifs in the promotor of TFEB target genes.
- MS-based analysis identified an increase of 18 newly synthesized lysosomal enzymes and accessory proteins during TFEB induction for 24 h, but only one by K3R.

In conclusion, acetylation of TFEB has been identified as a dominant cytoplasmic retention signal and represents a new fine-tuning level to control its nuclear translocation. Furthermore, TFEB is one regulatory factor for the biogenesis of lysosomes and autophagy depending on posttranslational modifications which are catalyzed by upstream cellular stress-sensing pathways involved in a complex interacting network to maintain cellular homeostasis.

Zusammenfassung

Die degradativen Funktionen der Lysosomen hängen von ~70 lysosomalen Hydrolasen und akzessorischen Proteinen sowie von ~250 integralen Membranproteinen ab. Der Transkriptionsfaktor EB (TFEB) wird als Master-Regulator der Biogenese von Lysosomen und der Autophagie angesehen. Die Aktivität von TFEB hängt von seiner subzellulären Lokalisierung ab, welche durch posttranslationale Modifikationen moduliert wird. Die mTORC1 vermittelte Phosphorylierung sequestriert TFEB im Cytosol. Wir haben sieben konservierte acetylierte Lysinreste (K116, K237, K256, K264, K274, K279 und K430) im TFEB im cytoplasmatischen TFEB von HeLa-Zellen durch MS-Analyse identifiziert. *In silico* Modellierung von menschlichem TFEB zeigte, dass die nicht acetylierten Lysinreste K237, K256 und K274 direkt an der Bindung von DNA beteiligt sind. Um die Rolle dieser acetylierten Reste für die TFEB Funktion zu untersuchen, wurden zwei Zellmodelle generiert, bei denen K237, K256 und K274 durch Alanin (K3A; Acetylierungs-Mimetikum) oder Arginin (K3R; Deacetylierungs-Mimetikum) im GFP-TFEB ersetzt und stabil und Doxycyclin-induzierbar in Tet3G HeLa-Zellen exprimiert. Die in der vorliegenden Arbeit durchgeführten Experimente führten zu folgenden neuen Erkenntnissen:

- TFEB-K3A, aber nicht K3R, wird im Cytoplasma zurückgehalten, auch in Kombination mit gleichzeitiger Alanin-Substitution der mTORC1 Phosphorylierungs-stellen (S142/211A). K274 ist der hauptsächlich acetylierte Rest und TFEB-K274A wird partiell, ein zweiter Austausch (K237/274A) wird vollständig sequestriert
- Die RNA-Sequenzierung unter zwei TFEB Expressionsbedingungen zeigte signifikante Veränderungen von mehreren tausend mRNAs, unter denen 190 bekannte TFEB-aktivierte Transkripte einschließlich von 23 Lysosomen/Autophagie-Genen waren. Die durch K3R aktivierten Genprofile waren geringer und unterschieden sich stark von dem TFEB-Wildtyp Profil. Das zeigt, dass 1. die Translokation von TFEB in den Kern direkt und sekundär zahlreiche Gene reguliert, und 2. Der K-R-Austausch die Erkennbarkeit von CLEAR-Motiven im Promotor von TFEB-Zielgenen reduziert.
- MS-basierte Analyse identifizierten 18 neu synthetisierte lysosomale Enzyme während der 24-stündigen Induktion von TFEB, aber nur ein Enzym durch K3R.

Zusammengefasst wurde die Acetylierung von TFEB als ein dominantes, cytoplasmatisches Retentionssignal identifiziert, das eine neue Ebene der Feinregulation zur Kontrolle der Kerntranslokation darstellt. Weiterhin ist TFEB ein regulatorischer Faktor für die Biogenese von Lysosomen und der Autophagie, der von posttranslationalen Modifikationen abhängt, die

von vorausgehenden zellulären Stress-Signalen gesteuert werden, die in einem komplexen Netzwerk integriert sind, um die zelluläre Homeöostase zu gewährleisten.

6. Abbreviation and Supplementary Tables

3D	three-dimensional
4EBP1	4E-binding protein 1
ACAT1	acetyl-CoA acetyltransferase 1
ACP5	lysosomal tartrate-resistant acid phosphatase
ACTB	actin
AD	activation domain
ADAM	a disintegrin and metalloprotease
ADAMTs	a disintegrin and metalloprotease with thrombospondin type I motifs
ALR	autophagosome-lysosome reformation
AMPK	AMP-activated kinase
bHLH-Zip	helix-loop-helix leucine zipper
BRD4	bromodomain-containing protein 4
CaN	calcineurin
CASTOR	arginine sensor
CLEAR	Coordinated Lysosomal Enhancement And Regulation
CRM-1	exportin-1
CTSB	cathepsin B
CTSS	cathepsin S
DBD	DNA binding domain
DEGs	differentially expressed genes
eIF2B	eukaryotic translation initiation factor
ELP3	elongator subunit 3
FLCN:FNIP1/2	folliculin:folliculin-interacting protein1/2
GATOR1	GAP towards Rags 1
GBA	β -glucocerebrosidase
GNPDA1	glucosamine-6-phosphate isomerase 1
GNPTAB	N-Acetylglucosamine-1-Phosphate Transferase Subunits α And β
GO	Gene Ontology
GPNMB	transmembrane type I glycoprotein non-metastatic protein B
GRB10	insulin receptor-binding protein
GSK3b	glycogen synthase kinase-3 β
HCT116	human colon cancer
HDAC2	histone-deacetylases 2
IPMK	inositol polyphosphate multikinase
IRS1	insulin receptor substrate 1
ISR	integrated stress response
LSDs	lysosomal storage disorders
m5C	5-methylcytosine
m6A	N6-methyladenosine
M6P	mannose 6-phosphate
m7G	N7-methylguanosine
MAFK4	MAF-oncogene protein family 4

MAP4K3	mitogen-activated protein kinase 3
MCOLN1	Mucolipin, TRP Cation Channel 1
MiT/TFE	microphthalmia/transcription factor E
mLST8	mammalian lethal with SEC13 protein 8
MLX	Max-like protein X
MPR	mannose 6-phosphate receptors
MPS	mucopolysaccharidoses
MS	mass-spectrometry
mSIN1	mammalian stress-activated map kinase-interacting protein 1
mTOR	mechanistic target of rapamycin
mTORC1	mTOR complex-1
NES	Nuclear Export Signal
NLS	Nuclear Localization Signal
PCA	principal component analyses
PCs	proprotein convertases
PRAS40	proline-rich AKT1 substrate 1
PSAP	pro-saposin
PTMs	posttranslational modifications
RAPTOR	Regulatory-associated protein of mTOR
RICTOR	rapamycin-insensitive companion of mTOR
S1P	site-1 protease
SAHA	suberoylanilide hydroxamic acid
SAM	S-adenosylmethionine
SGK1	serine/threonine-protein kinase
SIRT-1	sirtuin-1
STAT3	signal transducer and activator of transcription 3
STUB1	E3 ubiquitin ligase
TGN	trans Golgi network
TSA	trichostatin A
TSC	Tuberous Sclerosis Complex
ULK1	unc51-like autophagy activating kinase 1
WIPI1	autophagy-related WD repeat domain phosphoinositide-interacting protein 1
ZKSCAN3	zinc-finger transcription factor

Table S1: K3-to-alanine exchanges impair phosphorylation of TFEB at S211

	TFEB-wt		TFEB-K3A	
	cytoplasm	nucleus	cytoplasm	nucleus
TFEB protein	38.4 ^a ± 18.4	61.6 ± 18.4	82.1 ^a ± 11.0	17.9 ± 11.0
TFEB-pS142	47.0 ± 22.8 (1.2) ^b	53.0 ± 22.8 (0.9)	96.2 ± 4.4 (1.2) ^b	3.8 ± 4.4 (0.2)
TFEB-pS211	79.8 ± 13.7 (2.1)	20.2 ± 13.7 (0.3)	99.8 ± 0.4 (1.2)	0.2 ± 0.4 (-)

^a) mean percentage of total immunoreactivity in cytoplasm and nuclear fraction (n = 3-7)

^b) in brackets the pS/TFEB protein ratio

Table S2: α -L-Fucosidase, α -mannosidase, and β -hexosaminidase activities in cells and media of TFEB-wt and -K3R expressing cells after 3h dox + 21h chase in dox-free medium. Cell extract and concentrated media were used. Mean values are shown of enzyme assay specific activity for conditioned media [mU/ml] or cell extract [mU/mg]. The enzyme activities of non-induced HeLa TO cells were used as control and set to 1.

	Media		Cell extract	
	wt	K3R	wt	K3R
α -L-fucosidase (n=3)	0.72 ± 0.06	0.41 ± 0.13	0.68 ± 0.08	0.44 ± 0.22
β -galactosidase (n=2)	0.49 ± 0.05	0.50 ± 0.09	0.63 ± 0.07	0.61 ± 0.14
α -mannosidase (n=3)	0.42 ± 0.03	0.48 ± 0.21	1.26 ± 0.14	0.77 ± 0.23
β -hexosaminidase (n=2-3)	0.45 ± 0.01	0.49 ± 0.06	0.67 ± 0.01	0.74 ± 0.06

7. Bibliography

Akter F, Bonini S, Ponnaiyan S, Kögler-Mohrbacher B, Bleibaum F, Damme M, Renard BY, Winter D. Multi-Cell Line Analysis of Lysosomal Proteomes Reveals Unique Features and Novel Lysosomal Proteins. *Mol Cell Proteomics*. 2023 Mar;22(3):100509. doi: 10.1016/j.mcpro.2023.100509. Epub 2023 Feb 14. PMID: 36791992; PMCID: PMC10025164.

Annunziata I, van de Vlekkert D, Wolf E, Finkelstein D, Neale G, Machado E, Mosca R, Campos Y, Tillman H, Roussel MF, Andrew Weesner J, Ellen Fremuth L, Qiu X, Han MJ, Grosveld GC, d'Azzo A. MYC competes with MiT/TFE in regulating lysosomal biogenesis and autophagy through an epigenetic rheostat. *Nat Commun*. 2019 Aug 9;10(1):3623. doi: 10.1038/s41467-019-11568-0. PMID: 31399583; PMCID: PMC6689058.

Bajaj L, Lotfi P, Pal R, Ronza AD, Sharma J, Sardiello M. Lysosome biogenesis in health and disease. *J Neurochem*. 2019 Mar;148(5):573-589. doi: 10.1111/jnc.14564. Epub 2018 Oct 18. PMID: 30092616; PMCID: PMC6368902.

Ballabio A, Bonifacino JS. Lysosomes as dynamic regulators of cell and organismal homeostasis. *Nat Rev Mol Cell Biol*. 2020 Feb;21(2):101-118. doi: 10.1038/s41580-019-0185-4. Epub 2019 Nov 25. PMID: 31768005.

Bao J, Zheng L, Zhang Q, Li X, Zhang X, Li Z, Bai X, Zhang Z, Huo W, Zhao X, Shang S, Wang Q, Zhang C, Ji J. Deacetylation of TFEB promotes fibrillar A β degradation by upregulating lysosomal biogenesis in microglia. *Protein Cell*. 2016 Jun;7(6):417-33. doi: 10.1007/s13238-016-0269-2. Epub 2016 May 21. PMID: 27209302; PMCID: PMC4887328.

Battaglioni S, Benjamin D, Wälchli M, Maier T, Hall MN. mTOR substrate phosphorylation in growth control. *Cell*. 2022 May 26;185(11):1814-1836. doi: 10.1016/j.cell.2022.04.013. Epub 2022 May 16. PMID: 35580586.

Bahrani A, Bianconi V, Pirro M, Orafari HM, Sahebkar A. The role of TFEB in tumor cell autophagy: Diagnostic and therapeutic opportunities. *Life Sci*. 2020;244:117341.

Bouhamdani N, Comeau D, Turcotte S. A Compendium of Information on the Lysosome. *Front Cell Dev Biol*. 2021 Dec 15;9:798262. doi: 10.3389/fcell.2021.798262. PMID: 34977038; PMCID: PMC8714965.

Braulke T, Carette JE, Palm W. Lysosomal enzyme trafficking: from molecular mechanisms to human diseases. *Trends Cell Biol*. 2023 Jul 18:S0962-8924(23)00128-9. doi: 10.1016/j.tcb.2023.06.005. Epub ahead of print. PMID: 37474375.

Carey KL, Paulus GLC, Wang L, Balce DR, Luo JW, Bergman P, Ferder IC, Kong L, Renaud N, Singh S, Kost-Alimova M, Nyfeler B, Lassen KG, Virgin HW, Xavier RJ. TFEB Transcriptional Responses Reveal Negative Feedback by BHLHE40 and BHLHE41. *Cell Rep*. 2020 Nov 10;33(6):108371. doi: 10.1016/j.celrep.2020.108371. PMID: 33176151; PMCID: PMC7686957.

Cesana M, Tufano G, Panariello F, Zampelli N, Ambrosio S, De Cegli R, Mutarelli M, Vaccaro L, Ziller MJ, Cacchiarelli D, Medina DL, Ballabio A. EGR1 drives cell proliferation by directly stimulating TFEB transcription in response to starvation. *PLoS Biol.* 2023 Mar 8;21(3):e3002034. doi: 10.1371/journal.pbio.3002034. PMID: 36888606; PMCID: PMC9994711.

Chauhan S, Goodwin JG, Chauhan S, Manyam G, Wang J, Kamat AM, Boyd DD. ZKSCAN3 is a master transcriptional repressor of autophagy. *Mol Cell.* 2013 Apr 11;50(1):16-28. doi: 10.1016/j.molcel.2013.01.024. Epub 2013 Feb 21. PMID: 23434374; PMCID: PMC3628091.

Chen D, Wang Z, Zhao YG, Zheng H, Zhao H, Liu N, Zhang H. Inositol Polyphosphate Multikinase Inhibits Liquid-Liquid Phase Separation of TFEB to Negatively Regulate Autophagy Activity. *Dev Cell.* 2020 Dec 7;55(5):588-602.e7. doi: 10.1016/j.devcel.2020.10.010. PMID: 33290695.

Cui Z, Napolitano G, de Araujo MEG, Esposito A, Monfregola J, Huber LA, Ballabio A, Hurley JH. Structure of the lysosomal mTORC1-TFEB-Rag-Ragulator megacomplex. *Nature.* 2023 Feb;614(7948):572-579. doi: 10.1038/s41586-022-05652-7. Epub 2023 Jan 25. PMID: 36697823; PMCID: PMC9931586.

TFEBexplorer: An integrated tool to study genes regulated by the stress-responsive Transcription Factor EBRossella De Ceglia*, Diego Carrellaa*, Diletta Sicilianoa, Gennaro Gambardellaa,b, Gennaro Napolitanoa,c, Chiara Di Maltaa,c, Andrea Ballabioa,c,d,e and Diego di Bernardo

Dauden MI, Jaciuk M, Weis F, Lin TY, Kleindienst C, Abbassi NEH, Khatter H, Krutyholowa R, Breunig KD, Kosinski J, Müller CW, Glatt S. Molecular basis of tRNA recognition by the Elongator complex. *Sci Adv.* 2019 Jul 10;5(7):eaaw2326. doi: 10.1126/sciadv.aaw2326. PMID: 31309145; PMCID: PMC6620098.

Decressac M, Mattsson B, Weikop P, Lundblad M, Jakobsson J, Björklund A. TFEB-mediated autophagy rescues midbrain dopamine neurons from α -synuclein toxicity. *Proc Natl Acad Sci U S A.* 2013 May 7;110(19):E1817-26. doi: 10.1073/pnas.1305623110. Epub 2013 Apr 22. PMID: 23610405; PMCID: PMC3651458.

Deneubourg C, Ramm M, Smith LJ, Baron O, Singh K, Byrne SC, Duchen MR, Gautel M, Eskelinen EL, Fanto M, Jungbluth H. The spectrum of neurodevelopmental, neuromuscular and neurodegenerative disorders due to defective autophagy. *Autophagy.* 2022 Mar;18(3):496-517. doi: 10.1080/15548627.2021.1943177. Epub 2021 Aug 19. PMID: 34130600; PMCID: PMC9037555.

Di Malta C, Cinque L, Settembre C. Transcriptional Regulation of Autophagy: Mechanisms and Diseases. *Front Cell Dev Biol.* 2019 Jul 2;7:114. doi: 10.3389/fcell.2019.00114. PMID: 31312633; PMCID: PMC6614182.

Eskes ECB, van der Lienden MJC, Sjouke B, van Vliet L, Brands MMMG, Hollak CEM, Aerts JMFG. Glycoprotein non-metastatic protein B (GPNMB) plasma values in patients with chronic visceral acid sphingomyelinase deficiency. *Mol Genet Metab.* 2023 Aug;139(4):107631. doi: 10.1016/j.ymgme.2023.107631. Epub 2023 Jul 9. PMID: 37453187.

Franco-Juárez B, Coronel-Cruz C, Hernández-Ochoa B, Gómez-Manzo S, Cárdenas-Rodríguez N, Arreguin-Espinosa R, Bandala C, Canseco-Ávila LM, Ortega-Cuellar D. TFEB; Beyond Its Role as an Autophagy and Lysosomes Regulator. *Cells*. 2022 Oct 7;11(19):3153. doi: 10.3390/cells11193153. PMID: 36231114; PMCID: PMC9562866.

Gambardella G, Staiano L, Moretti MN, De Cegli R, Fagnocchi L, Di Tullio G, Polletti S, Braccia C, Armirrotti A, Zippo A, Ballabio A, De Matteis MA, di Bernardo D. GADD34 is a modulator of autophagy during starvation. *Sci Adv*. 2020 Sep 25;6(39):eabb0205. doi: 10.1126/sciadv.abb0205. PMID: 32978159; PMCID: PMC7518873.

Hemesath TJ, Steingrímsson E, McGill G, Hansen MJ, Vaught J, Hodgkinson CA, Arnheiter H, Copeland NG, Jenkins NA, Fisher DE. microphthalmia, a critical factor in melanocyte development, defines a discrete transcription factor family. *Genes Dev*. 1994 Nov 15;8(22):2770-80. doi: 10.1101/gad.8.22.2770. PMID: 7958932.

Hiesberger T, Hüttler S, Rohlmann A, Schneider W, Sandhoff K, Herz J. Cellular uptake of saposin (SAP) precursor and lysosomal delivery by the low density lipoprotein receptor-related protein (LRP). *EMBO J*. 1998 Aug 17;17(16):4617-25. doi: 10.1093/emboj/17.16.4617. PMID: 9707421; PMCID: PMC1170791.

Hook V, Yoon M, Mosier C, Ito G, Podvin S, Head BP, Rissman R, O'Donoghue AJ, Hook G. Cathepsin B in neurodegeneration of Alzheimer's disease, traumatic brain injury, and related brain disorders. *Biochim Biophys Acta Proteom*. 2020 Aug;1868(8):140428. doi: 10.1016/j.bbapap.2020.140428. Epub 2020 Apr 17. PMID: 32305689; PMCID: PMC7261628.

Hsu CL, Lee EX, Gordon KL, Paz EA, Shen WC, Ohnishi K, Meisenhelder J, Hunter T, La Spada AR. MAP4K3 mediates amino acid-dependent regulation of autophagy via phosphorylation of TFEB. *Nat Commun*. 2018 Mar 5;9(1):942. doi: 10.1038/s41467-018-03340-7. PMID: 29507340; PMCID: PMC5838220.

Ignacio BJ, Dijkstra J, Mora N, Slot EFJ, van Weijsten MJ, Storkebaum E, Vermeulen M, Bongers KM. THRONCAT: metabolic labeling of newly synthesized proteins using a bioorthogonal threonine analog. *Nat Commun*. 2023 Jun 8;14(1):3367. doi: 10.1038/s41467-023-39063-7. PMID: 37291115; PMCID: PMC10250548.

Jaaks P, Bernasconi M. The proprotein convertase furin in tumour progression. *Int J Cancer*. 2017 Aug 15;141(4):654-663. doi: 10.1002/ijc.30714. Epub 2017 May 15. PMID: 28369813.

Kendall RL, Holian A. The role of lysosomal ion channels in lysosome dysfunction. *Inhal Toxicol*. 2021 Feb;33(2):41-54. doi: 10.1080/08958378.2021.1876188. Epub 2021 Feb 25. PMID: 33627009.

Keshishian H, Burgess MW, Gillette MA, Mertins P, Clauser KR, Mani DR, Kuhn EW, Farrell LA, Gerszten RE, Carr SA. Multiplexed, Quantitative Workflow for Sensitive Biomarker Discovery in Plasma Yields Novel Candidates for Early Myocardial Injury. *Mol Cell Proteomics*. 2015 Sep;14(9):2375-93. doi: 10.1074/mcp.M114.046813. Epub 2015 Feb 27. PMID: 25724909; PMCID: PMC4563722.

Kollmann K, Pestka JM, Kühn SC, Schöne E, Schweizer M, Karkmann K, Otomo T, Catala-Lehnen P, Failla AV, Marshall RP, Krause M, Santer R, Amling M, Bräulke T, Schinke T. Decreased bone formation and increased osteoclastogenesis cause bone loss in mucopolidosis II. *EMBO Mol Med*. 2013 Dec;5(12):1871-86. doi: 10.1002/emmm.201302979. Epub 2013 Oct 15. PMID: 24127423; PMCID: PMC3914524.

Lambert SA, Jolma A, Campitelli LF, Das PK, Yin Y, Albu M, Chen X, Taipale J, Hughes TR, Weirauch MT. The Human Transcription Factors. *Cell*. 2018 Feb 8;172(4):650-665. doi: 10.1016/j.cell.2018.01.029. Erratum in: *Cell*. 2018 Oct 4;175(2):598-599. PMID: 29425488.

Li Y, Xu M, Ding X, Yan C, Song Z, Chen L, Huang X, Wang X, Jian Y, Tang G, Tang C, Di Y, Mu S, Liu X, Liu K, Li T, Wang Y, Miao L, Guo W, Hao X, Yang C. Protein kinase C controls lysosome biogenesis independently of mTORC1. *Nat Cell Biol*. 2016 Oct;18(10):1065-77. doi: 10.1038/ncb3407. Epub 2016 Sep 12. PMID: 27617930.

Li L, Friedrichsen HJ, Andrews S, et al. A TFEB nuclear export signal integrates amino acid supply and glucose availability. *Nat Commun* 2018;9:2685.

Li T, Yin L, Kang X, Xue W, Wang N, Zhang J, Yuan P, Lin L, Li Y. TFEB acetylation promotes lysosome biogenesis and ameliorates Alzheimer's disease-relevant phenotypes in mice. *J Biol Chem*. 2022 Dec;298(12):102649. doi: 10.1016/j.jbc.2022.102649. Epub 2022 Oct 27. PMID: 36441024; PMCID: PMC9694136.

Loregger A, Raaben M, Nieuwenhuis J, Tan JME, Jae LT, van den Hengel LG, Hendrix S, van den Berg M, Scheij S, Song JY, Huijbers IJ, Kroese LJ, Ottenhoff R, van Weeghel M, van de Sluis B, Brummelkamp T, Zelcer N. Haploid genetic screens identify SPRING/C12ORF49 as a determinant of SREBP signaling and cholesterol metabolism. *Nat Commun*. 2020 Feb 28;11(1):1128. doi: 10.1038/s41467-020-14811-1. PMID: 32111832; PMCID: PMC7048761

Maric G, Rose AA, Annis MG, Siegel PM. Glycoprotein non-metastatic b (GPNMB): A metastatic mediator and emerging therapeutic target in cancer. *Onco Targets Ther*. 2013 Jul 9;6:839-52. doi: 10.2147/OTT.S44906. PMID: 23874106; PMCID: PMC3711880.

Martina JA, Chen Y, Gucsek M, Puertollano R. mTORC1 functions as a transcriptional regulator of autophagy by preventing nuclear transport of TFEB. *Autophagy*. 2012 Jun;8(6):903-14. doi: 10.4161/auto.19653. Epub 2012 May 11. PMID: 22576015; PMCID: PMC3427256.

Martina JA, Puertollano R. Rag GTPases mediate amino acid-dependent recruitment of TFEB and MITF to lysosomes. *J Cell Biol*. 2013 Feb 18;200(4):475-91. doi: 10.1083/jcb.201209135. Epub 2013 Feb 11. PMID: 23401004; PMCID: PMC3575543.

Martina, J.A., Diab, H.I., Lishu, L., Jeong-A, L., Patange, S., Raben, N., and Puertollano, R. (2014). The nutrient-responsive transcription factor TFE3 promotes autophagy, lysosomal biogenesis, and clearance of cellular debris. *Sci. Signal*. 7, ra9

Martínez-Fábregas J, Tamargo-Azpilicueta J, Diaz-Moreno I. Lysosomes: multifunctional compartments ruled by a complex regulatory network. *FEBS Open Bio*. 2022 Apr;12(4):758-774. doi: 10.1002/2211-5463.13387. Epub 2022 Mar 8. PMID: 35218162; PMCID: PMC8972048.

Martínez-Fábregas J, Prescott A, van Kasteren S, Pedrioli DL, McLean I, Moles A, Reinheckel T, Poli V, Watts C. Lysosomal protease deficiency or substrate overload induces an oxidative-stress mediated STAT3-dependent pathway of lysosomal homeostasis. *Nat Commun*. 2018 Dec 17;9(1):5343. doi: 10.1038/s41467-018-07741-6. PMID: 30559339; PMCID: PMC6297226.

Medina DL, Fraldi A, Bouche V, Annunziata F, Mansueto G, Spampanato C, Puri C, Pignata A, Martina JA, Sardiello M, Palmieri M, Polishchuk R, Puertollano R, Ballabio A. Transcriptional activation of lysosomal exocytosis promotes cellular clearance. *Dev Cell*. 2011 Sep 13;21(3):421-30. doi: 10.1016/j.devcel.2011.07.016. Epub 2011 Sep 1. PMID: 21889421; PMCID: PMC3173716.

Medina DL, Di Paola S, Peluso I, Armani A, De Stefani D, Venditti R, et al. Lysosomal calcium signalling regulates autophagy through calcineurin and TFEB. *Nat Cell Biol*. 2015;17:288–99.

McGlinchey RP, Lacy SM, Walker RL 3rd, Lee JC. Cathepsin K is a potent disaggregase of α -synuclein fibrils. *Biochem Biophys Res Commun*. 2020 Sep 3;529(4):1106-1111. doi: 10.1016/j.bbrc.2020.06.155. Epub 2020 Jul 31. PMID: 32819572; PMCID: PMC7478362.

Möller K, Sigurbjornsdottir S, Arnthorsson AO, Pogenberg V, Dilshat R, Fock V, Brynjolfsdottir SH, Bindesboll C, Bessadottir M, Ogmundsdottir HM, Simonsen A, Larue L, Wilmanns M, Thorsson V, Steingrímsson E, Ogmundsdottir MH. MITF has a central role in regulating starvation-induced autophagy in melanoma. *Sci Rep*. 2019 Jan 31;9(1):1055. doi: 10.1038/s41598-018-37522-6. PMID: 30705290; PMCID: PMC6355916.

Moloney EB, Moskites A, Ferrari EJ, Isacson O, Hallett PJ. The glycoprotein GPNMB is selectively elevated in the substantia nigra of Parkinson's disease patients and increases after lysosomal stress. *Neurobiol Dis*. 2018 Dec;120:1-11. doi: 10.1016/j.nbd.2018.08.013. Epub 2018 Aug 24. PMID: 30149180; PMCID: PMC6748034.

Munson MJ, Allen GF, Toth R, Campbell DG, Lucocq JM, Ganley IG. mTOR activates the VPS34-UVRAG complex to regulate autolysosomal tubulation and cell survival. *EMBO J*. 2015 Sep 2;34(17):2272-90. doi: 10.15252/embj.201590992. Epub 2015 Jul 2. PMID: 26139536; PMCID: PMC4585463.

Murugesan V, Liu J, Yang R, Lin H, Lischuk A, Pastores G, Zhang X, Chuang WL, Mistry PK. Validating glycoprotein non-metastatic melanoma B (gpNMB, osteoactivin), a new biomarker of Gaucher disease. *Blood Cells Mol Dis*. 2018 Feb;68:47-53. doi: 10.1016/j.bcmd.2016.12.002. Epub 2016 Dec 13. PMID: 28003098; PMCID: PMC5468511.

Napolitano G, Esposito A, Choi H, Matarese M, Benedetti V, Di Malta C, Monfregola J, Medina DL, Lippincott-Schwartz J, Ballabio A. mTOR-dependent phosphorylation controls TFEB nuclear export. *Nat Commun*. 2018 Aug 17;9(1):3312. doi: 10.1038/s41467-018-05862-6. PMID: 30120233; PMCID: PMC6098152.

Napolitano G, Di Malta C, Ballabio A. Non-canonical mTORC1 signaling at the lysosome. *Trends Cell Biol*. 2022 Nov;32(11):920-931. doi: 10.1016/j.tcb.2022.04.012. Epub 2022 May 30. PMID: 35654731.

Palmieri M, Impey S, Kang H, di Ronza A, Pelz C, Sardiello M, Ballabio A. Characterization of the CLEAR network reveals an integrated control of cellular clearance pathways. *Hum Mol Genet.* 2011 Oct 1;20(19):3852-66. doi: 10.1093/hmg/ddr306. Epub 2011 Jul 13. PMID: 21752829.

Paquette M, El-Houjeiri L, C Zirden L, Puustinen P, Blanchette P, Jeong H, Dejgaard K, Siegel PM, Pause A. AMPK-dependent phosphorylation is required for transcriptional activation of TFEB and TFE3. *Autophagy.* 2021 Dec;17(12):3957-3975. doi: 10.1080/15548627.2021.1898748. Epub 2021 Mar 18. PMID: 33734022; PMCID: PMC8726606.

Park JY, Sohn HY, Koh YH, Jo C. A splicing variant of TFEB negatively regulates the TFEB-autophagy pathway. *Sci Rep.* 2021 Oct 26;11(1):21119. doi: 10.1038/s41598-021-00613-y. PMID: 34702966; PMCID: PMC8548335.

Pernemalm M, Sandberg A, Zhu Y, Boekel J, Tamburro D, Schwenk JM, Björk A, Wahren-Herlenius M, Åmark H, Östenson CG, Westgren M, Lehtiö J. In-depth human plasma proteome analysis captures tissue proteins and transfer of protein variants across the placenta. *Elife.* 2019 Apr 8;8:e41608. doi: 10.7554/eLife.41608. PMID: 30958262; PMCID: PMC6519984.

Ploper D, Taelman VF, Robert L, Perez BS, Titz B, Chen HW, Graeber TG, von Euw E, Ribas A, De Robertis EM. MITF drives endolysosomal biogenesis and potentiates Wnt signaling in melanoma cells. *Proc Natl Acad Sci U S A.* 2015 Feb 3;112(5):E420-9. doi: 10.1073/pnas.1424576112. Epub 2015 Jan 20. PMID: 25605940; PMCID: PMC4321275.

Platt FM, d'Azzo A, Davidson BL, Neufeld EF, Tifft CJ. Lysosomal storage diseases. *Nat Rev Dis Primers.* 2018 Oct 1;4(1):27. doi: 10.1038/s41572-018-0025-4. Erratum in: *Nat Rev Dis Primers.* 2018 Oct 18;4(1):36. Erratum in: *Nat Rev Dis Primers.* 2019 May 17;5(1):34. PMID: 30275469.

Pogenberg V, Ogmundsdóttir MH, Bergsteinsdóttir K, Schepsky A, Phung B, Deineko V, Milewski M, Steingrímsson E, Wilmanns M. Restricted leucine zipper dimerization and specificity of DNA recognition of the melanocyte master regulator MITF. *Genes Dev.* 2012 Dec 1;26(23):2647-58. doi: 10.1101/gad.198192.112. PMID: 23207919; PMCID: PMC3521630.

Puertollano R, Ferguson SM, Brugarolas J, Ballabio A. The complex relationship between TFEB transcription factor phosphorylation and subcellular localization. *EMBO J.* 2018 Jun 1;37(11):e98804. doi: 10.15252/embj.201798804. Epub 2018 May 15. PMID: 29764979; PMCID: PMC5983138.

Qian M, Sleat DE, Zheng H, Moore D, Lobel P. Proteomics analysis of serum from mutant mice reveals lysosomal proteins selectively transported by each of the two mannose 6-phosphate receptors. *Mol Cell Proteomics.* 2008 Jan;7(1):58-70. doi: 10.1074/mcp.M700217-MCP200. Epub 2007 Sep 11. PMID: 17848585.

Reczek D, Schwake M, Schröder J, Hughes H, Blanz J, Jin X, Brondyk W, Van Patten S, Edmunds T, Saftig P. LIMP-2 is a receptor for lysosomal mannose-6-phosphate-independent targeting of beta-glucocerebrosidase. *Cell.* 2007 Nov 16;131(4):770-83. doi: 10.1016/j.cell.2007.10.018. PMID: 18022370.

Roczniak-Ferguson A, Petit CS, Froehlich F, Qian S, Ky J, Angarola B, Walther TC, Ferguson SM. The transcription factor TFEB links mTORC1 signaling to transcriptional control of lysosome homeostasis. *Sci Signal*. 2012 Jun 12;5(228):ra42. doi: 10.1126/scisignal.2002790. PMID: 22692423; PMCID: PMC3437338

Rodriguez-Gil JL, Baxter LL, Watkins-Chow DE, Johnson NL, Davidson CD, Carlson SR, Incao AA; NISC Comparative Sequencing Program; Wallom KL, Farhat NY, Platt FM, Dale RK, Porter FD, Pavan WJ. Transcriptome of HP β CD-treated Niemann-Pick disease type C1 cells highlights GPNMB as a biomarker for therapeutics. *Hum Mol Genet*. 2021 Nov 30;30(24):2456-2468. doi: 10.1093/hmg/ddab194. PMID: 34296265; PMCID: PMC8643505.

Rose KWJ, Taye N, Karoulis SZ, Hubmacher D. Regulation of ADAMTS Proteases. *Front Mol Biosci*. 2021 Jun 29;8:701959. doi: 10.3389/fmolb.2021.701959. PMID: 34268335; PMCID: PMC8275829.

Rose AA, Annis MG, Dong Z, Pepin F, Hallett M, Park M, Siegel PM. ADAM10 releases a soluble form of the GPNMB/Osteoactivin extracellular domain with angiogenic properties. *PLoS One*. 2010 Aug 10;5(8):e12093. doi: 10.1371/journal.pone.0012093. PMID: 20711474; PMCID: PMC2919417.

Ryu HY, Kim LE, Jeong H, Yeo BK, Lee JW, Nam H, et al. GSK3B induces autophagy by phosphorylating ULK1. *Exp Mol Med*. 2021;53:369–83.

Sakamaki JI, Wilkinson S, Hahn M, Tasdemir N, O'Prey J, Clark W, Hedley A, Nixon C, Long JS, New M, Van Acker T, Tooze SA, Lowe SW, Dikic I, Ryan KM. Bromodomain Protein BRD4 Is a Transcriptional Repressor of Autophagy and Lysosomal Function. *Mol Cell*. 2017 May 18;66(4):517-532.e9. doi: 10.1016/j.molcel.2017.04.027. PMID: 28525743; PMCID: PMC5446411.

Saftig P, Klumperman J. Lysosome biogenesis and lysosomal membrane proteins: trafficking meets function. *Nat Rev Mol Cell Biol*. 2009 Sep;10(9):623-35. doi: 10.1038/nrm2745. Epub 2009 Aug 12. PMID: 19672277.

Sambri I, Ferniani M, Campostrini G, Testa M, Meraviglia V, de Araujo MEG, Dokládal L, Vilardo C, Monfregola J, Zampelli N, Vecchio Blanco FD, Torella A, Ruosi C, Fecarotta S, Parenti G, Staiano L, Bellin M, Huber LA, De Virgilio C, Trepiccione F, Nigro V, Ballabio A. RagD auto-activating mutations impair MiT/TFE activity in kidney tubulopathy and cardiomyopathy syndrome. *Nat Commun*. 2023 May 15;14(1):2775. doi: 10.1038/s41467-023-38428-2. PMID: 37188688; PMCID: PMC10185561.

Sancak Y, Bar-Peled L, Zoncu R, Markhard AL, Nada S, Sabatini DM. Ragulator-Rag complex targets mTORC1 to the lysosomal surface and is necessary for its activation by amino acids. *Cell*. 2010 Apr 16;141(2):290-303. doi: 10.1016/j.cell.2010.02.024. Epub 2010 Apr 8. PMID: 20381137; PMCID: PMC3024592.

Sardiello M, Palmieri M, di Ronza A, Medina DL, Valenza M, Gennarino VA, Di Malta C, Donaudy F, Embrione V, Polishchuk RS, Banfi S, Parenti G, Cattaneo E, Ballabio A. A gene network regulating lysosomal biogenesis and function. *Science*. 2009 Jul 24;325(5939):473-7. doi: 10.1126/science.1174447. Epub 2009 Jun 25. PMID: 19556463.

Sato S, Roberts K, Gambino G, Cook A, Kouzarides T, Goding CR. CBP/p300 as a co-factor for the Microphthalmia transcription factor. *Oncogene*. 1997 Jun 26;14(25):3083-92. doi: 10.1038/sj.onc.1201298. PMID: 9223672.

Saxton RA, Sabatini DM. mTOR Signaling in Growth, Metabolism, and Disease. *Cell*. 2017 Mar 9;168(6):960-976. doi: 10.1016/j.cell.2017.02.004. Erratum in: *Cell*. 2017 Apr 6;169(2):361-371. PMID: 28283069; PMCID: PMC5394987.

Settembre C, Di Malta C, Polito VA, Arencibia MG, Vetrini F, Erdin S, et al. TFEB links autophagy to lysosomal biogenesis. *Science* 2011; 332:1429–33.

Settembre, C., Zoncu, R., Medina, D.L., Vetrini, F., Erdin, S., Erdin, S., Huynh, T., Ferron, M., Karsenty, G., Vellard, M.C., et al. (2012). A lysosome-to-nucleus signalling mechanism senses and regulates the lysosome via mTOR and TFEB. *EMBO J*. 31, 1095–1108.

Settembre C, De Cegli R, Mansueto G, Saha PK, Vetrini F, Visvikis O, et al. TFEB controls cellular lipid metabolism through a starvation-induced autoregulatory loop. *Nat Cell Biol*. 2013 ;15:647–58.

Sha Y, Rao L, Settembre C, Ballabio A, Eissa NT. STUB1 regulates TFEB-induced autophagy-lysosome pathway. *EMBO J*. 2017 Sep 1;36(17):2544-2552. doi: 10.15252/embj.201796699. Epub 2017 Jul 28. PMID: 28754656; PMCID: PMC5579343.

Shirakabe K, Omura T, Shibagaki Y, Mihara E, Homma K, Kato Y, Yoshimura A, Murakami Y, Takagi J, Hattori S, Ogawa Y. Mechanistic insights into ectodomain shedding: susceptibility of CADM1 adhesion molecule is determined by alternative splicing and O-glycosylation. *Sci Rep*. 2017 Apr 10;7:46174. doi: 10.1038/srep46174. PMID: 28393893; PMCID: PMC5385562.

Slade L, Pulinilkunnil T. The MiTF/TFE Family of Transcription Factors: Master Regulators of Organelle Signaling, Metabolism, and Stress Adaptation. *Mol Cancer Res*. 2017 Dec;15(12):1637-1643. doi: 10.1158/1541-7786.MCR-17-0320. Epub 2017 Aug 29. PMID: 28851811.

Song H, Feng X, Zhang H, Luo Y, Huang J, Lin M, Jin J, Ding X, Wu S, Huang H, Yu T, Zhang M, Hong H, Yao S, Zhao Y, Zhang Z. METTL3 and ALKBH5 oppositely regulate m⁶A modification of *TFEB* mRNA, which dictates the fate of hypoxia/reoxygenation-treated cardiomyocytes. *Autophagy*. 2019 Aug;15(8):1419-1437. doi: 10.1080/15548627.2019.1586246. Epub 2019 Mar 17. PMID: 30870073; PMCID: PMC6613905.

Stevens LM, Sijbesma E, Botta M, MacKintosh C, Obsil T, Landrieu I, Cau Y, Wilson AJ, Karawajczyk A, Eickhoff J, Davis J, Hann M, O'Mahony G, Doveston RG, Brunsveld L, Ottmann C. Modulators of 14-3-3 Protein-Protein Interactions. *J Med Chem*. 2018 May 10;61(9):3755-3778. doi: 10.1021/acs.jmedchem.7b00574. Epub 2017 Oct 19. PMID: 28968506; PMCID: PMC5949722.

Sun Y, Wang H, Qu T, Luo J, An P, Ren F, Luo Y, Li Y. mTORC2: a multifaceted regulator of autophagy. *Cell Commun Signal*. 2023 Jan 5;21(1):4. doi: 10.1186/s12964-022-00859-7. PMID: 36604720; PMCID: PMC9814435.

Sun H, Li K, Liu C, Yi C. Regulation and functions of non-m⁶A mRNA modifications. *Nat Rev Mol Cell Biol*. 2023 Oct;24(10):714-731. doi: 10.1038/s41580-023-00622-x. Epub 2023 Jun 27. PMID: 37369853.

Takla M, Keshri S, Rubinsztein DC. The post-translational regulation of transcription factor EB (TFEB) in health and disease. *EMBO Rep*. 2023 Nov 6;24(11):e57574. doi: 10.15252/embr.202357574. Epub 2023 Sep 20. PMID: 37728021; PMCID: PMC10626434.

Tan A, Prasad R, Lee C, Jho EH. Past, present, and future perspectives of transcription factor EB (TFEB): mechanisms of regulation and association with disease. *Cell Death Differ*. 2022 Aug;29(8):1433-1449. doi: 10.1038/s41418-022-01028-6. Epub 2022 Jun 23. PMID: 35739255; PMCID: PMC9345944.

Tsou PS, Sawalha AH. Glycoprotein nonmetastatic melanoma protein B: A key mediator and an emerging therapeutic target in autoimmune diseases. *FASEB J*. 2020 Jul;34(7):8810-8823. doi: 10.1096/fj.202000651. Epub 2020 May 23. PMID: 32445534; PMCID: PMC7501235.

Vara-Ciruelos D, Russell FM, Hardie DG. The strange case of AMPK and cancer: Dr Jekyll or Mr Hyde? [†]. *Open Biol*. 2019 Jul 26;9(7):190099. doi: 10.1098/rsob.190099. Epub 2019 Jul 10. PMID: 31288625; PMCID: PMC6685927.

van der Lienden MJC, Gaspar P, Boot R, Aerts JMFG, van Eijk M. Glycoprotein Non-Metastatic Protein B: An Emerging Biomarker for Lysosomal Dysfunction in Macrophages. *Int J Mol Sci*. 2018 Dec 24;20(1):66. doi: 10.3390/ijms20010066. PMID: 30586924; PMCID: PMC6337583.

Vega-Rubin-de-Celis S, Peña-Llopis S, Konda M, Brugarolas J. Multistep regulation of TFEB by MTORC1. *Autophagy*. 2017 Mar 4;13(3):464-472. doi: 10.1080/15548627.2016.1271514. Epub 2017 Jan 5. PMID: 28055300; PMCID: PMC5361595.

Wang Y, Huang Y, Liu J, Zhang J, Xu M, You Z, Peng C, Gong Z, Liu W. Acetyltransferase GCN5 regulates autophagy and lysosome biogenesis by targeting TFEB. *EMBO Rep*. 2020 Jan 7;21(1):e48335. doi: 10.15252/embr.201948335. Epub 2019 Nov 21. PMID: 31750630; PMCID: PMC6945067.

Wang Z, Yang C, Guan D, Li J, Zhang H. Cellular proteins act as surfactants to control the interfacial behavior and function of biological condensates. *Dev Cell*. 2023 Jun 5;58(11):919-932.e5. doi: 10.1016/j.devcel.2023.04.004. Epub 2023 Apr 24. PMID: 37098348.

Yang C, Wang X. Lysosome biogenesis: Regulation and functions. *J Cell Biol*. 2021 Jun 7;220(6):e202102001. doi: 10.1083/jcb.202102001. Epub 2021 May 5. PMID: 33950241; PMCID: PMC8105738.

Yang XJ, Seto E. Lysine acetylation: codified crosstalk with other posttranslational modifications. *Mol Cell*. 2008 Aug 22;31(4):449-461. doi: 10.1016/j.molcel.2008.07.002. PMID: 18722172; PMCID: PMC2551738.

Zhang J, Wang J, Zhou Z, Park JE, Wang L, Wu S, Sun X, Lu L, Wang T, Lin Q, Sze SK, Huang D, Shen HM. Importance of TFEB acetylation in control of its transcriptional activity and lysosomal function in response to histone deacetylase inhibitors. *Autophagy*. 2018;14(6):1043-1059. doi: 10.1080/15548627.2018.1447290. Epub 2018 Jul 30. PMID: 30059277; PMCID: PMC6103407.

Zhao GQ, Zhao Q, Zhou X, Mattei MG, de Crombrughe B. TFEC, a basic helix-loop-helix protein, forms heterodimers with TFE3 and inhibits TFE3-dependent transcription activation. *Mol Cell Biol*. 1993 Aug;13(8):4505-12. doi: 10.1128/mcb.13.8.4505-4512.1993. PMID: 8336698; PMCID: PMC360062.

8. Acknowledgements

This doctoral thesis is based on studies performed from November 2020 to December 2023 at the Zentrum für Experimentelle Medizin, Institut für Osteologie und Biomechanik, UKE, Germany. I am very thankful for Prof. Dr. Thomas Bräulke who guided me in the realisation and completion of this project, teaching me how to develop critical thinking, and for giving me the opportunity to work on this very competitive field (as someone said in a conference, nowadays it's frightening to deal with TFEB).

Many thanks also to my working group, Dr. rer. nat. Malte Klüssendorf and Jane Rehberg, for always being willing to help me. Moreover, many thanks to Manu and Gianmarco, for bringing a bit of Italy to the office.

I am thankful for having been part of the LysFOR2526 symposium, allowing me to present and discuss my project annually to a group of experts in the field. Thanks to Sara for always being there for me and for keeping this friendship from Uni Perugia!

I am grateful for the opportunity to actively participate in international congresses with poster and talks - they were a huge opportunity to build connections, and to meet other PhD students (we were always on the same boat).

I would like to thank also all the people in my personal life that helped me going through this doctorate away from my home: to my bf, Elena, Silvia, Arianna, Veronica, Laura, and Benedetta, grazie per avermi supportato (e sopportato). To my *new* family, Luca and Lavinia, and thanks to my mother, for taking on her shoulders also my problems. A special thanks to Roxy, for listening my podcast and for always being there when I needed you most.

Thanks to all the beautiful people that I met here in Hamburg, you made these cold days warmer.

Finally, thanks who left, and thanks who stayed, till the very end.

9. Curriculum vitae

Laudicina Anastasia,

12.04.1996

Spoletto (PG), Italy

Working experiences

PhD non-medical program

University Medical Center Hamburg-Eppendorf UKE), Hamburg, Germany 2020-now

Supervisor: Prof. Dr. rer. nat. Thomas Braulke

Internship visiting student

University Medical Center Hamburg-Eppendorf UKE), Hamburg, Germany 2019

Supervisor: Prof. Dr. rer. nat. Thomas Braulke

Internship Master Degree

University of Perugia, Perugia, Italy 2018

Supervisor: Prof. Tommaso Beccari

Internship Bachelor Degree

University of Perugia, Perugia, Italy 2017

Supervisor: Prof. Roberta Spaccapelo

Education

Master Degree in Pharmaceutical Biotechnologies (LM-9)

University of Perugia, Perugia, Italy 2018-2020

Supervisor: Prof. Tommaso Beccari Lab

Bachelor Degree in Biotechnologies (L-2)

University of Perugia, Perugia, Italy 2015-2018

Supervisor: Prof. Roberta Spaccapelo

High School

Liceo Scientifico A. Volta, Spoleto (PG), Italy 2010-2015

Languages

Italian (native speaker)

English (fluent)

Poster presentation:

1. International FOR2625 Symposium on LYSOSOMES & AUTOPHAGY, 5th -6th May 2022 Berlin, Germany;
2. 24th European Study Group on Lysosomal Diseases (ESGLD) Workshop and Graduate Course, 7th -11th September 2022, Lancaster, UK;
3. Gordon Research Conference: Lysosomal Diseases 14th – 19th May 2023, Barcelona,

Oral presentation:

1. 1st retreat progress report members of the FOR2625 Symposium, 28 January 2022, online
2. 2nd retreat progress report members of the FOR2625 Symposium 21 September 2022, Kiel, Germany
3. 24th European Study Group on Lysosomal Diseases (ESGLD) Workshop and Graduate Course, 7th -11th September 2022, Lancaster, UK, *winner of the best flash-talk award*
4. 3rd retreat progress report members of the FOR2625 Symposium 2nd -4th November 2023, Jena, Germany

10. Eidesstattliche Versicherung

Ich versichere ausdrücklich, dass ich die Arbeit selbständig und ohne fremde Hilfe verfasst, andere als die von mir angegebenen Quellen und Hilfsmittel nicht benutzt und die aus den benutzten Werken wörtlich oder inhaltlich entnommenen Stellen einzeln nach Ausgabe (Auflage und Jahr des Erscheinens), Band und Seite des benutzten Werkes kenntlich gemacht habe.

Ferner versichere ich, dass ich die Dissertation bisher nicht einem Fachvertreter an einer anderen Hochschule zur Überprüfung vorgelegt oder mich anderweitig um Zulassung zur Promotion beworben habe.

Ich erkläre mich einverstanden, dass meine Dissertation vom Dekanat der Medizinischen Fakultät mit einer gängigen Software zur Erkennung von Plagiaten überprüft werden kann.

Unterschrift: Quastasa dardiana